CHARACTERIZATION OF HEMODIALYSIS MEMBRANES: MEMBRANE STRUCTURE AND FUNCTION

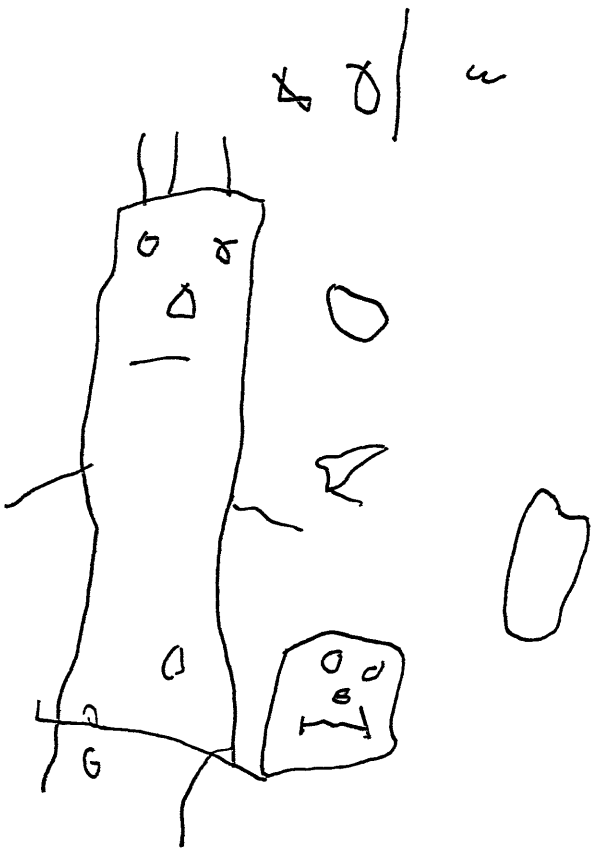

Arnold Broek

CHARACTERIZATION OF HEMODIALYSIS MEMBRANES: MEMBRANE STRUCTURE AND FUNCTION

PROEFSCHRIFT

ter verkrijging van
de graad van doctor aan de Universiteit Twente,
op gezag van de rector magnificus,
prof. dr. Th.J.A. Popma,
volgens besluit van het College voor Promoties
in het openbaar te verdedigen
op vrijdag 3 december 1993 te 16.45 uur.

door

Arnold Peter Broek
geboren op 29 augustus 1965
te Vlaardingen

Dit proefschrift is goedgekeurd door de promotor prof. dr. ing. H. Strathmann, de co-promotor prof. dr. C.A. Smolders en de assistent-promotor dr. D. Bargeman.

VOORWOORD

Soms vragen mensen hoe het toch mogelijk is dat je vier jaar lang onderzoek kunt doen naar de gaatjes in bloedfilters; zoiets moet wel ongelofelijk saai zijn. Voor mij is het heel belangrijk geweest om te kunnen werken in een omgeving die stimulerend is. Daarom ook zijn mensen aan wie je wat kunt vragen, die je in bescherming nemen of met wie je gewoon lekker kunt 'ouwehoeren' heel belangrijk. Graag zou ik een aantal van deze 'auteurs die niet op de voorkant staan' willen bedanken.

Herman Teunis, jou wil ik danken voor het grote aandeel dat je hebt gehad in het experimentele werk.

Erik Sprengers, bedankt voor je enthousiaste en coöperatieve begeleiding. Hoewel je misschien wel de direktst belanghebbende was, heb je me toch zeer veel ruimte, vertrouwen en waardering gegeven.

Dick Bargeman, belast met de dagelijkse 'zorg' voor mijn functioneren, je hebt me de ruimte gegeven om zelfstandig te kunnen werken. Op de momenten dat het nodig was, was je aanwezig.

Heiner Strathmann en Kees Smolders, bedankt voor de collegiale sfeer waarin ik van jullie heb mogen leren.

Mijn kamergenoten, Antoine, Emile, Monique en Wei, het was me een waar genoegen om met jullie de kamer te mogen delen.

Petrus Cuperus, het ene jaar dat we collega's waren, was duidelijk veel te kort, gelukkig wacht je nog een taak als paranimf. En ook die andere paranimf, John Heeks, al besef je dat misschien niet, ik heb veel van je geleerd en met veel plezier.

Dan zijn er nog vele anderen die op een of andere manier, bewust of onbewust, een bijdrage hebben geleverd. Remko Boom bedankt voor je hulp op velerlei gebied, Jan Heezen voor je hulp bij het computeren, Wim Lengton voor de zorg waarmee je analyses hebt uitgevoerd, Ingrid Wienk, Alie Bos en Monique Beerlage voor jullie correctiewerk, Clemens Padberg voor je hulp bij het GPC werk, Ineke Pünt voor je diffusiecoëfficientmetingen, Peter Bleeker voor je bijdrage aan hoofdstuk 5, Katrin Ebert voor je Duitse samenvatting. En al die andere lieve, aardige, belangstellende en hulpvaardige collega's uit de membraan-groep.

Tenslotte wil mijn familie bedanken, in het bijzonder mijn ouders. Piet en Wil bedankt voor jullie maar niet aflatende zorgzaamheid, liefde en belangstelling voor mijn leven en zijn. Ik wou dat iedereen zulke fijne ouders had.

En dan Annet, uit blijdschap om elkaar zijn we getrouwd, wat valt daar eigenlijk nog aan toe te voegen?

Arnold

Acknowledgement

Organon Teknika b.v. is gratefully acknowledged for their financial support of this work.

CIP-DATA KONINKLIJKE BIBLIOTHEEK, DEN HAAG

Broek, Arnold Peter

Characterization of hemodialysis membranes: membrane structure and function / Arnold Peter Broek. - [S.l. : s.n.]. - Ill.
Thesis Enschede. - With ref. - With summary in Dutch.
ISBN 90-9006544-X
Subject headings: hemodialysis membranes / membrane characterization.

Druk: Alfa, Enschede
Cover: Arnold Broek, 1969, reproduction

Voor Annet
Voor Johan

CONTENTS

1

HEMODIALYSIS AND ARTIFICIAL KIDNEYS
- a general introduction -

1.1 Historical background, economic aspects and principles

Since ancient times people have believed that diseases result from impurities in the body. Methods of purifying the organism and correcting the body's humoral balance have been disputed throughout the centuries. The blood purification health maintenance program of the 17th and 18th century for the well-to-do was: 'adequate purgation every week, application of a strong emetic once a month, and blood-letting twice a year, in the spring and in the fall' [1]. In our modern times extra-corporal blood purification techniques like hemodialysis are basically used to treat people which suffer from kidney failure. Nevertheless the availability of these techniques still is reserved to the countries that can afford the required medical infra-structure.

Just before World War I, about 60 years after Graham did his famous dialysis experiments, Abel and co-workers were the first to report on blood purification by means of dialysis [2]. Their dialysis membranes, hand-made collodium tubes, were named an artificial kidney. The first hemodialysis treatment on a human being suffering from kidney failure was reported in 1925 by Haas [3]. During World War II, in 1943, the Dutchmen Kolff and Berk developed their rotating drum high efficiency dialyzer equipped with cellophane tubing membrane [4]. It took another two years before, for the first time in history, a patient survived his kidney failure owing to hemodialysis. Since that time hemodialysis has developed from a highly risky pioneering enterprise to a well-established and save blood purification treatment with an average 5 years survival up to 90% [5].

World-wide 460,000 kidney failure patients are treated with hemodialysis nowadays, the number of patients is increasing by 7 to 8 percent annually. In Western Europe about 400 patients per million inhabitants are dialyzed. This patient ratio is largely dependent on the level of medical infra-structure but also ethic and religious factors play a role. In Japan for example, the patient ratio is about 800 per million because of cultural reasons relatively few patients undergo kidney transplantation. The average costs of hemodialysis are more than US$ 32,000 per patient per year [6].

Hemodialysis still is by far the most important synthetic membrane application market. In 1991 the world market sales of membrane and

membrane modules for hemodialysis were one billion US$, which is about 40% of the total synthetic membrane market [7]. This number is even more significant when it is considered that membranes used for hemodialysis are produced in bulk and therefore relatively cheap. Some important manufacturers of blood purification equipment are Baxter and CD Medical (USA), Akzo (the Netherlands), Fresenius (Germany), Toray (Japan), Kuraray (Japan) and the Gambro group (Sweden). The dialysis division of the Gambro group is a holding of the Swedish company Gambro, the French Hospal and the American Cobe.

Hemodialysis is applied to the treatment of patients which suffer from chronic or acute kidney failure to remove toxic metabolic wastes like urea, uric acid and creatinine from their blood. During a hemodialysis run arterial blood is passed over one side of the artificial kidney membrane, while a dialysate solution containing a buffered and isotonic mixture of dextrose and salts is circulated on the other side. The composition of the dialysate is set to maintain the correct ionic balance in the blood. Heparin is added to the blood stream to prevent the blood from clotting. In the generally used hollow fiber artificial kidney the blood is pumped through the lumen of the hollow fibers and the dialysate is pumped in counter-current flow through the interstice between the fibers. The concentration difference across the membrane between blood and dialysate stream causes small solutes to diffuse through the membrane while larger molecules like proteins and blood cells are rejected. The hemodialysis process is schematically shown in Figure 1.

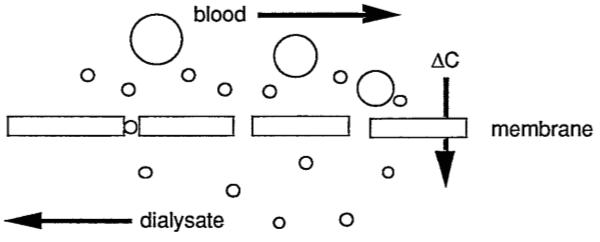

Figure 1 *The basic principle of (hemo)dialysis. The concentration difference ΔC causes the diffusion of the small solutes through the pores of the membrane, the larger particles are retained.*

An additional aim of hemodialysis is the removal of excess body fluid, and therefore the process is also driven by a small pressure difference, typically of 0.2 bar. This pressure difference is high enough to produce 1-4 liter 'urine' which is not produced by the kidney of the patient. For the ordinary low-flux hemodialysis membranes the contribution of the pressure difference to the transport of metabolic wastes is in general negligible.

People suffering from chronic kidney failure should preferably have their blood cleaned continuously. For practical and economic reasons, however, dialysis is performed only two or three times a week. A typical hemodialysis treatment lasts from 4 to 6 hours, during which the patient is confined to bed. Hemodialysis therefore puts a large demand on the patient's social life. As an alternative, approximately 15% of the world's patient population is treated with a therapy named 'peritoneal dialysis (PD)' [6]. For this process the patient's own peritoneum is used as the dialysis membrane. PD is performed by regularly (3-5 times each day) introducing 1 to 3 liters of a dialysate solution into the abdominal cavity of the patient. By diffusion the metabolic waste products are transported from the blood and surrounding tissues into the dialysis solution. Removal from the body of waste products and excess water occurs when the dialysate is drained. Although PD patients are much more sensitive to infections many patients prefer this technique because with PD they are not restricted to treatment in a dialysis clinic [8].

Although modern dialysis techniques are good enough to guarantee an acceptably high survival rate, many chronic dialysis patients suffer from a lack of complete well-being. The ultimate goal for these patients is to receive a donor kidney. In general, however, there is a time gap between the diagnosis of kidney failure and the moment a donor kidney becomes available. Hemodialysis is used to bridge this time gap. In the Netherlands the average time gap is about two years [9].

1.2 Artificial kidney development

Several developments have resulted in important improvements of the modern artificial kidney since the first successful dialysis treatment by Kolff. In 1967 the first hollow fiber artificial kidney device was reported, combining a large surface to volume ratio with a low blood priming volume [10]. Since the early 1970s hollow fibers made of cuprophan®, a thinner regenerated cellulose film made by the cuprammonium process, have replaced the cellophane membranes. Nowadays hollow fiber cuprophan is the standard for dialysis membranes, although the contribution of other, synthetic polymeric materials is becoming more and more important.

One of the major drawbacks of regenerated cellulose membranes is their lack of biocompatibility. The many hydroxyl groups of the cellulose are thought to play an important role in the observed complement activation in the blood of dialysis patients [11]. An ideally biocompatible material should neither evoke thrombogenic, toxic, allergic or inflammatory reactions, nor immunologic reactions, carcinogenic effects or deterioration of adjacent tissue [12]. Although the clinical relevance of most of the determined biocompatibility parameters is controversial, it has forced artificial kidney manufacturers to explore

alternative membrane materials. Since the early 1980s different synthetic polymeric materials with improved biocompatibility have become available. The relative contribution of these materials to the total dialysis market is growing. In Table 1, an overview of commercially available artificial kidney membrane materials is shown.

Table 1 *Commercially available artificial kidney membrane materials [13a-c].*

Polymer	Trade-name	Manufacturer
cellulose	cuprophan, cellophane	Akzo
modified cellulose	hemophan	Akzo
cellulose acetate (CA)		CD Medical, Akzo, Baxter
saponified cellulose ester		
polyacrylonitrile (PAN)		Hospal
polymethylmethacrylate (PMMA)		Toray
ethylene vinylalcohol copolymer	EVAL	Kuraray
polysulfone (PSf)		Fresenius
polycarbonate		
polyamide (PA)		
PA/polyvinylpyrrolidone (PVP) blends	polyflux	Gambro
polycarbonate/polyether blends	gambrane	Gambro

Another important factor for the development of artificial kidneys has been the so-called 'middle molecule hypothesis' which was raised in 1972 by Babb *et al.* [14]. This hypothesis states that the 'middle molecules', i.e. (toxic) molecules with a molecular weight between 500 and 2000 g/mole, are responsible for the lack of well-being suffered by hemodialysis patients. The permeabilities of the ordinary hemodialysis membranes are relatively low towards these molecules. During an ordinary hemodialysis session the middle molecules are not adequately removed and accumulate in the patient's body. The clinical relevance of the middle molecule hypothesis has not been proven yet [15,16]. Still it has triggered the development of artificial kidneys with an enhanced capacity to remove the middle molecules.

The desirability of removing higher-molecular weight solutes has been revived recently, especially in connection with the suspected importance of certain low-molecular weight proteins. Normally, these proteins are catabolized in the kidney but in chronic hemodialysis patients they are found in elevated concentrations. Prominent among these is β2-microglobulin (M = 11.8 kg/mole), of which elevated concentrations lead to systemic amyloidosis (resulting in a rheumatic syndrome) in patients on long-term hemodialysis [17,18].

In order to enhance the capacity of artificial kidneys to remove middle and larger molecules two different approaches are followed. Firstly, new dialysis strategies like hemofiltration and hemodiafiltration have been developed. The hemofiltration (HF) process is comparable with the ultrafiltration (UF) process, the driving force for mass transport is a hydrostatic pressure difference rather than the concentration difference used for hemodialysis. Since the transport is convective the transport of the middle molecules is enhanced. HF also leads to a change, i.e. a decrease of the blood volume, which has to be compensated by addition of a proper solution either before or after the filtration process. This makes the process relatively expensive. The hemodiafiltration (HDF) process makes use of a combination of a pressure and a concentration difference. The three different operation modes for artificial kidneys are shown in Figure 2.

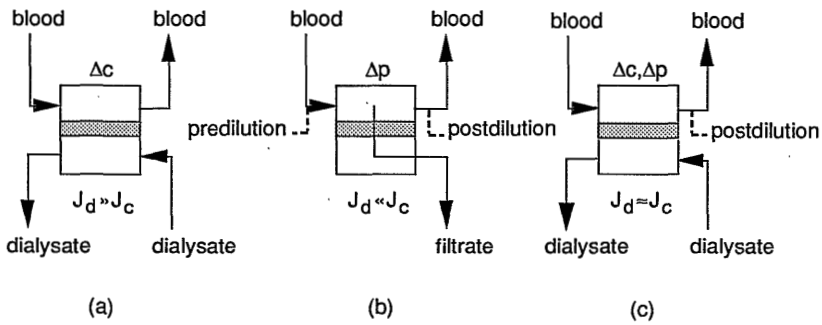

Figure 2 *The three different operation modes for artificial kidneys, a: hemodialysis; b: hemofiltration; c: hemodiafiltration. J_d is the diffusive flux, J_c the convective flux, Δc and Δp are the concentration and the pressure difference across the membrane, after Strathmann et al. [19].*

Secondly, so-called 'high-flux' membranes with an enhanced permeability towards the middle and larger molecules have been developed. Since these membranes also have an enhanced hydraulic permeability care must be taken to avoid fatal dehydration of the patient. Another 'hot topic' related to the use of high-flux membranes is the so-called backfiltration [20,21], i.e. the permeation of endotoxins (bacterial residues) from contaminated dialysate to the patient's blood. For polyamide high-flux membranes it is claimed that the permeation of endotoxins is prevented by a combined rejection/absorption mechanism [22].

The artificial kidney has to be sterile and pyrogen free in order to avoid contamination of the patient's blood. Current dialyzers for clinical use are sterilized by either ethylene oxide (EtO) gas, autoclave or gamma-irradiation [23]. It is known that small amounts of residual EtO can cause an allergic

reaction in some patients [24]. Material degradation was reported for autoclaved and gamma-irradiated membranes [25,26,27]. The sterilization method also influences the choice of housing and potting materials.

1.3 Mass transfer in hollow fiber artificial kidneys

In clinical practice the artificial kidney device is generally regarded as a 'black box' and its performance is expressed in terms of a 'clearance rate' Q_{cl} and an 'ultrafiltration capacity' UFR. The clearance Q_{cl} is referring to the volume of blood which is cleared of a certain substance per unit of time. For hemodialysis with a negligible convective mass transport it is defined by equation 1:

$$Q_{cl} = Q_{b,i} \cdot \frac{(c_{b,i} - c_{b,o})}{c_{b,i}} \qquad (1)$$

where Q_{cl} is the clearance rate, $Q_{b,i}$ the blood flow at the inlet and $c_{b,i}$ and $c_{b,o}$ are the concentrations in the blood at the inlet and outlet respectively.

The clearance rate is not a simple function of only the membrane permeability but depends also on other factors such as total membrane area, fiber and device geometry and linear flow velocities of blood and dialysate.

The ultrafiltration capacity is basically referring to the capacity to remove body fluids by means of a pressure difference. It is often determined at a pressure difference of 0.2 bar.

For an ideal counter-current configuration the relation between clearance rate and the overall permeability of the membrane is given by [28,29]:

$$Q_{cl} = \frac{Q_b Q_d \left[1 - \exp\left(\frac{-PA(Q_d - Q_b)}{Q_b Q_d}\right)\right]}{Q_d - Q_b \exp\left(\frac{-PA(Q_d - Q_b)}{Q_b Q_d}\right)} \qquad (2)$$

where Q_b is the blood flow, Q_d the dialysate flow, A the total membrane surface area and P the overall membrane permeability.

For a hollow-fiber artificial kidney the membrane surface area is calculated from the logarithmic mean surface area:

$$A = NL\pi \frac{d_o - d_i}{\ln(d_o/d_i)} \qquad (3)$$

where N is the total number of fibers, L the effective fiber length, and d_o and d_i are the outer and inner fiber diameter in the wet state.

In practice, the ideal counter-current conditions are never met. Due to channelling, mixing effects and convective fluxes deviations from the ideal situation occur. Channelling is caused by the preferential flow of the blood or dialysate through specific parts of the device. Noda *et al.* [30] showed that channelling of the dialysate can cause a substantial deviation from the theoretical performance. The effect was found to be the most prominent in the case of loosely packed devices and for equal volumetric blood and dialysate flow. Park and Chang [31] showed with advanced tracer techniques that also in the fiber lumen a significant degree of channelling can exist. Lumen flow was found to occur preferentially through the center of the fiber bundle. The channelling was found to be dependent on the manifold design, Reynolds number and pressure drop along the fibers. Van Bekkum and Segal [32] showed by means of computer calculations that in a properly designed device a uniform flow distribution through the fibers can be obtained.

Mixing effects in the blood or dialysate stream can also be responsible for deviations from the counter-current configuration. Assuming a well-mixed dialysate circuit (instead of plug flow) allows one to estimate the maximal effect of back mixing (Figure 3). The malfunction of the device is most significant for high membrane permeabilities, i.e. small solutes.

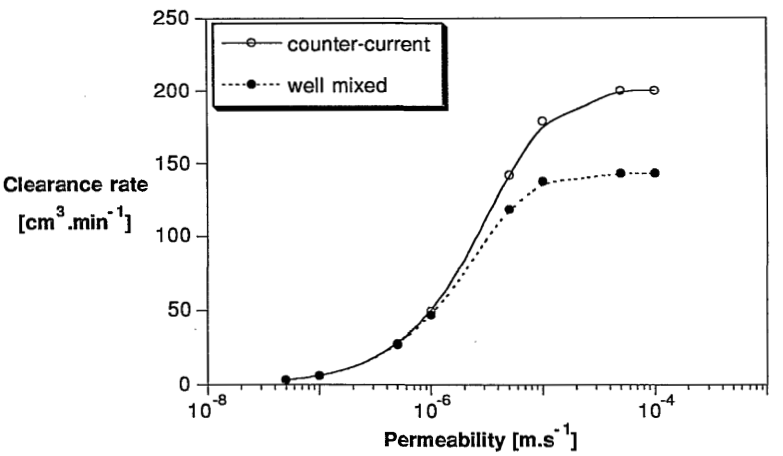

Figure 3 *The effect of a well-mixed dialysate circuit on the device performance (Q_b=200 cm³.min⁻¹, Q_d=500 cm³.min⁻¹, A=1 m², data calculated from Eqn. 2 and from an equation given by Jonsson [33]).*

The permeability P used in Eqn. 2 is an overall membrane permeability. Adjacent to the membrane wall, stagnant liquid films are formed which cause an additional resistance against diffusion through the membrane. The

resistances of these boundary layers are influenced by the device and fiber geometry, flow conditions and solute size. The situation near the membrane wall is schematically shown in Figure 4.

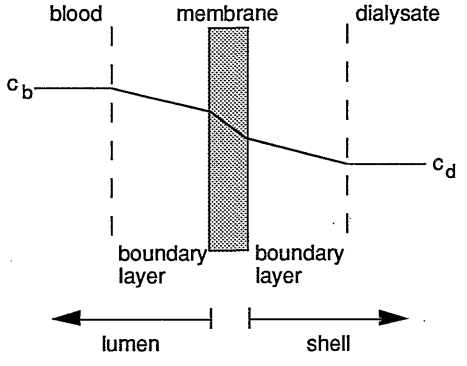

Figure 4 *Schematic representation of the concentration profiles in hemodialysis.*

The relation between the overall and the true membrane permeability is given by Eqn. 4. The equation is an analogue of the resistance-in-series model used for electric circuits.

$$\frac{1}{P} = \frac{1}{P_m} + \frac{1}{P_b} + \frac{1}{P_d} \qquad (4)$$

where P_m is the true membrane permeability and P_b and P_d are the permeabilities of the boundary layers in the fiber lumen and in the interstice between the fibers.

Figure 5 shows the estimated contribution of the boundary layers to the overall resistance against diffusion for a typical low-flux hemodialysis device. As can be seen, the effect of the boundary layers is most prominent for small solutes. Recently, Futselaar *et al.* [34] reported on the development of hollow fiber devices in which the dialysate flow is locally perpendicular to the direction of the fibers. As a consequence of this transverse flow principle the influence of the dialysate boundary layer can be diminished.

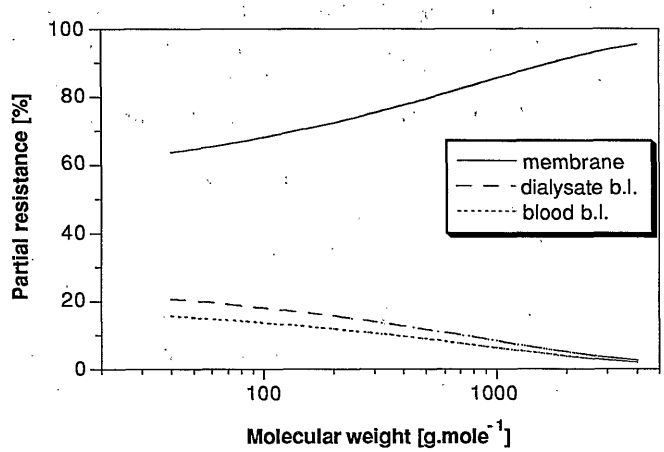

Figure 5 *Partial resistances of the membrane and of the boundary layers (b.l.) in the blood and dialysate compartment as a function of the molecular weight of the solute. Data are for a typical low-flux hemodialysis device.*

For a proper estimation of the overall membrane permeability one has to know the contributions of the membrane and boundary layers to the total resistance. In general the flow in a hollow fiber artificial kidney is governed by a laminar flow regime. The permeability of the boundary layer in the fiber lumen can be estimated from Eqn. 5:

$$Sh_b = \frac{P_b d_i}{D_b} \qquad (5)$$

where Sh_b is the Sherwood number for the fiber lumen, D_b the diffusion coefficient of the solute in the fiber lumen and d_i the internal fiber diameter. With a hydrodynamically installed flow regime, the Sherwood number reaches an asymptotic value of about 4. The exact value of the asymptotic Sh_b is ranging from 3.65-4.37 [28,29], 3.66 [35], 4.25-4.35 [36] to 4.36 [37]. Klein *et al.* [38] adapted an average value of 4. The asymptotic Sherwood number is reached provided that the following condition is satisfied [28,29,35]:

$$Gz_b = \frac{\bar{v}_b d_i^2}{L D_b} < 2.5\text{-}10 \qquad (6)$$

where Gz_b is the Graetz number for the fiber lumen and $\bar{v}_b$ the average liquid velocity in the fiber lumen and L the effective fiber length.

Angierski *et al.* [39] and Kreulen [40] pointed out that the distribution of the fiber diameters around the average which is normally present (about 10%) can have a large impact on the actually obtained apparent permeability. The value can significantly deviate from the value calculated on basis of the average diameter.

Much more difficult is the estimate of the boundary layer in the interstice between the fibers. As mentioned before, the observed permeability of the membrane is also influenced by channelling and mixing. Furthermore the packing of the fibers in the device is never completely regular and the position of the fibers in the device is not always fixed. A number of relations between boundary layer permeability, device geometry and flow conditions are proposed by various authors [28,41]. In general, the discrepancy between the different relations is considerable.

1.4 The structure of this thesis

The main objective of this thesis is to study the relation between the structure and mass transfer performance of cellulosic hollow-fiber hemodialysis membranes. As indicated in this general introduction, the relation is rather complex because in the practical (clinical) situation several disturbing factors play a role. Throughout this work special attention is paid to three different types of hollow-fiber hemodialysis membranes: cuprophan®, hemophan® and RC-HP400A. The cuprophan and RC-HP400A membranes are made of a regenerated cellulose. The hemophan membranes are made of a regenerated and modified cellulose. In order to improve its biocompatibility, the cellulose has been modified with a small amount (degree of substitution 0.01-0.03) of N,N-di-ethyl-aminoethyl (DEAE) ether groups. The DEAE groups have a weak anion exchange capacity. The RC-HP400A fiber is a so-called high-flux type membrane.

Chapter 2 gives an overview of the present knowledge about cellulosic dialysis membranes. The chapter is divided in three sections. The first section deals with the chemical and physical features of regenerated cellulosic materials. In the second section, the two main mass transport models proposed for the transport through cellulose membranes are discussed. In the third section, the characterization of porous membranes is discussed. Special attention is paid to find suitable characterization methods for cellulosic hollow-fiber hemodialysis membranes.

The characterization of cellulosic membranes by means of thermoporometry/calorimetric measurements is discussed in Chapter 3. Thermoporometry is a wet-state membrane characterization method to determine the pore size distribution and porosity of meso-porous membranes. It

is based on the calorimetric analysis of the liquid-solid transformation of liquid filled porous materials. On the other hand, calorimetric measurements have extensively been used to study the states of water in water swollen hydrogels. Chapter 3 aims at bringing the two concepts together.

Chapter 4 presents the characterization of cellulosic hemodialysis membranes by means of an inverse size exclusion chromatography (i-SEC) technique. I-SEC is a wet-state characterization method to determine the pore size distribution and porosity of porous materials. The technique can also be used to study the interaction between test molecules and membrane materials.

In Chapter 5, the results of mass transport measurements with cellulosic hemodialysis membranes are presented. Special attention is paid to the influence of the NaCl concentration of feed and dialysate on the transport of the test molecules creatinine and vitamin B12.

Chapter 6 is a general discussion to compare the results of the calorimetric, inverse SEC and mass transport measurements. It is shown that for the transport through the membranes of interest both the pore structure and the interaction between permeating molecule and membrane play an important role.

1.5 Symbols

A	total membrane surface area [m^2]
$c_{b,i}$	concentration in the blood stream at the inlet [$mole.m^{-3}$]
$c_{b,o}$	concentration in the blood stream at the outlet [$mole.m^{-3}$]
D_b	diffusion coefficient of the solute in the fiber lumen [$m^2.s^{-1}$]
d_o	outer fiber diameter [m]
d_i	inner fiber diameter [m]
Gz_b	Graetz number in the fiber lumen [-]
J_c	convective flux through the membrane [$mole.m^{-2}.s^{-1}$]
J_d	diffusive flux through the membrane [$mole.m^{-2}.s^{-1}$]
L	effective fiber length [m]
N	total number of fibers [-]
P	overall diffusive membrane permeability [$m.s^{-1}$]
P_m	true diffusive membrane permeability [$m.s^{-1}$]
P_b	permeability boundary layer in the fiber lumen [$m.s^{-1}$]
P_d	permeability boundary layer in the fiber interstice [$m.s^{-1}$]
Q_{cl}	clearance rate [$m^3.s^{-1}$]
$Q_{b,i}$	blood flow at inlet [$m^3.s^{-1}$]
Q_b	blood flow [$m^3.s^{-1}$]
Q_d	dialysate flow [$m^3.s^{-1}$]
Sh_b	Sherwood number in the fiber lumen [-]
$\bar{v}_b$	average liquid velocity in the fiber lumen [$m.s^{-1}$]

1.6 References

[1] H. Klinkmann, *Historical overview of renal failure therapy*, In: H. Klinkmann, L.C. Smeby (eds.), Terminal renal failure: therapeutic problems and potentials, Basel etc., Karger, Contrib. Nephrol., 78 (1990) 1-23

[2] J.J. Abel, L.G. Rowntree, B.B. Turner, *On the removal of diffusible substances from the circulating blood by means of dialysis*, Trans. Ass. Am. Physicians, 28 (1913) 50-54

[3] G. Haas, *Versuche der Blutauswaschung am Lebenden mit Hilfe der Dialyse*, Klin. Wochenschrift, 4 (1925) 13-14

[4] W.J. Kolff, H.Th.J. Berk, *De kunstmatige nier: een dialysator met een groot oppervlak*, Ned. Tijdschr. Geneeskd., 87 (1943) 1684

[5] F.P. Brunner et al., *Figures from combined report on regular dialysis and transplantation in Europe XIX, 1989*, Proc. Eur. Dial. Transplant Ass. - Eur. Renal Ass., Vienna, 5-8 September 1990, p. 27

[6] Gambro, *Annual report Gambro group 1991*, Lund, 1992

[7] H. Strathmann, *Industrial utilization of membranes and membranes processes*, In: P. Aimar, P. Aptel (eds.), Membrane processes, water treatment - pervaporation, Récents progrès en génie des procédés, 6, 21 (1992) 17-26

[8] M.I. Sorkin, J.A. Diaz-Buxo, *Physiology of peritoneal dialysis*, In: J.T. Daugirdas, S. Todd (eds.), Handbook of Dialysis, Boston etc., Little Brown, 1988, 167-181

[9] F.P. Brunner et al., *Figures from combined report on regular dialysis and transplantation in Europe XIX, 1989*, Proc. Eur. Dial. Transplant Ass. - Eur. Renal Ass., Vienna, 5-8 September 1990, p. 75

[10] B.J. Lipps, R.D. Stewart, H.A. Perkins, G.W. Holmes, E.A. McLain, M.R. Rolfs, P.D. Oja, *The hollow fiber artificial kidney*, Trans. Am. Soc. Artif. Int. Organs, 13 (1967) 200

[11] P.R. Craddock, J. Fehr, A.P. Dalmaso, K. Brigham, H. Jacob, *Hemodialysis leukopenia: pulmonary vascular leukostasis resulting from complement activation by dialyzer cellophane membranes*, J. Clin. Invest., 59 (1977) 879-888

[12] H. Klinkmann, *The role of biomaterials in the application of artificial organs*, In: J. Paul, J. Gaylor, J. Courtney, T. Gilchrist (eds.), Biomaterials in artificial organs, London, Macmillan, (1984) 1-8

[13 a] J.C. Van Stone, *Hemodialysis Apparatus*, In: J.T. Daugirdas, S. Todd (eds.), Handbook of Dialysis, Boston etc., Little Brown, 1988, 21-40

[b] several manufacturers brochures

[c] R.A. Ward, P.W. Feldhoff, E. Klein, *Membrane materials for therapeutic applications in medicine*, In: D.R. Lloyd (ed.), Materials science of synthetic membranes, ACS symposium series, Washington, 1985

[14] A.L. Babb, P.C. Farrell, D.A. Uvelli, B.H. Scribner, *Hemodialyzer evaluation by examination of solute molecular weight spectra: implications for the square-meter-hour hypothesis*, Trans. Am. Soc. Artif. Intern. Organs, 18 (1972) 18

[15] H. Brunner, H. Mann, *What remains of the 'middle molecule' hypothesis today?*, In: M.J. Lysaght, E. Wetzels, H.J. Gurland (eds.), Disputed issues in renal failure therapy, Basel etc., Karger, Contrib. Nephrol., 44 (1985) 14-34

[16] C.K. Colton, *Analysis of membrane processes for blood purification*, Blood Purif., 5 (1987) 202-251

[17] G.A. Kozeny, J.E. Hano, *Rheumatic disease*, In: J.T. Daugirdas, S. Todd (eds.), Handbook of Dialysis, Boston etc., Little Brown, 1988, 515-523

[18] P.D. Gorevic, T.T. Casey, W.J. Stone, C.R. Di Raimondo, F.C. Prelli, B. Frangione, *Beta-2 microglobulin is an amyloidogenic protein in man*, J. Clin. Invest., 76 (1985)

[19] H. Strathmann, H. Göhl, *Membranes for blood purification: state of the art and new developments*, In: H. Klinkmann, L.C. Smeby (eds.), Terminal renal failure: therapeutic problems, possibilities and potentials, Basel etc., Karger, Contrib. Nephrol., 78 (1990) 119-141.

[20] S. Stiller, H. Mann, H. Brunner, *Backfiltration in hemodialysis with highly permeable membranes*, In: E. Streicher, G. Seyffart (eds.), Highly permeable membranes, Basel etc., Karger, Contrib. Nephrol., 46 (1985) 23-32

[21] U. Baurmeister, J. Vienken, V. Daum, *High-flux dialysis membranes: Endotoxin transfer by backfiltration can be a problem*, Nephrol. Dial. Transplant., 4 (1989) 89-93

[22] H. Göhl, R. Buck, H. Strathmann, *Basic features of the polyamide membranes*, In: S. Shaldon, K.M. Koch (eds.), Polyamide - The evolution of a synthetic membrane for renal therapy, Basel etc., Karger, Contrib. Nephrol., 96 (1992) 1-25

[23] S. Takesawa, S. Ohmi, Y. Konno, M. Sekiguchi, S. Shitaokoshi, T. Takahashi, H. Hidai, K. Sakai, *Varying methods of sterilisation, and their effect on the structure and permeability of dialysis membranes*, Nephrol. Dial. Transplant., 1 (1987) 254-257

[24] J. Poothullil, A. Shimizu, R.P. Day, J. Dolovich, *Anaphylaxis from the product of ethylene oxide gas*, Ann. Intern. Med., 82 (1975) 58-60

[25] E. Klein, F.F. Holland, A. Donnaud, A. Lebeouf, K. Eberle, *Diffusive and hydraulic permeabilities of commercially available cellulosic hemodialysis films and hollow fibers*, J. Membrane Sci., 2 (1977) 349-364

[26] S. Takesawa, S. Satoh, H. Hidai, M. Sekiguchi, K. Sakai, *Degradation by gamma irradiation of regenerated cellulose membranes for clinical dialysis*, Trans. Am. Soc. Artif. Intern. Organs, 33 (1987) 584-587

[27] A.P. Broek, H.A. Teunis, D. Bargeman, E.D. Sprengers, C.A. Smolders, *Characterization of hollow fiber hemodialysis membranes: pore size distribution and performance*, J. Membrane Sci., 73 (1992) 143-152

[28] J.E. Sigdell, *Calculation of combined diffusive and convective mass transfer*, Int. J. Artif. Organs, 5 (1982) 361-372

[29] J.E. Sigdell, *A mathematical theory for the capillary artificial kidney*, Stuttgart, Hippokrates Verlag, 1974

[30] I. Noda, D.G. Brown-West, C.C. Grytte, *Effect of flow maldistribution on hollow fiber dialysis - experimental studies*, J. Membrane Sci., 5 (1979) 209-225

[31] J.K. Park, H.N. Chang, *Flow distribution in the fiber lumen side of a hollow-fiber module*, Am. Industr. Chem. Eng. Sci., 32 (1986) 1937-1947

[32] M. v. Bekkum, G. Segal, *Flow and pressure distributions of blood in dialysers*, Int. J. Artif. Organs, 14 (1991) 576

[33] G. Jonsson, *Dialysis*, In: M. Bungay et al. (eds.), Synthetic membranes: science engineering and applications, Reidel, 1986, 625-645

[34] H. Futselaar, T. Reith, I.G. Racz, *The transverse flow microfiltration module: a process-technical and economical evaluation*, In: P. Aimar, P. Aptel (eds.), Membrane preparation, fouling - emerging processes, Récents progrès en génie des procédés, 6, 22 (1992) 239-244

[35] W.J. Beek, K.M.K. Muttzall, *Transport phenomena*, London, Wiley, 1975, Chapter 3

[36] C.K. Colton, E.G. Lowrie, *Hemodialysis: physical principles and technical considerations*, In: B.M. Brenner, F.C. Rector (eds.), The Kidney, vol. II, 2nd edn., Philadelphia, Saunders, 1981, p. 2425

[37] I. Noda, C.C. Grytte, *Mass transfer in regular arrays of hollow fibers in counter-current dialysis*, Am. Inst. Chem. Eng. J., 25 (1979) 113-122

[38] E. Klein, F. Holland, A. Lebeouf, A. Donnaud, J.K. Smith, *Transport and mechanical properties of hemodialysis hollow fibers*, J. Membrane Sci., 1 (1976) 371-396

[39] B.R. Angierski, P. Lötzsch, R. Tietze, *Einfluß der Faserdurchmesserverteilung auf*

den Stofftransportkoeffizienten bei Hohlfasermembranen für die Dialyse, Chem. Techn., 42 (1990) 426-428

[40] H. Kreulen, *Microporous membranes in gas separation processes using a liquid phase*, PhD Thesis, University of Twente, 1993, p. 60

[41] H. Futselaar, *The transverse flow membrane module*, PhD Thesis, University of Twente, 1993, p. 98

2

CELLULOSIC HEMODIALYSIS MEMBRANES
- properties and characterization -

2.1 Chemical and physical properties of celluloses

Technologically spoken, cellulose denotes the residues obtained by subjecting vegetable materials to certain pulping processes. The pulps consist mainly of cellulose and closely related materials but may differ in amount and nature of the non-cellulosic constituents. Cellulose in the chemical sense, is a polysaccharide of sufficient chain length to be insoluble in water and in dilute acid or alkaline solutions at ordinary temperatures [1]. The cellulose molecules consist of anhydroglucose units linked together through a 1,4 β-glucosidic linkage as shown in Figure 1. The molecules typically have a degree of polymerization (DP) of 3000-7000 glucose units [2]. The anhydroglucose units are ordered in a syndiotactic way, every second unit is rotated 180° with respect to its neighbors. The units are in the chair conformation. All of its pendant groups, the hydroxyl groups and the β-glucosidic oxygen are in the equatorial position. As a result, cellulose and its derivatives are linear, rodlike (at low molecular weight) and rather inflexible molecules. The large number of hydroxyl groups render it extremely hydrophilic so that the water swollen cellulose exhibits a hydrogel character. However, because of its structural regularity and the capacity to form inter-molecular hydrogen bonds cellulose is not soluble in water. Celluloses always contain a small number of carboxylic groups which give the molecule a slightly negative charge. Typical values are 1 carboxylic group per 100-1000 glucose units for wood cellulose and 1 per 100-500 for cotton cellulose [3,4].

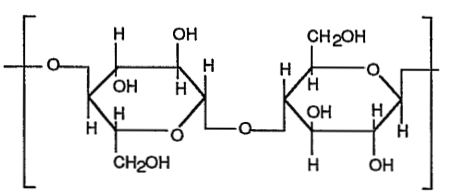

Figure 1 *Structure of the basic cellobiose unit of the cellulose molecule.*

Regenerated cellulose has been recovered in a solid form from a homogeneous

solution of cellulose. Amongst the various industrial processes that are applied for the production of regenerated cellulose, the viscose process is the most important one [5]. In this process the cellulose is recovered from a cellulose sodium xanthate solution[1]. When the material is extruded into fibers the product is called 'viscose rayon' and when extruded into sheets, 'cellophane'. The viscose rayons are extensively used for the production of textile materials.

In the cuoxam or cuprammonium process the cellulose is first treated with aqueous NaOH at a high temperature and pressure to depolymerize the cellulose partly and to remove hemicellulose. The pre-treated cellulose is dissolved in a cuoxam solution, an aqueous solution containing $CuSO_4.3Cu(OH)_2.H_2O$, NH_3 and NaOH. The cellulose is recovered by precipitation in a dilute aqueous solution of sulfuric acid. The cuprammonium process is applied by Akzo (Enka) for the production of the well-known hemodialysis membranes made of cuprophan® and hemophan® [5]. Owing to the cuprammonium process the average degree of polymerization drops to 300-400 [2].

The ability of hydroxyl groups to form secondary valence hydrogen bonds is - together with the stiff and straight chain nature of the cellulose molecule - the reason for the high tendency to organize into crystallites and crystalline strands (elementary fibrils), the basic elements of the supra-molecular structure of cellulose fibers. The dimensions of the elementary fibrils differ only slightly for native or regenerated celluloses [3]. Their length ranges between 12 and 20 nm (=24-40 glucose units) and their width between 2.5 and 4.0 nm. In solid cellulose, high-order micro-crystalline structures 'crystalline regions' alternate with those of a distinctly lower order 'amorphous regions'. Cellulose is polymorphous, i.e. depending on the origin or the conditions during isolation or conversion, cellulose can adopt various crystal lattice structures. X-ray spectrographic studies showed that the structure of the crystalline regions of native cellulose is different from that of regenerated celluloses, i.e. the dimensions of the crystalline unit cell are different. Cellulose I is found in native cellulose and is by far the most common in nature, regenerated celluloses mainly contain cellulose II. The regenerated celluloses show different macroscopic properties such as moisture and dye sorption, accessibility, mechanical and viscoelastic properties and overall crystallinity [1]. For instance, the crystallinity of the native celluloses is roughly 70% while for the regenerated celluloses it is about 35% [6].

With regard to the supra-molecular structure of cellulose various structural models have been proposed. The classical one is the 'fringed micelle' model, according to which the crystalline regions (micellae) are joined by

[1] Cellulose sodium xanthate is prepared by treating cellulose swollen in an aqueous solution of sodium hydroxyde with carbon disulfide gas. The cellulose is recovered in an aqueous solution of sulfuric acid.

cellulose chains which in turn are constituents of several micellae. Since X-ray diffraction studies indicated that most crystalline regions extend only for a few hundred Ångstrom units, which is less than the complete extended length of the polymer chains, it was assumed that the crystalline regions contain only sections of molecules [7].

More recently the fringed fibril model has been proposed [7]. According to this model, polymer crystallites are formed from polymer molecules which fold back on themselves in the shapes of spirals. In such a situation, individual molecules do not participate in both crystalline and amorphous regions. In the case of highly crystalline polymers the amorphous regions may represent only chain ends and small sized dislocations within the crystallites.

Despite the enormous effort invested during the last 100 years or more, the supra-molecular structure of native and regenerated cellulose are still not completely elucidated. Also the validity of the fringed micelle and the fringed fibril model are still under dispute [3].

Cellulose is a hydrophilic material and in water the material swells. The extent of swelling is very much dependent on the type of cellulose. Table 1 shows some typical swelling values of different cellulosic materials. When cellulose is swollen the water opens the inter-fibrillar interstices and swells the less-ordered surface and interlinking regions of the fibrillar elements. The water molecules break the inter-molecular hydrogen bonding, and increase the inter-molecular distance of the cellulose chains [4]. Hence, as shown in Figure 2, water filled holes or channels are formed through which eventually mass transport can occur.

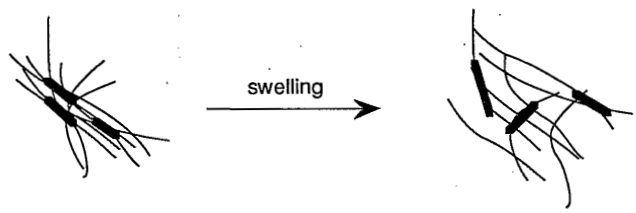

Figure 2 *Schematic representation of the effect of swelling on the cellulose matrix. The swelling causes the formation of water filled holes or channels. The thick lines indicate the crystalline regions.*

For the swollen celluloses it has been proposed that at least two types of water can be distinguished. Generally, a discrimination is made between so-called 'bound' or 'non-freezing' water and 'free' or 'bulk' water. The states of water are discussed in two- or three state models [8-10]. These models will be discussed in detail in Chapter 3.

Table 1 *Typical swelling values of different cellulosic materials [3].*

Material	Swelling [%]
Cotton	18
Viscose, continuous filament	74
Cuprammonium rayon	86
Cellulose triacetate	10
Cellulose tripropionate	2.5
Cellulose tributyrate	1.8
Cellulose tristearate	1.0

2.2 Mass transport through cellulosic membranes

2.2.1 Pores versus segment mobility

Already in 1930 McBain and Kistler [11] reported that dry cellulosic films are practically impermeable to ethanol and other organic solvents. If the films were first soaked in water, however, ethanol passed through readily, and when the alcohol was replaced by other solvents, these also passed through. From these phenomena they concluded that pores do not exist in dry cellulosic films and that they develop only upon swelling. Indeed a remarkable change in properties occurs when a cellulose film is swollen. It is known that a dry regenerated cellulose film has gas selective properties whereas a water swollen film can be applied to separate high and low molecular weight molecules in a solution [12]. The change in characteristic size of the permeant is at least one order of magnitude.

Water swollen celluloses exhibit a hydrogel character. Gels cover a spectrum from one phase or homogeneous dynamic solutions (where the entropy of mixing is the chief factor responsible for retention of the solvent, and 'pores' are neither constant in size nor location) to two phase or heterogeneous rigid porous structures (where capillary forces are responsible for retention of the solvent) [13].

In accordance with that, essentially two models have been proposed to explain the mechanism of solute migration in water swollen cellulosic materials; the models are shown in Figure 3. The oldest model, the *pore model*, is based on the hypothesis that the swollen cellulose contains a permanent network of interconnected water filled channels or pores through which mass transport can occur. Since the 1930s, pore models have been used to explain the dyeing behavior of textile materials, the modelling of size exclusion chromatography and supported catalysts and the permselective behavior of

membranes.

The *free volume* or *segment mobility model* describes the transport of solutes through the amorphous parts of the cellulose. The rate of diffusion is determined by the mobility of the polymer chain segments. The free volume interpretation of diffusion data has been been presented by several authors from the late 1950s [14-16]. Rosenbaum [17] used the free volume approach to explain the transport of dyes in polyacrylonitrile fibers. Yasuda *et al.* [18-20] extended the theory to water swollen gel systems.

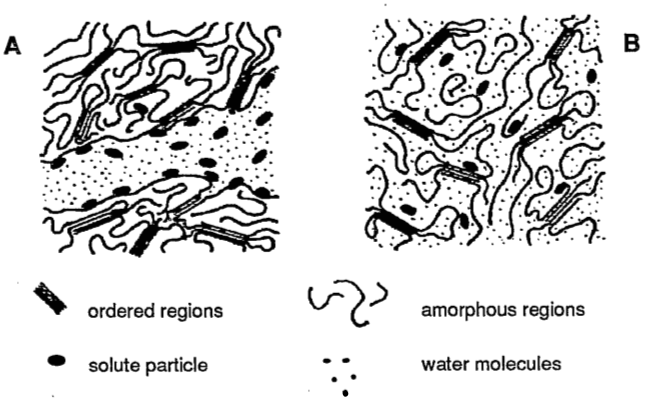

Figure 3 *The two models used to explain the transport of solutes through cellulosic materials, a: pore model; b: free volume or segment mobility model, after Rohner and Zollinger [21].*

The main difference between the pore model and the free volume approach lies in the physical meaning of the pores [12]. In the pore model, more-or-less fixed pores are assumed, and the principles that apply to macroscopic phenomena, such as Poiseuille's law, are also assumed to hold for the sub-microscopic and molecular level. The 'pores' considered in the free volume membrane concept are fixed neither in size nor in location. In this concept the term pore might be misleading, deGennes [22] used the term 'macro-molecular mesh'. As a consequence of the plasticizing effect of water, the hydrated, more-or-less free sections in the amorphous regions of the macromolecules exhibit a fair degree of mobility so that size and shape of the solvent-filled holes may continuously change. The geometry of the polymer network sets the upper limit for the size of such pores and hence also for the size of the permeant molecule that can pass. The rate of diffusion is governed by the probability that the permeant molecule finds a sufficiently large hole at its location. The pores considered in this concept may be described as the 'free volume' since the total amount of such holes per volume unit of membrane phase represents the free volume accessible to the transport of permeants. Yasuda *et al.* [12] pointed out that in

the free volume concept the 'non-porous' membrane can be permeable to many permeants whereas according to the pore model the same membrane would be impermeable by definition to permeants above a certain size.

2.2.2 Transport equations

Starting point for many studies on mass transport through membranes are the phenomenological transport equations, derived by Kedem and Katchalsky [23]:

$$J_v = L_p(\Delta p - \sigma\Delta\pi) \quad (1)$$

$$J_s = P_m\Delta c_s + (1-\sigma)J_v\bar{c}_s \quad (2)$$

where J_v is the solvent volume flux, L_p the hydraulic permeability coefficient, Δp the applied pressure difference across the membrane, σ the Staverman reflection coefficient , $\Delta\pi$ the osmotic pressure difference, J_s the solute flux, P_m the diffusive membrane permeability coefficient, Δc_s the concentration difference and $\bar{c}_s$ the average solute concentration in the membrane.

The Kedem and Katchalsky equations treat the membrane as a 'black box'. The membrane characteristics are expressed by three parameters - the solute permeability coefficient P_m, the solvent permeability coefficient L_p and the Staverman reflection coefficient σ. In the case of a dialysis process the transport is purely diffusive and Eqn. 2 turns into a very simple form:

$$J_s = P_m\Delta c_s \quad (3)$$

The membrane parameter of interest for a diffusion or dialysis process is the diffusive membrane permeability coefficient P_m.

2.2.3 Pore model

Before the analysis of Kedem and Katchalsky was presented, the basic pore model had been developed by several authors. Already in 1936 Ferry [24] derived simple equations showing that the sieve constant for a certain solute increases gradually (and not by a step function) from 0 to 1 as the pore size is progressively increased.

For diffusion through pores, the diffusion coefficient refers to solute diffusion through the solvent filled pores. If the pores are large compared with the solutes the only effect of the presence of the membrane is a reduction of the area through which diffusion can occur (porosity). In case the pores do not run

perpendicular to the membrane surface, an additional effect is caused by the prolonged pathway that has to be traversed by the diffusing solutes. The determination of this so-called 'tortuosity' is a complex task, and in practical situations it is often used as a lumping factor. Wolf and Strieder [25] calculated tortuosity factors for a random fiber bed of overlapping cylinders of several radii.

When interaction forces between membrane material and solute are present, a correction has to be made by means of a solubility distribution coefficient K_s. The diffusive membrane permeability coefficient can be written as:

$$P_m = \frac{K_s \varepsilon D}{\tau \Delta x} \qquad (4)$$

where K_s is the solubility distribution coefficient, ε the volume porosity of the membrane, D the free diffusion coefficient of the solute, τ the tortuosity factor and Δx the membrane thickness.

Eqn. 4 holds as long as the pores are large compared with the permeating solute. In the case that both sizes are in the same order of magnitude the diffusion is hindered because of two reasons.

First, because of steric hindrance, the equilibrium partitioning of the solute in the pore is affected. The distribution coefficient K is defined as the ratio of the mean concentration inside the pores divided by the bulk solution concentration at equilibrium. Because the center of a molecule can not approach the pore wall closer than its radius, the fraction accessible pore volume is smaller than 1. The partitioning of rigid molecules in inert porous networks was described by Giddings *et al.* [26] among others. Using the theory of statistical mechanics they derived relations for the partitioning of solutes of different geometry, in pores of different geometry and for different pore size distributions. The partitioning of random-flight macromolecules in pores of various shapes was analyzed by Casassa *et al.* [27-29]. Their theory is based on the calculation of changes in entropy of a macromolecule as it leaves the mobile phase (solution) to enter the sorbent pores. Recently the effect of long and short range interactions on the partitioning of macromolecules in pores was described by Deen *et al.* [30,31].

The second effect of the presence of the pore is a reduction of the mobility of the solute, which is due to an enhanced hydrodynamic drag. The mobility of a molecule depends on the position within the pore cross section, the diffusion coefficient is determined by averaging the mobility over the cross section. The oldest calculations, for rigid metal balls in tubes, were done by Faxén in 1923 already [32]. Pappenheimer *et al.* [33] considered a spherical molecule in a pore of circular cross section. Instead of averaging the mobility over the pore

cross section, they substituted its value at the pore centerline. This centerline approximation is known as the Renkin equation [34]. The results were incorporated into the 'capillary pore model' by Haberman and Sayre [35] and Verniory [36]. For a rigid non-adsorbing spherical solute diffusing through a cylindrical pore, the diffusive membrane permeability coefficient is given by:

$$P_m = \frac{\varepsilon f(q) K(q) D}{\tau^2 \Delta x} \tag{5}$$

With:

$$f(q) = \frac{1-2.105q+2.087q^3-1.707q^5+0.726q^6}{1-0.759q^5} \tag{6}$$

$$K(q) = (1-q)^2 \tag{7}$$

$$q = \frac{r}{R_p} \tag{8}$$

where P_m is the diffusive membrane permeability coefficient, ε the volume porosity of the membrane, D the free diffusion coefficient of the solute, τ the tortuosity factor, Δx the membrane thickness, r the radius of the solute and R_p the pore radius. Note that for the cylindrical pore geometry the squared tortuosity is introduced in the formulae (the surface porosity is the ratio of the volume porosity and the tortuosity).

The factor f(q) of Eqn. 6 is the drag or wall correction factor as derived by Pappenheimer *et al.* [33] and Renkin [34]. The factor K(q) was derived by Giddings *et al.* [26]. Several alternative relations for rigid spherical solutes in cylindrical pores have been proposed by other authors, an overview of these is given by Deen [37]. Also some relations have been proposed for different solute and pore geometries. In Figure 4, the hydrodynamic correction functions of Eqns. 6 and 7 are shown. In general, a rather strong dependence of the hindrance factors on the ratio q is predicted. For example, for a solute whose radius is only one-tenth of that of the pore, the macroscopically observable diffusivity is already some 40% below the bulk solution value.

More recently, attempts are made to derive transport equations for the transport of flexible macromolecules through porous supports. For completeness we refer to the work of Deen *et al.* [38,39] and Anderson *et al.* [40].

For the cylindrical pore model the solvent permeability coefficient is given by a relation based on the Hagen-Poiseuille equation assuming a bundle of parallel cylindrical pores:

$$L_p = \frac{\varepsilon R_p^2}{8\eta\tau^2\Delta x} \qquad (9)$$

where η is the dynamic viscosity of the solvent.

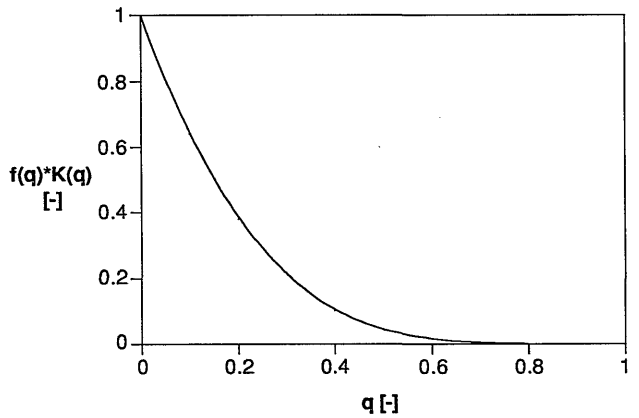

Figure 4 *Dependence of hydrodynamic correction functions on q for non-interacting rigid spheres in cylindrical pores.*

2.2.4 Free volume model

The free volume approach for the transport through polymers was developed by several authors starting from the 1950s [14-16]. Yasuda *et al.* [18-20] used the free volume theory to study the transport through water swollen cellulose membranes. Reinhart and Peppas [41] extended the theory to include the effects of cross-linking.

The basis for the free volume theory is that the homogeneously swollen polymer consists of a volume fraction ε of water (solvent) and a fraction $(1-\varepsilon)$ of polymer. The polymer is impermeable to the solute so that diffusion may only proceed through the water phase. Hence, the free volume of the system available for permeation is approximately equal to the volume fraction of water. The solute can diffuse through the membrane if it finds a succession of holes larger than the solute size. A general expression for the diffusion coefficient is given by Eyring's rate theory:

$$D = \nu.\exp\left(\frac{-\Delta G}{kT}\right) = \nu.\exp\left(\frac{\Delta S}{k}\right)\exp\left(\frac{-\Delta H}{kT}\right) \qquad (10)$$

where ν is the translational oscillating frequency of the solute, ΔG, ΔS and ΔH are the free energy, entropy and enthalpy of activation for diffusion, k is the Boltzmann constant and T the absolute temperature.

Yasuda *et al.* [20] assumed that the polymer is sufficiently swollen so that the enthalpic contribution to the diffusion coefficient is the same for the diffusion of the solute in the swollen polymer as for its diffusion in pure solvent. It was also assumed that the average jump distance for the molecule is the same in both media. The entropy term contains two major contributions: (1) the conformational probability of formation of a hole sufficiently large for the passage of the diffusing molecule, $\exp(-V^*/V_f)=\exp(-Bq_2/V_f)$ and (2) the probability $\varphi(q_2)$ of finding that space in the swollen medium. In these expressions, V_f is the total free volume in the membrane, V^* a characteristic volume parameter, q_2 the effective cross section of the permeant, and B a proportionality factor. The free volume of the system is approximately equal to the volume fraction of water. The reduction in diffusion coefficient is given by:

$$\frac{D_{eff}}{D} = \varphi(q_2).\exp\left[\frac{Bq_2}{V_f}\left(\frac{1}{\varepsilon}-1\right)\right] \qquad (11)$$

where D_{eff} is the effective diffusion coefficient in the membrane.

If the solute molecule is sufficiently small, it can be assumed that there is no sieving effect, i.e. $\varphi(q_2)=1$. In that case a plot of $\ln(D_{eff}/D)$ versus $1/\varepsilon$ or q_2 should yield a straight line. Yasuda *et al.* [20] indeed found a straight line behavior for several membranes including a swollen cellulose film. Using data of Colton [42] they found for a swollen cuprophan membrane that the sieving effect was not significant for molecules up to the size of albumin (M=66,000 g.mole^{-1}). The results of Yasuda *et al.* are replotted in Figure 5. The theoretical effect of sieving was shown by Yasuda *et al.* by using several differential hole distribution functions.

The diffusive membrane permeability coefficient is given by:

$$P_m = \frac{KD\varepsilon}{\tau\Delta x}\varphi(q_2).\exp\left[\frac{-Bq_2}{V_f}\left(\frac{1}{\varepsilon}-1\right)\right] \qquad (12)$$

Peppas and Reinhart [43] and Meadows and Peppas [44] described the sieving mechanism in terms of the network mesh size ξ. They postulated that the sieving probability is proportional to the volume fraction of mesh sizes larger than a certain critical mesh size.

Later Vrentas and Duda *et al.* gave, in a series of papers, a more exact treatment of the free volume theory. The highlights of their analysis were presented by Peppas and Lustig [45].

Based on scaling laws derived by deGennes, Lustig and Peppas [46,47] developed a relation for the reduction in diffusion coefficient. The relation was shown to give excellent agreement with measured data for swollen polymers with polymer volume fractions between 0.05 and 0.74.

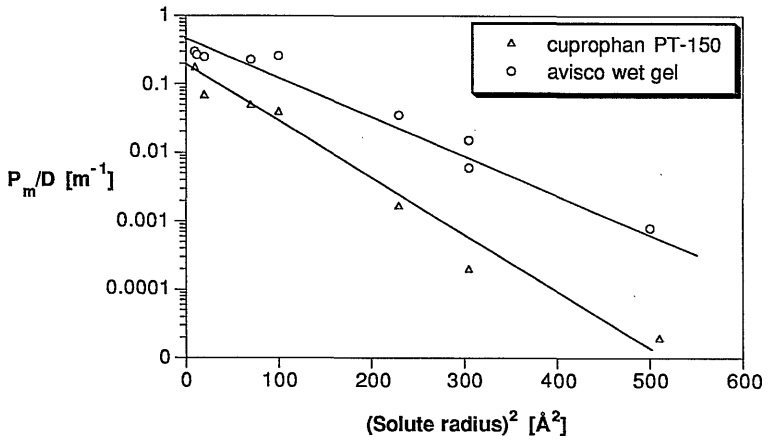

Figure 5 *Plot of P_m / D for gel cellophane and cuprophan, replotted from Yasuda et al. [20].*

2.2.5 Discrimination between pore and free volume model

According to Hori and Zollinger [48] there has been a considerable amount of discussion in the scientific literature regarding which model corresponds better to reality. Nevertheless, none of the papers were dealing with a differentiation between the two models by experiments that falsify one mechanism and at the same time not falsify the other mechanism. Hori and Zollinger [48] and Rohner and Zollinger [21] tried to make such a comparison for different membranes. Their main conclusion was that no membrane could be described completely by either one of these models. Both mechanisms of transport seem to occur simultaneously, the extent of contribution of the mechanisms is dependent upon the type of membrane. For cellulosic materials they concluded that diffusion is governed to a large extent, though not exclusively, by pore diffusion. According to Peppas and Lustig [45], the free volume theory is successful in systems which are sufficiently concentrated to permit significant contact between effective chains.

2.3 Characterization of cellulosic hemodialysis membranes

2.3.1 Characterization of porous membranes

As pointed out in Chapter 1, the performance of an artificial kidney is not a simple function of the permeability of the membrane. Figure 6 shows the complexity of the model input factors relating membrane structure and artificial kidney performance. Even the condition of the dialysis patient is known to have impact on the final result. It is obvious that the prediction of the artificial kidney performance, 'simply' from the structure of the membrane, is a very difficult job.

Reading this, one could draw the pessimistic conclusion that the processes are too complex to follow a fundamental approach. On the other hand, however, many of the disturbing factors such as fouling and boundary layers are caused just by the existence of the membrane wall, and therefore by its characteristic structure. Detailed knowledge on membrane structure parameters and their relation to the production process can help the manufacturer to choose optimal production conditions. So the characterization of the porous structure of the membrane provides a good starting point in order to understand the relation between membrane structure and performance.

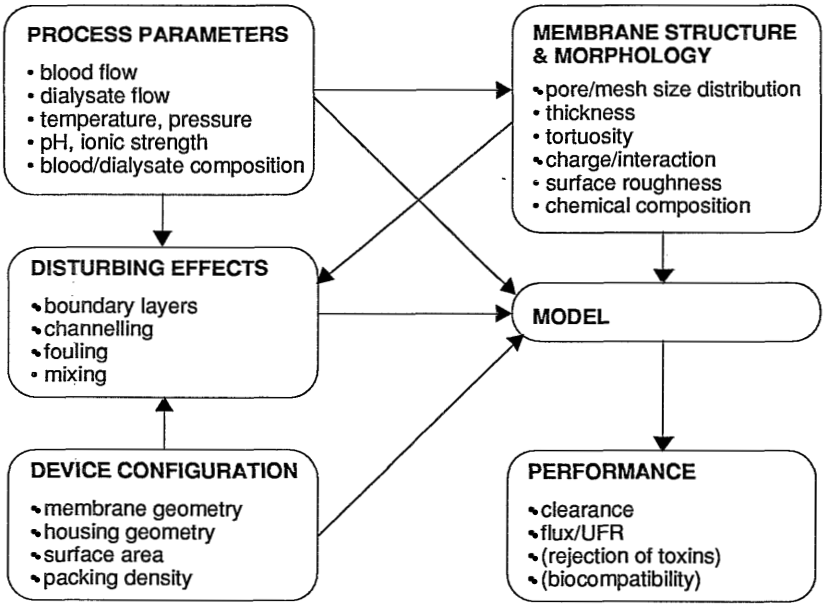

Figure 6 *Complexity of the model input factors relating membrane structure and artificial kidney performance.*

In principle, two different pathways can be followed depending on the final aim of the characterization. The first is to try to obtain a detailed knowledge of the membrane structure and to predict from that the experimental performance. The second possibility is to search for those structure parameters which give the best fit with the experimental performance observations. The first pathway is the most fundamental one. The latter is probably the easiest one, but in many cases, the derived structure parameters will not necessarily correspond with the real properties. For cellulosic membranes, for which it is not even clear whether the holes present are real pores or not, it is obvious that following this pathway may lead to results which have not too much physical meaning.

Two types of characteristic parameters can be defined: *performance related parameters* such as diffusive permeability or retention and *morphology related parameters* such as pore shape and size and (surface) porosity [49]. The development of consistent theories on membrane structure and performance needs the linkage between both types of parameters by a model. For the ideal model, describing reality, the performance related and the morphology related parameters will be consistent with each other. As long as the model is not perfect there will very probably be a discrepancy between the two classes of parameters and one should be aware of that.

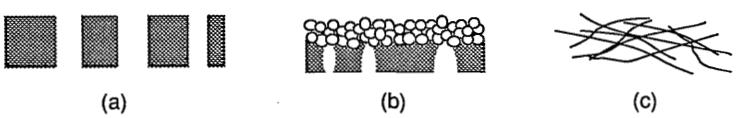

Figure 7 *Different pore morphologies found in porous membranes, a: cylindrical; b: nodular structure in top layer of UF membranes; c: 'random' fiber orientation.*

Figure 7 shows some typical pore geometries found in porous membranes. The pores in swollen cellulosic dialysis membranes have the closest resemblance to the type of morphology shown in 7c. A fundamental problem of membrane characterization is that for a quantitative evaluation, all the available characterization techniques force the investigator to make an assumption about the pore geometry. Generally, the exact pore geometry of a membrane is not known and for practical reasons simplified pore geometries, e.g. the cylindrical pore geometry are assumed. In nearly all cases the models chosen are gross simplifications of the real system, and the parameters obtained are strictly related to the model and/or method chosen. Besides, it is not the average pore size of a certain pore which is the determining factor for permeation but its smallest constriction [49].

The International Union of Pure and Applied Chemistry (IUPAC) adopted the following classification for the sizes of pores [50]:

- macro-porous >50 nm
- meso-porous 2 nm<pore size<50 nm
- micro-porous <2 nm

For the classification of hydrogel membranes Peppas and Lustig [46] suggested a somewhat different classification:

- macro-porous >20 nm
- micro-porous 5 nm<pore size<20 nm
- non-porous mesh size <5 nm

Apart from the confusing use of the indications macro- and micro-porous, also these classifications illustrate the rather vague transition from porous to non-porous. The IUPAC micropores are supposed to be non-porous according to the definition of Peppas and Lustig. We have chosen to stick to the classification adopted by the IUPAC.

As mentioned before, the most fundamental approach to elucidate the relation between membrane structure and performance would be to characterize the structure and to predict from that the performance. Unfortunately, only a few membrane characterization techniques do not incorporate some kind of mass transport measurement. As a consequence, in many cases the determined structure parameters are somehow performance related.

Stimulated by the development of modern computers, several recent attempts have been made to simulate membrane structures by computer calculations. Stochastical simulations by Arnold and Davies [51] of the structure of macro-porous stretched poly(tetrafluoroethylene) resulted in representations of the membrane morphology having a very close resemblance with scanning electron microscopy micrographs. Comparable results were described by Lim *et al.* [52] for macro-porous ceramic membranes. MacDonald [53] simulated the diffusion of macromolecules through porous media by means of a two-dimensional computer model.

When the mechanism of separation shifts to a molecular level the simulations should be at a correspondingly more refined scale. Smit *et al.* [54] and Wessling [55] used molecular dynamics to simulate the structure of dense polymeric membranes used for gas separation. Smit used the simulated membrane structure to explain the permeation behavior of CO_2 in a polyimide. Wessling found for the polymers poly(ethylene terephthalate) and poly(ethylene isophthalate) a reasonable correlation between the simulations and experimental X-ray scattering data.

All the simulations have in common that a lot of computer time has to be invested before any results can be obtained. At the present stage, the calculation time still forms the bottle-neck. Because the supra-molecular structure of

(swollen) cellulose is, due to its semi-crystalline character, even more complex we refrained from following this approach.

By far the majority of scientific studies have followed the less fundamental approach, i.e. to search for those structure parameters which give the best fit with the experimental performance observations. Most of the work has been concentrated on the determination of a pore size (distribution) from mass transport measurements; the most well-known example is the determination of a pore size from the rejection of the membrane. A pore size (distribution) can be deduced from performance data by using the following equation:

$$Z = \frac{1}{V_p}\int_0^\infty W(r).f_v(r)\,dr \qquad (13)$$

where Z is the observed phenomenological coefficient, V_p the pore volume of the membrane, W(r) a model dependent weighing factor and $f_v(r)$ the pore volume distribution function.

Eqn. 13 is a so-called 'Fredholm equation of the first kind' which is known to represent an *ill-posed mathematical problem* [56,57]. For all practical purposes, this implies that minor errors in the initial data will have a considerable effect on the calculated results. Furthermore, it was shown by Gorbunov [57] and Wendt *et al.* [58] that the solute flux and the equilibrium distribution of solutes in pores are only weakly dependent on the type of pore size distribution. Mass transport measurements should therefore not be expected to yield very valuable information on the shape of the pore size distribution curve. Mason *et al.* [59,60] and Leypoldt [56] have extensively reviewed the problem of accounting for the sieving effect when translating retention data into a pore size distribution. All these authors conclude that there is not a single solution to that problem unless some assumption is made about the shape of the pore size distribution curve.

A log-normal distribution function was substituted, for instance, by Michaels [61] and Aimar *et al.* [62] to determine the pore size distribution of ultrafiltration membranes from retention measurements. The same function was used by Gorbunov [57] and Knox and Ritchie [63] to determine the pore size distribution of various supports from inverse size exclusion chromatography data. Several other functions were suggested by various authors, an overview is given by Tam [64]. An interesting development in this field is the growing interest for the possible fractal nature of membranes. Tam *et al.* [65] determined the fractal dimensions of several synthetic membranes. They showed that the pore morphology of these membranes can be well described by fractal theories.

2.3.2 Choice of the characterization method

When searching for suitable characterization methods to characterize cellulosic dialysis membranes one has to take into account the specific features of these membranes. As indicated, the pores in these membranes only develop upon swelling in water. For an appropriate characterization, the membranes therefore have to be examined in the water swollen state. Dry-state characterization methods or methods using other liquids as a swelling agent will give misleading information. Dialysis membranes are typically used to separate low- and high-molecular weight molecules which means that the pore sizes are in the range of a few nanometers. All membranes used in this study are of the hollow fiber type, so a characterization method should be able to deal with this membrane geometry. An advantage of cellulosic dialysis membranes is that these usually do not have a skin- or top-layer, i.e. the porosity is the same throughout the membrane. The separation characteristics are achieved over the complete membrane thickness. In the following section, an overview of available membrane characterization methods for porous membranes is given. The techniques are discussed in terms of their suitability to characterize the hollow fiber cellulosic membranes investigated in this study in the wet state. At the end of this section, Table 2 summarizes the characterization methods discussed.

Scanning Electron Microscopy (SEM)
SEM in combination with a cryo-preparation technique is in principle a wet-state characterization technique. The resolution of the present microscopes however, is probably not good enough to make the pores of swollen cellulosic membranes visible.

Transmission Electron Microscopy (TEM)
Despite its higher resolution, TEM is probably not a suitable method. The sample preparation techniques needed to prepare the water swollen samples makes it very difficult to retain the original water swollen structure. Nevertheless, recently Sheldon [66] reported on TEM studies revealing the fine structure of UF membranes. Sheldon used a special preparation technique involving rapid freezing, deep-etching and replication of the fracture surface to prepare the samples from the water swollen state. One of the membranes investigated was an Amicon YM10 membrane made of regenerated cellulose with a nominal molecular weight cut-off of 10,000 g.mole^{-1}. For this membrane, the separating surface of the regenerated cellulose was composed of closely packed fibers with a diameter of about 5.5 nm. Distinct pores were found between the fibers with diameters in the range between 4-10 nm. The YM10 membrane had a clean water flux of about 30 L.h^{-1}.bar^{-1} which is very well

comparable with the flux of a high-flux hemodialysis membrane. Sheldon pointed out that the replica technique does not often give a true representation of the overall membrane structure because fractures may not create true cross-sections and the replicas themselves are often fragmented.

Atomic Force Microscopy (AFM)

The new AFM technique is in principle suitable for the characterization of structures with a characteristic size of a few nanometers. Water swollen and dry samples can be investigated without further preparation. Recently, several papers were published showing AFM micrographs of dry and water swollen cuprophan and hemophan hemodialysis membranes [67,68]. The pictures revealed remarkable differences in macroscopic morphology between the cuprophan and hemophan samples. However, because of the rough surface morphology of the samples, the authors were not able to reach the magnifications needed to make the pores visible.

Gas adsorption/desorption

The analysis of adsorption and desorption isotherms is one of the most frequently used and well-known characterization techniques for porous solids [69]. It is based on the capillary condensation of vapor in the pores. For the characterization of cellulosic membranes this technique will fail because it is a dry state characterization technique.

Nuclear Magnetic Resonance (NMR)

Recently, Gallegos and Smith [70] and Glaves and Smith [71] reported on a wet-state NMR technique to determine pore sizes. Unfortunately, for pore sizes smaller than 5 nm this technique has to be calibrated with porous materials of well-defined pores and preferably of the same material to get significant data. Because these standards do not exist, the NMR technique is less suitable.

Bubble pressure

The bubble pressure technique is based on the measurement of the pressure necessary to blow air through a water-filled porous material [72]. The physical basis for the bubble pressure technique is given by the Laplace equation:

$$\Delta p = \frac{2\gamma\cos(\theta)}{R_p} \qquad (14)$$

where Δp is the applied pressure difference, γ the interfacial tension, θ the contact angle and R_p the pore radius.

An air bubble will escape from a pore when its radius is equal to that of the pore. This means that the contact angle θ is 0° and $\cos(\theta)=1$. Since the surface tension at the water-air interface is relatively high (72 $mN.m^{-1}$),

relatively high pressures are needed to detect the smallest pores. Assuming a pore radius of 3 nm for the cuprophan membrane, a pressure of 48 MPa is needed to find these pores. Such a pressure will certainly destroy the structure of the hollow fiber membrane. Moreover, the replacement of the water in the pores by air will cause a change in pore morphology.

Liquid displacement

The liquid displacement technique is closely related to the bubble pressure method [73,74]. Instead of air a second liquid immiscible with water and with a lower interfacial tension is used which allows the use of lower pressures. With the system water/isobutanol/methanol (25/15/7 v/v/v) an interfacial tension of 0.35 $mN.m^{-1}$ can be reached. For a pore of 3 nm this means that a pressure of only 0.23 MPa is sufficient. Still this technique is not very useful for the characterization of cellulosic dialysis membranes because of the solvent pairs used. In the system mentioned, the water activity is certainly not high enough to swell the membrane completely (i.e. water has been saturated with the other components).

Mercury porosimetry

Also the mercury porosimetry technique is based on the Laplace equation. Since it is a dry-state characterization method it is not suitable for the characterization of cellulosic hemodialysis membranes. Besides, too high pressures would be needed to fill the pores.

Permporometry

Permporometry is a relatively new technique to measure the active pores of meso-porous membranes [75,49]. The technique is based on the controlled blocking of pores by condensation of a vapor, present as a component of a gas mixture, and the simultaneous measurement of the diffusive gas flux through the open pores of the membrane. Permporometry is a dry-state characterization method and therefore not suitable for the characterization of cellulosic hemodialysis membranes.

Thermoporometry

Thermoporometry also is a relatively new characterization technique to determine the pore size distribution and porosity of meso-porous materials. The method, developed by Brun *et al.* [76], is based on the observation that in a liquid filled porous material the solidification temperature of the liquid is dependent on the size of the pores. The minimal size of a stable crystal (R_c) is inversely proportional to the extent of undercooling. A liquid contained in the pores of a porous material will therefore crystallize (or melt) at the temperature where the pore radius R_p equals R_c. The melting or solidification thermogram

can be monitored in a differential scanning calorimeter (DSC) and translated to a pore size (distribution). Thermoporometry provides equations relating the pore radius R_p and the apparent transition energy W_a with the extent of undercooling ΔT. For cylindrical pores filled with melting ice, Brun *et al.* derived the following equations:

$$R_p = \frac{-32.33}{\Delta T} + 0.68 \qquad [nm] \qquad (15)$$

$$W_a = -0.155\Delta T^2 - 11.39\Delta T - 332 \qquad [J.g^{-1}] \qquad (16)$$

where R_p is the pore radius, W_a the apparent transition energy and ΔT the extent of undercooling $\Delta T = T - T_o$, with T_o the normal phase transition temperature of the liquid (0 °C for water) and T the temperature where the phase transition is actually observed when this liquid is contained in pores.

Thermoporometry is a wet-state characterization method which can therefore be helpful in the characterization of water swollen cellulosic membranes. The parameters obtained are not performance related. As a consequence, all pores including 'dead-end' pores are determined.

Several authors applied thermoporometry to study the pore size distribution of membranes used for blood purification [77,78]. Recently we reported on the effect of different sterilization methods for artificial kidneys on the porosity and pore size distribution of hemophan hemodialysis membranes [79,80].

Though not using the relations derived by Brun *et al.* also other authors determined the pore sizes of regenerated celluloses from the lowering of the melting-point of ice [81,82].

Diffusion measurements

Diffusion measurements can be used to determine the pore size (distribution) of a membrane. Of course the results are transport related and may therefore not have too much physical meaning. An indirect method to characterize the morphology of hemodialysis membranes was proposed by Klein *et al.* [83]. By fitting diffusive solute and pure water permeability data to the capillary pore model presented in equations 5-9 they could obtain values for the surface porosity and an average effective pore radius for several membrane types. The method was extended by Sakai *et al.* [84,85] who introduced the tortuosity factor in the model.

Klein *et al.* pointed out that the method is only valid if the ε/τ^2 term of the Eqns. 5 and 9 are equal which is true if L_p and P_m can be measured for the same solute, i.e. water and/or D_2O/HTO. Sakai *et al.* also used other solute/solvent pairs. Their results were found to be only slightly dependent on

the solutes used. Typical values reported for cuprophan dialysis membranes were an effective pore radius of 2-3 nm, a surface porosity of 32% and a tortuosity factor of 2 [83-86]. The fact that consistent results could be obtained possibly is an indication that cuprophan has a relatively narrow pore size distribution. With a relatively broad pore size distribution, it is difficult to hold the concept of an average or effective pore size because this value must be dependent on the solute or solvent that is permeating. Large molecules can only permeate through the larger pores of the membrane while small molecules can permeate through both the large and the small pores. Small pores do not contribute to the transport of large molecules which means that the effective pore size obtained from permeation experiments must depend on the dimensions of the permeant. Analogous arguments can be given for the porosity and tortuosity factor.

Peeters [87] reported on the use of diffusion experiments with the penetrant system polystyrene/ethylacetate to characterize polyimide ultrafiltration membranes. An advantage of diffusion experiments with polymers is that these are not hindered by the existence of boundary layers because the main resistance against diffusion is caused by the membrane.

Retention measurements

A retention measurement is the most generally applied technique to determine the pore size (distribution) of meso-porous membranes. Also, this technique will only yield performance related structure parameters. Several complications can frustrate the application of the technique. A prominent complication is caused by concentration polarization, i.e. the permeant concentration near the membrane wall is higher than its bulk value. The observed retention coefficients have to be corrected for this phenomenon. For hollow fiber membranes in particular, the correction can be quite complicated. The conditions, i.e. wall and bulk concentration, pressure drop etc. change along the length of the fiber. The observed concentration in the permeate is the result of the different contributions along the length of the fiber.

Klein *et al.* [88] proposed a complex calculation procedure to calculate the true membrane retention of a hollow fiber membrane. Recently, El-Kalay [89] presented a simplified intrinsic rejection coefficient model for capillary hollow fibers. Van den Berg and Smolders [90] showed that only for relatively simple systems the results of concentration polarization models give a reasonable prediction.

An alternative way to circumvent or to diminish the problem of concentration polarization was proposed by Hanemaayer *et al.* [91]. They used a mixture of oligo-saccharides for their retention measurements. Because the oligo-saccharides are relatively small, the disturbance by concentration polarization is diminished. For a low cut-off regenerated cellulose a pore radius of 2.3-3 nm was reported.

The flow-induced deformation of the permeating molecules may cause another complication. Because of this deformation, the molecules will have a characteristic size which is different from its radius of gyration and hard to determine. Several authors reported on the flow induced deformation of polymer molecules [92,93].

The last, but not least, complication can arise when there is a physical interaction (adsorption) between the membrane and the solute. In particular the results obtained with molecules which carry a charge such as proteins should be treated with care.

The calculation of the pore size distribution from corrected retention data basically consists of minimizing the differences between a set of experimental and a set of model calculated data [61,94]. A graphical procedure was proposed by Aimar *et al.* [62].

The complexity of the disturbing processes, especially for the hollow fiber geometry, make retention measurements less suitable as a characterization method.

Inverse size exclusion chromatography (i-SEC)

Size exclusion chromatography is extensively used for analytical purposes to separate molecules on the basis of their size. It is also applied as a standard technique for the determination of the size/molecular weight of molecules. If well-defined tracer molecules are taken instead, the technique can be used to study the morphology of porous materials (i-SEC). Several authors applied the i-SEC technique to study the morphology of cellulosic materials used in the paper and textile industry [95-102].

SEC is based on the principle that, depending on its size, a molecule is more or less able to penetrate into the pores of a porous material. The measured elution volume of a tracer is a function of the distribution coefficient of the tracer in the material:

$$V_e = V_o + K.V_p^t \qquad (17)$$

where V_e is the elution volume of the tracer, V_o the void volume of the column, V_p^t total pore volume of the column and K the distribution coefficient.

For non-adsorbing molecules the distribution coefficient is a function of exclusively the size and shape of the tracer molecule and of the pore size distribution and the shape of the pores of the porous material. By applying equilibrium partitioning models and by using well-defined tracers a pore size distribution can be derived from a set of distribution coefficient data.

I-SEC is a wet-state membrane characterization method and the obtained membrane morphology parameters are performance related. In contrast with retention measurements, i-SEC measurements are not disturbed

by concentration polarization. Also, because the material is cut into small pieces the method is not hampered by the hollow fiber geometry. Care should be taken to avoid adsorption and flow induced deformation of the tracers.

To summarize, Table 2 gives an overview of available characterization techniques for porous membranes and their applicability to characterize cellulosic membranes in the wet state. Because of the specific features of swollen cellulose membranes only a few of the characterization methods may be expected to yield valuable information. In the remaining chapters of this thesis the results of three of these techniques, i.e., thermoporometry, i-SEC and diffusion experiments will be discussed.

Table 2 *Membrane characterization techniques for porous membranes and their applicability to characterize cellulosic hollow-fiber membranes in the wet state.*

Method	wet-state	pore radius	hollow fiber	applicability
Cryo-SEM	+/-	-/+	+	-/+
TEM	-/+	+	+	-/+
AFM	+	-/+	+	-/+
Gas adsorption	-	+	+	-
NMR	+	-	+	-
Bubble point	-	-	+/-	-
Liquid displacement	-/+	-/+	+	-/+
Mercury porosimetry	-	-	+	-
Permporometry	-	+	+	-
Thermoporometry	+	+	+	+
Diffusion measurements	+	+	+	+
Retention/cut-off	+	+	-/+	+/-
Inverse SEC	+	+	+	+

2.4 Symbols

B	proportionality factor [-]
Δc_s	concentration difference solute across the membrane [mole.m^{-3}]
$\bar{c}_s$	average solute concentration [mole.m^{-3}]
D	free diffusion coefficient of the solute [m^2.s^{-1}]
D_{eff}	effective diffusion coefficient of the solute [m^2.s^{-1}]
f(q)	wall correction factor defined by Eqn. 6 [-]
$f_v(q)$	differential pore volume distribution function [m^3.kg^{-1}.nm^{-1}]
ΔG	free energy of activation for diffusion [J.mole^{-1}]
ΔH	enthalpy of activation for diffusion [J.mole^{-1}]
J_v	volume flux [m^3.m^{-2}.s^{-1}]
J_s	solute flux [mole.m^{-2}.s^{-1}]

K	distribution coefficient [-]
K_s	solubility distribution coefficient [-]
$K(q)$	steric hindrance distribution coefficient [-]
k	Boltzmann constant [$J.K^{-1}$]
L_p	hydraulic permeability coefficient [$m^3.m^{-2}.s^{-1}.Pa.^{-1}$]
Δp	pressure difference [Pa]
P_m	diffusive membrane permeability coefficient [$m.s^{-1}$]
q	ratio of solute radius and pore radius [-]
q_2	effective cross section of the permeant [m^2]
R_c	minimal radius of a stable ice crystal [m]
R_p	pore radius [m]
r	solute radius [m]
ΔS	entropy of activation for diffusion [$J.mole^{-1}$]
T	absolute temperature [K]
T_o	normal phase transition temperature [K]
ΔT	freezing point depression [K]
V_e	elution volume of the tracer [m^3]
V_o^t	void volume of the SEC column [m^3]
V_p^t	total pore volume of the SEC column [m^3]
V_f	total free volume in the membrane [$m^3.kg^{-1}$]
V_p	pore volume of the membrane [$m^3.kg^{-1}$]
V^*	characteristic volume parameter [$m^3.kg^{-1}$]
$W(r)$	model dependent weighing factor, units model dependent
W_a	apparent transition energy [$J.kg^{-1}$]
Δx	membrane thickness [m]
Z	observed phenomenological coefficient, units experiment dependent
ε	volume porosity of the membrane [-]
γ	surface tension [$N.m^{-1}$]
η	dynamic viscosity [Pa.s]
ν	translational oscillating frequency of the solute [$m^2.s^{-1}$]
$\Delta\pi$	osmotic pressure difference [Pa]
θ	contact angle [°]
σ	Staverman reflection coefficient [-]
τ	tortuosity factor of the membrane [-]
ξ	network mesh size [m]

2.5 References

[1] E. Ott, H.M. Spurlin, M.W. Grafflin (eds.), *Cellulose and cellulose derivatives. part I*, New York etc., Wiley, 1954

[2] W. Bobeth, *Textile Faserstoffe*, Springer-Verlag, Berlin etc., 1993, p.18

[3] H. Krässig, R.G. Steadman, K. Schliefer, W. Albrecht, *Cellulose*, In: W. Gerhartz et al. (eds.), Ullmann's Encyclopedia of Industrial Chemistry, Weinheim, VCH, 5th edition, vol. A5, 1986, p. 375-418

[4] P.H. Hermans, *Physics and chemistry of cellulose fibers*, New York etc., Elsevier, 1949, p. 83

[5] W. Albrecht, B. Wulfhorst, H. Külter, *Celluloseregeneratfasern*, Chemiefasern/ Textilindustrie, 40/92 (1990) 1041-1057

[6] N.M. Bikales, L. Segal (eds.), *Cellulose and cellulose derivatives. part IV*, New York etc., Wiley, 1971

[7] R.E. Kesting, *Synthetic Polymeric Membranes*, New York etc., McGraw-Hill, 1971
[8] A. Higuchi, J. Komiyama, T. Iijima, *The states of water in gel cellophane membranes*, Polym. Bull., 11 (1984) 203-208
[9] S.W. Kim, J.R. Cardinal, S. Wisniewski, G.M. Zentner, *Solute permeation through hydrogel membranes*, In: S.P. Rowland (ed.), Water in Polymers, Washington, ACS, 1980, p. 347-359
[10] Z. Morita, H. Ishida, H. Shimamoto, *Anion permeability of cellulosic membranes. I Porosity of water-swollen membranes*, J. Membrane Sci., 46 (1989) 283-298
[11] J.W. McBain, S.S. Kistler, *Membranes for high-pressure ultrafiltration*, Trans. Faraday Soc., 26 (1930) 157-162
[12] H. Yasuda, C.E. Lamaze, *Permselectivity of solutes in homogeneous water-swollen polymer membranes*, J. Macromol. Sci. Phys., B5 (1971) 111-134
[13] A.H. Muhr, J.M.V. Blanshard, *Diffusion in gels*, Polymer, 23 (1982) 1012-1026
[14] M.H. Cohen, D. Turnbull, *Molecular transport in liquids and gases*, J. Chem. Phys., 31 (1959) 1164-1169
[15] H. Fujita, A. Kishimoto, K. Matsumoto, *Concentration and temperature dependence of diffusion coefficients for systems of poly(methyl acrylate) and n-alkyl acetates*, Trans. Faraday Soc., 56 (1960) 424-437
[16] J.S. Vrentas, J.L. Duda, *Diffusion in polymer-solvent systems, I. Reexamination of the free-volume theory*, J. Polym. Sci. Polym. Phys., 15 (1977) 403-416
[17] S. Rosenbaum, *Dyeing of polyacrylonitrile fibers: I. Rates of diffusion with malachite green and diffusion model*, J. Appl. Polym. Sci., 7 (1963) 1225-1242
[18] H. Yasuda, C.E. Lamaze, L.D. Ikenberry, *Permeability of solutes through hydrated polymer membranes. Part I Diffusion of sodium chloride*, Makromol. Chem., 118 (1968) 19-35
[19] H. Yasuda, L.D. Ikenberry, C.E. Lamaze, *Permeability of solutes through hydrated polymer membranes. Part II Permeability of water soluble organic solutes*, Makromol. Chem., 125 (1969) 108-118
[20] H. Yasuda, A. Peterlin, C.K. Colton, K.A. Smith, E.W. Merrill, *Permeability of solutes through hydrated polymer membranes. Part III Theoretical background for the selectivity of dialysis membranes*, Makromol. Chem., 126 (1969) 177-186
[21] R.M. Rohner, H. Zollinger, *Porosity versus segment mobility in dye diffusion kinetics - A differential treatment: dying of acrylic fibers*, Textile Res. J., 56 (1986) 1-13
[22] P.G. deGennes, *Scaling concepts in polymer physics*, Ithaca N.Y., Cornell University Press, 1979
[23] O. Kedem, A. Katchalsky, *Thermodynamics analysis of the permeability of biological membranes to non-electrolytes*, Biochim. Biophys. Acta, 27 (1958) 229-246
[24] J.D. Ferry, *Statistical evaluation of sieve constants in ultrafiltration*, J. Gen. Physiol., 20 (1936) 95-104
[25] J.R. Wolf, W. Strieder, *Surface and void tortuosities for a random fiber bed: overlapping, parallel cylinders of several radii*, J. Membrane Sci., 49 (1990) 103-115
[26] J.C. Giddings, E. Kucera, C.P. Russell, M.N. Myers, *Statistical theory for the equilibrium distribution of rigid molecules in inert porous networks. Exclusion chromatography*, J. Phys. Chem., 72 (1968) 4397-4408
[27] E.F. Casassa, *Equilibrium distribution of flexible polymer chains between a macroscopic solution phase and small voids*, J. Polym. Sci.: Polym. Lett., 5 (1967) 773-778
[28] E.F. Casassa, Y. Tagami, *Equilibrium model for gel permeation chromatography of flexible polymer chains*, Macromolecules, 2 (1969) 14-26
[29] E.F. Casassa, *Comments on exclusion of polymer chains from small pores and its relation to gel permeation chromatography*, Macromolecules, 9 (1976) 182-185

[30] M.G. Davidson, W.M. Deen, *Equilibrium partitioning of long-chain polymers between bulk solution and pores in the presence of short-range attractions*, J. Polym. Sci.: Polym. Phys., 28 (1990) 2555-2563

[31] N.P. Lin, W.M. Deen, *Effects of long-range polymer-pore interactions on the partitioning of linear polymers*, Macromolecules, 23 (1990) 2947-2955

[32] H. Faxén, *Die Bewegung einer starren Kugel langs der Achse eines mit zahrer Flussigkeit gefullten Rohres*, Arkiv. Mat. Astron. Fys., 17 (1923) 217

[33] J.R. Pappenheimer, E.M. Renkin, L.M. Borrero, *Filtration, diffusion, and molecular sieving through capillary membranes. The pore theory of capillary permeability*, Am. J. Physiol., 167 (1951) 13-46

[34] E.M. Renkin, *Filtration, diffusion and molecular sieving through porous cellulose membranes*, J. Gen. Physiol., 38 (1954) 225-243

[35] W.L. Haberman, R.M. Sayre, David Taylor Model Basin Report no. 1143, Washington, U.S. Navy Dept., 1958

[36] A. Verniory, R. Du Bois, P. Decoodt, J.P. Gassee, P.P. Lambert, *Measurement of the permeability of biological membranes*, J. Gen. Physiol., 62 (1973) 489-507

[37] W.M. Deen, *Hindered transport of large molecules in liquid-filled pores*, Am. Inst. Chem. Eng. J., 33 (1987) 1409-1425

[38] M.G. Davidson, W.M. Deen, *Hydrodynamic theory for the hindered transport of flexible macromolecules in porous membranes*, J. Membrane Sci., 35 (1988) 167-192

[39] R.J. Phillips, W.M. Deen, J.F. Brady, *Hindered transport in fibrous membranes and gels: effect of solute size and fiber configuration*, J. Colloid Interf. Sci., 139 (1990) 363-373

[40] I. Kathawalla, J.L. Anderson, *Pore size effects on diffusion of polystyrene in dilute solution*, Ind. Eng. Chem. Res., 27 (1988) 866-871

[41] C.T. Reinhart, N.A. Peppas, *Solute diffusion in swollen membranes. Part II Influence of crosslinking on diffusive properties*, J. Membrane Sci., 18 (1984) 227-239

[42] C.K. Colton, K.A. Smith, E.W. Merrill, P.C. Farrell, *Permeability studies with cellulosic membranes*, J. Biomed. Mater. Res., 5 (1971) 459-488

[43] N.A. Peppas, C.T. Reinhart, *Solute diffusion in swollen membranes. Part I A new theory*, J. Membrane Sci., 15 (1983) 275-287

[44] D.L. Meadows, N.A. Peppas, *Solute diffusion in swollen membranes. Part III Non-equilibrium thermodynamics aspects of solute diffusion in polymer network membranes*, Chem. Eng. Commun., 31 (1984) 101-119

[45] N.A. Peppas, S.R. Lustig, *Solute diffusion in hydrophilic network structures*, In: N.A. Peppas (ed.), Hydrogels in medicine and pharmacy. I Fundamentals, Boca Raton (Florida), CRC Press, 1986, p. 57-84

[46] S.R. Lustig, N.A. Peppas, *Scaling concepts in controlled release*, Proc. Symp. Controlled Rel. Bioact. Mater., 11 (1984) 104

[47] S.R. Lustig, N.A. Peppas, *Scaling laws for solute diffusion in equilibrium swollen gels*, Polym. Prepr., 26 (1985) 72-73

[48] T. Hori, H. Zollinger, *The role of water in the dyeing process*, Text. Chem. Colorist, 18 (1986) 19-25

[49] F.P. Cuperus, C.A. Smolders, *Characterization of UF membranes. Membrane characteristics and characterization techniques*, Adv. Coll. Interf. Sci., 34 (1991) 135-173

[50] *IUPAC Reporting Physisorption Data*, Pure Appl. Chem., 57 (1985) 603

[51] S.T. Arnold, G.A. Davies, *A stochastic model to simulate the structure of stretched polymer membranes*, Proceedings 5th World Filtration Congress, Nice, 1990, p. 541-547

[52] J.H.F. Lim, X. Jia, R. Jafferali, G.A. Davies, *Statistical models to describe the structure of porous ceramic membranes*, Sep. Sci. Tech., 28 (1993) 821-854

[53] R.A. MacDonald, *Modelling macromolecular diffusion through a porous medium*, J. Membrane Sci., 68 (1992) 93-106

[54] E. Smit, M.H.V. Mulder, C.A. Smolders, H. Karrenbeld, J. van Eerden, D. Feil, *Modelling of the diffusion of carbon dioxide in polyimide matrices by computer simulation*, J. Membrane Sci., 73 (1992) 247-257

[55] M. Wessling, *Relaxation phenomena in dense gas separation membranes*, PhD Thesis, University of Twente, Enschede, The Netherlands, 1993

[56] J.K. Leypoldt, *Determining pore size distributions of ultrafiltration membranes by solute sieving - Mathematical limitations*, J. Membrane Sci., 31 (1987) 289-305

[57] A.A. Gorbunov, L.Y. Solovyova, V.A. Pasechnik, *Fundamentals of the theory and practice of polymer gel permeation chromatography as a method of chromatographic porosimetry*, J. Chromatography, 448 (1988) 307-332

[58] R.P. Wendt, E.A. Mason, E.H. Bressler, *Effect of heteroporosity on flux equations for membranes*, Biophys. Chem., 4 (1976) 237-247

[59] E.A. Mason, R.P. Wendt, E.H. Bressler, *Similarity relations (dimensional analysis) for membrane transport*, J. Membrane Sci., 6 (1980) 283-298

[60] K.D. Knierim, E.A. Mason, *Heteroporous sieving membranes: rigorous bounds on pore-size distributions and sieving curves*, J. Membrane Sci., 42 (1989) 87-107

[61] A.S. Michaels, *Analysis and prediction of sieving curves for ultrafiltration membranes: a universal correlation?*, Sep. Sci. Technol., 15 (1980) 1305-1322

[62] P. Aimar, M. Meireles, V. Sanchez, *A contribution to the translation of retention curves into pore size distributions for sieving membranes*, J. Membrane Sci., 54 (1990) 321-338

[63] J.H. Knox, H.J. Ritchie, *Determination of pore size distribution curves by size exclusion chromatography*, J. Chromatography, 387 (1987) 65-84

[64] C.M. Tam, A.Y. Tremblay, *Membranes as fractals, implications and consequences*, Desalination, 90 (1993) 77-91

[65] C.M. Tam, T. Matsuura, A.Y. Tremblay, *The fractal nature of membranes*, J. Colloid Interf. Sci., 147 (1991) 206-212

[66] J.M. Sheldon, *The fine structure of ultrafiltration membranes. I. Clean membranes*, J. Membrane Sci., 62 (1991) 75-86

[67] P. Dietz, P.K. Hansma, O. Inacker, H.D. Lehmann, K.H. Herrmann, *Surface pore structures of micro- and ultrafiltration membranes imaged with the atomic force microscope*, J. Membrane Sci., 65 (1992) 101-111

[68] K. Kasper, K.H. Herrmann, P. Dietz, P.K. Hansma, O. Inacker, H.D. Lehmann, *Investigation of dialysis membranes with atomic force microscopy*, Ultramicroscopy, 42-44 (1992) 1181-1188

[69] S.J. Gregg, K.S.W. Sing, *Adsorption, surface area and porosity*, 2nd edition, London etc., Academic Press, 1982

[70] D.P. Gallegos, D.M. Smith, *A NMR technique for the analysis of pore structure: Determination of continuous pore size distributions*, J. Colloid Interf. Sci., 122 (1988) 143-153

[71] C.L. Glaves, D.M. Smith, *Membrane pore structure analysis via NMR spin lattice relaxation experiments*, J. Membrane Sci., 46 (1989) 167-184

[72] H. Bechold, Z. Phys. Chem., 60 (1907) 356

[73] H. Bechold, M. Schlesinger, K. Silbereisen, *Porenweite von Ultrafiltern*, Kolloid-Z., 55 (1931) 172-198

[74] F. Erbe, *Blockierungsphänomene bei Ultrafiltern*, Kolloid-Z., 59 (1932) 195-206

[75] C. Eyraud, M. Betemps, J.F. Quinson, F. Chatelut, M. Brun, B. Rasneur, *Détermination de la répartition des rayons de pores d'un ultrafiltre par: permporométrie gaz-liquide*, Bull. Soc. Chim. France, 7-8 (1984) I-237-244

[76] M. Brun, A. Lallemand, J.F. Quinson, C. Eyraud, *A new method for the*

simultaneous determination of the size and the shape of pores: the thermoporometry, Thermochim. Acta, 21 (1977)-59-88

[77] J. Desbrieres, M. Rinaudo, M. Brun, J.F. Quinson, *Relation entre le taux de retention et la distribution de pores dans une membrane d'ultrafiltration*, J. Chim. Phys., 78 (1981) 187-191

[78] F.P. Cuperus, D. Bargeman, C.A. Smolders, *Critical points in the analysis of membrane pore structures by thermoporometry*, J. Membrane Sci., 66 (1992) 45-53

[79] A.P. Broek, D. Bargeman, E.D. Sprengers, C.A. Smolders, *Characterization of hemophan hemodialysis membranes by thermoporometry*, Int. J. Artificial Organs, 15 (1992) 25-28

[80] A.P. Broek, H.A. Teunis, D. Bargeman, E.D. Sprengers, C.A. Smolders, *Characterization of hollow fiber hemodialysis membranes: pore size distribution and performance*, J. Membrane Sci., 73 (1992) 143-152

[81] T. Tatsuguchi, K. Sakai, *Determination of structure and permeability of drawn hollow fibers dialysis membranes of regenerated cellulose*, In: N.N. Li (ed.), Ext. Abstr. ICOM'90, Chigago, NAMS, 1990, 1238-1239

[82] T. Kobayashi, M. Todoki, M. Kimura, Y. Fujii, T. Takeyama, H. Tanzawa, *Permeability and structure of PMMA stereocomplex hollow fiber membrane for hemodialysis*, In: E. Drioli, M. Nakayaki (eds.), Membranes and membrane processes, New York, Plenum Press, 1986, p. 507-513

[83] E. Klein, F.F. Holland, K. Eberle, *Comparison of experimental and calculated permeability and rejection coefficients for hemodialysis membranes*, J. Membrane Sci., 5 (1979) 173-188

[84] K. Sakai, S. Takesawa, R. Mimura, H. Ohashi, *Structural analysis of hollow fiber dialysis membranes for clinical use*, J. Chem. Eng. Jpn., 20 (1987) 351-356

[85] K. Sakai, H. Chiba, A. Naitoh, *Determination of the pore radius of regenerated cellulose membranes by a dyeing technique*, J. Membrane Sci., 37 (1988) 101-112

[86] R.P. Wendt, E. Klein, E.H. Bressler, F.F. Holland, R.M. Serino, H. Villa, *Sieving properties of hemodialysis membranes*, J. Membrane Sci., 5 (1979) 23-49

[87] M. Peeters, *Karakterisering van ultrafiltratiemembranen*, Master Thesis, University of Twente, Enschede, The Netherlands, 1992

[88] E. Klein, F.F. Holland, K. Eberle, R.P. Wendt, *Ultrafiltration rates and rejection of solutes by cellulosic hollow fibers*, In: A.F. Turbak (ed.), Synthetic membranes: Hyper- and ultrafiltration uses, Washington, ACS, 154 (1981) 75-108

[89] M.A. El-Kalay, *A simplified intrinsic rejection coefficient model for capillary hollow fibers*, J. Membrane Sci., 49 (1990) 241-252

[90] G. van den Berg, C.A. Smolders, *Concentration polarization phenomena during dead-end ultrafiltration of protein mixtures. The influence of solute-solute interactions*, J. Membrane Sci., 47 (1989) 1-24

[91] J.H. Haanemaaijer, T. Robbertsen, Th. van de Boomgaard, C. Olieman, P. Both, D.G. Schmidt, *Characterization of clean and fouled ultrafiltration membrane*, Desalination, 68 (1988) 93-108

[92] Q.T. Nguyen, J. Neel, *Characterization of ultratfiltration membranes. Part IV. Influence of the deformation of macromolecular solutes on the transport through UF-membranes*, J. Membrane Sci., 14 (1983) 111-128

[93] S. Daoudi, F. Brochard, *Flows of flexible polymer solutions in pores*, Macromol., 11 (1978) 751-758

[94] J. Kassotis, J. Schmidt, L.T. Hodgins, H.P. Gregor, *Modelling of the pore size distribution of ultrafiltration membranes*, J. Membrane Sci., 22 (1985) 61-76

[95] J.E. Stone, A.M. Scallan, *Structural model for the cell wall of water swollen pulp fibers*, Cell. Chem. Technol., 2 (1968) 343-358

[96] J.E. Stone, E. Treiber, B. Abrahamson, *Accessibility of regenerated cellulose to solute molecules of a molecular weight of 180 to 2*106*, Tappi, 52 (1969) 108-110

[97] S.P. Rowland, N.R. Bertoniere, *Chemical methods of studying supra-molecular structure*, In: T.P. Nevell, S.H. Zeronian (eds.), Cellulose chemistry and its application, Chichester, Ellis Horwood, 1985, 112-137

[98] L.F. Martin, S.P. Rowland, *Gel permeation properties of decrystallized cotton cellulose*, J. Chromatography, 28 (1967) 139-142

[99] K. Bredereck, E. Bader, U. Schmitt, *Die Bestimmung der Porenstruktur wassergequollener Zellulosefasern*, Textilveredlung, 24 (1989) 142-150

[100] K. Bredereck, A. Blüher, A. Hoffmann-Frey, *Die Bestimmung der Porenstruktur von Cellulosefasern durch Ausschlußmessung*, Das Papier, 44 (1990) 648-656

[101] K. Bredereck, A. Blüher, *Die Ammoniak-Vorbehandlung und ihre Auswirkung auf die Veredlung*, Melliand Textilber., 72 (1991) 446-454

[102] M. Grünwald, E. Burtscher, O. Bobleter, *HPLC determination of the pore distribution and chromatographic properties of cellulose textile materials*, J. Appl. Polym. Sci., 39 (1990) 301-317

3

CHARACTERIZATION OF HEMODIALYSIS MEMBRANES BY DIFFERENTIAL SCANNING CALORIMETRY: THERMOPOROMETRY

3.1 Introduction

States of water in swollen polymers

The structure and performance of cellulosic hemodialysis membranes are strongly dependent on the extent of swelling of the membrane. When a dry membrane is brought into contact with water it swells, the water increases the inter-fibrillar distance of the cellulose fibrils and as a result water-filled pathways or pores are formed. The swollen membrane can be employed to separate high-molecular weight solutes from low-molecular weight solutes in a solution, e.g. proteins from salts. The dry membrane resembles a dense polymeric film which has gas selective properties. Only in the water swollen state, the membranes exhibit the properties that are required for the hemodialysis process. Therefore, for an adequate determination of the pore morphology wet-state characterization techniques have to be applied.

In order to explain the mass transport properties of cellulosic membranes essentially two models have been proposed. The first one, is the pore model which assumes a permanent network of water filled channels, i.e. the pores, through which the solutes can permeate. The second one, the free volume model, considers the swollen membrane as a homogeneous system in which the plasticizing effect of water causes the mobility of polymer chains. On average there will be a certain volume of water filled holes or pores through which transport can occur. The rate of transport is determined by the probability that the permeant finds a sequence of sufficiently large holes.

It is obvious that the role of water in these membranes is a very important one. Since the late 1960s, numerous experimental studies have been executed to elucidate the state of water in swollen (cellulosic) membranes. The state of adsorbed water has been discussed in two-, three- and more state models. The exact origin of the proposed models is in some cases hard to determine, many authors tend to accept the models as being well-established. The interpretation of the experimental data, however, is not always unequivocal. It is considered useful therefore to give a rather extensive overview of the present knowledge about water in polymers. Special attention is paid to the interpretation of the thermograms of water swollen polymers.

Already in the 1940s Magne *et al.* [1] suggested that water swollen cellulose contains a certain amount of 'non-freezing' water. This state of water was considered to originate from (strong) interaction of water with the hydrophilic groups of cellulose molecules. Because of the interaction water does not freeze at temperatures (far) below 0 °C. Many authors adopted this picture of two types of water [2-5]. One type having a strong interaction with the polymer, i.e. the 'non-freezing' or 'bound' water and a second type showing the properties of bulk water, i.e. the 'free' water. The two state model of water has been useful in explaining the perm-selectivity of biological and cellulose acetate reverse osmosis membranes. Schultz *et al.* [6] reported that the non-freezing water in cellulose acetate and in porous glass membranes exists as a salt free ~2.2 nm thick liquid-crystalline hydration sheath lining the interface of the membrane pores. As a result, pores with a radius smaller than this 2.2 nm have good salt retention properties. Sourirajan postulated the existence of a layer of demineralized water already in 1963 [7].

A popular molecular model of liquid water is the 'flickering cluster' model suggested by Frank and Wen [8]. It suggests that water consists of a mixture of clusters of about 50 to 100 water molecules. The stability of a cluster is the result of a resonance effect in the highly hydrogen bonded structure. Schultz and Asunmaa [9] suggested that the adsorption interaction of a cluster with a polar or a hydrogen bonding group at a macromolecular surface will increase this resonance effect, thereby increasing the cluster size and its stability. If the surface density of the hydrogen bonding groups is sufficiently high, these adsorbed clusters will interact with each other, resulting in additional resonance, size and stability until an almost continuous hydration sheath of clusters is formed.

However, Luck *et al.* [10] and Toprak *et al.* [5] showed by means of infrared studies that even near saturation the water sorbed in desalination membranes of different materials has a low degree of association and that the bonds between water and membrane interfaces are considerably weaker than those in liquid water. At high water content, dimers and larger clusters of water molecules appear.

According to Hoeve [11], at first glance little reason seems to exist for water to be strongly bound to polymers because the energy of interaction between water molecules in bulk water is quite large. In order to explain the non-freezing behavior of water Hoeve suggested that in the narrow, fixed polymer interstices, i.e. small pores, space requirements are insufficient to form three-dimensional ice crystals. The cluster/crystal size is imposed by the polymer network. Other options available to the water molecules are to remain in the interstices in liquid form or to form ice outside the polymer as a separate phase. The latter option involves breakage of hydrogen bonds between water molecules and polymer groups. The fixed positions of the polymer chains

prevent formation of hydrogen bonds between the polymer groups, which could provide compensation in the case of (flexible) polymer solutions. Since the energy of hydrogen bond rupture is comparatively high a lower free energy is obtained if liquid-like water remains in the interstices. If at higher water contents, or for more flexible polymer chains, sufficient polymer mobility exists, water diffuses out of the interstices and forms ice as a separate phase. This ice will give rise to a melting peak at 0 °C. The polymer shrinks, internal hydrogen bonds are formed and dehydration occurs without a net loss of hydrogen bonds. The amount of non-freezing water is dependent on the flexibility of the polymer and on the size of its interstitial spaces, rather than on the strength of the bonds that can be formed with water. If so, bound water is an unfortunate term when used to denote non-freezing water.

The ideas of Hoeve are, to some extent, supported by a mechanism proposed by Burghoff and Pusch [12]. They explained the occurrence of a melting peak at 0 °C in the heat capacity-temperature curve of an asymmetric cellulose acetate membrane by a freeze drying effect. At a water content near saturation a part of the frozen water has been *driven out* of the membrane by freeze drying. This water, on the macroscopic surface of the membrane, cannot return into the pores during the gradual heating because it is frozen. Therefore it melts at 0 °C like bulk water and thus creates the corresponding peak in the heat capacity-temperature curves. According to Burghoff and Pusch this water obviously does not represent an independent state of water within the membrane. The appearance of water at the surface of the asymmetric membrane after a calorimetric run was indeed observed by Burghoff and Pusch.

Katayama and Fujiwara [13] analyzed the states of water in cross-linked polyacrylamide gels by nuclear magnetic resonance (NMR) measurements. The amount of non-frozen water at -35 °C increased abruptly when the cross-linking density of the gel exceeded a certain value. Water confined to restrictive geometries is known to supercool deeply and sometimes remains unfrozen [14]. Murase *et al.* [15] suggested that non-frozen water may not necessarily be bound water and that some of the water, compartmentalized in small holes, of gels may also remain unfrozen. Consequently, not only the hydration properties of polymers and the trapping effect of water owing to their interstitial structure but also the compartmentalization effect owing to the network of gels may be important.

A helpful picture is sketched by Chan and Harrison [16]. Water which is miscible with another liquid, e.g. alcohol, is molecularly dispersed and can be categorized as dissolved water. If it is dispersed, but specifically associated with another molecule or ion, then it is frequently described as 'bound water'. Neither of these states will freeze, since freezing is a cooperative function of water aggregates and so the molecular dispersions give rise to nonfreezable states of water. When small amounts of water are adsorbed in a space

restricted environment such as in a polymer it can be expected that hydrogen bonding and aggregation will be affected. Nonetheless, water in polymers is generally perceived to form mobile clusters. If the water molecules aggregate in large enough clusters they will freeze. Very large clusters will exhibit the properties of bulk water, while smaller aggregates may not. Freezable water that can be distinguished from bulk water by a change in some bulk property such as freezing point is often referred to as a cluster or droplet.

The compartimentalization effect may also be the cause for the anomalous crystallization of water during heating of frozen samples as reported by Higuchi *et al.* [17] and by Murase *et al.* [15,18]. Higuchi *et al.* reported the occurrence of an exothermic peak at about -2 °C in the melting thermogram of water swollen cellophane membranes. This exothermic peak was only observed for heating rates of 1.25 °C.min^{-1} or less. The observations were explained by the (re)crystallization of water during the sub-zero melting process. When the heating rate is sufficiently low, there will be enough time for melted ice to recrystallize near the surrounding ice that provides nuclei for the growth of additional ice at temperatures below 0 °C. In the experimental procedure described by Higuchi *et al.* the heating rate was chosen equal to the rate used for cooling of the sample, and hence not chosen independently. Since low cooling rates were used it might also be possible that already during cooling the water freezes at the surface of the membrane.

Murase *et al.* [18] performed differential scanning calorimetry (DSC) measurements with gels having different pore sizes, i.e. the size of the compartments formed by the cross-linked network. They concluded that compartmentalized water crystallizes during heating if the compartment is appropriately small in size. Murase *et al.* [15] investigated three different sephadex® (cross-linked dextran) gels with chromatographic exclusion limits of 1500, 5000 and 150,000 g.mole^{-1} by means of DSC and electron spin resonance (ESR) measurements. The occurrence of an exothermic effect at about -12 °C was most prominent for the gel with the moderate compartment size, with a water content of about 50% and when frozen rapidly. Furthermore they concluded that the extent of the continuity between the adjacent compartments in the gel was an important factor. The ESR measurements confirmed the DSC results. Murase *et al.* explained their observations by changes in the network structure during cooling and heating. The change in network structure during heating enables the diffusion of water molecules and triggers ice formation of non-frozen compartmentalized water. If sufficient continuity between the compartments exists, i.e. at high enough swelling values, the water in some of the compartments can be ice-seeded from the outside and so it will freeze if the cooling is not too fast. In that case the exothermic effect will be less pronounced or even absent.

Belfort and Sinai [19] studied the adsorption of water on various types of

porous glass by means of NMR measurements. They suggested the 'fragmented cluster model', which was claimed to be consistent with the infrared (IR) results of Luck *et al.* [10] for porous glass and Toprak *et al.* [5] for cellulose acetate. According to the fragmented cluster model some minimum coverage of water is necessary for a particular pore size before the first layers of adsorbed water can structure themselves into clusters. At a coverage below this critical value, the adsorbed water molecules or monomers are relatively isolated. Above this minimum coverage less restricted and probably dimers and higher clusters of water enter the pores during adsorption. A minimum amount of water must be adsorbed, however, before bulk-like properties can be established. Belfort and Sinai predicted a minimum pore radius of 1.6 to 2.6 nm for the establishment of water with bulk-like properties. The model proposed is in fact a three-state model, two states of water, i.e. 'hydrate' and 'transition state' water, are formed before water with bulk-like properties can be observed.

Three-state models were also presented by various other authors [20-29]. For instance, Jhon and Andrade [22] suggested that there are at least three kinds of water in hydrogels: 'hydration' water and 'interfacial' water having a certain ordered arrangement and finally 'normal' or 'bulk-like' water. As they indicated, the interfacial water may represent a range of possible interfacial structures depending on the local environment. The authors tried to support their hypothesis by experimental data (IR, NMR, thermal expansion) from several literature sources. We feel, however, that the evidence given was not completely convincing.

Nakamura and Hatakeyama [21] categorized water adsorbed on cellulose samples as one of three kinds: 'free' water, 'freezing bound' water and 'non-freezing bound' water. Free water is defined as the water in polymers whose melting temperature and enthalpy are equal to those of pure water. Bound water is the water restricted by the hydroxyl groups of cellulose, the transition temperature of this water is lower than that of pure water. Non-freezing water is a kind of bound water whose transition is not detected in the first-order transition. The non-freezing water is considered to have a strong interaction with the cellulose molecules. The freezing bound water was later accounted for by Hatakeyama *et al.* [23,24] to reflect the disordered structure of ice which is frozen irregularly due to strong interaction with hydroxyl groups. No experimental evidence, however, was presented for this explanation. According to Hatakeyama [23] more than 8 water molecules are required in order to form a crystalline structure. When the number of water molecules are insufficient to form hexagonal ice crystals, they must form an irregular structure or remain in an amorphous arrangement.

Determination of pore size distribution

Several authors assumed a capillary condensation mechanism to be responsible for the occurrence of a phase transition peak at temperatures below 0 °C (freezing bound or interfacial water). By applying the Kelvin equation they could determine a pore size (distribution) for their porous materials [30-32]. Kobayashi *et al.* [31] determined the pore sizes of polymethylmethacrylate hollow fiber membranes used for blood purification. For a low-flux hemodialysis membrane they reported a pore radius of 2 nm and for a high-flux type a pore radius of 2.9 nm. Recently, Tatsuguchi and Sakai [32] determined the pore sizes of hollow fiber hemodialysis membranes made of regenerated cellulose; pore radii between 2.5 and 3 nm were reported.

Thermoporometry is a characterization technique to determine the pore size (distribution) and porosity of meso-porous materials. The method, developed by Brun *et al.* [33], is based on the calorimetric analysis of the liquid-solid transformation in liquid filled porous materials. It is a wet-state characterization technique which can therefore be helpful in the characterization of water swollen hemodialysis membranes.

Several authors applied the thermoporometry technique to study the pore size distribution of membranes used for blood purification. Desbrieres *et al.* [34] investigated the porous structure of a commercially available AN69 (modified polyacrylonitrile) membrane. Cuperus *et al.* [35] studied a cellulose acetate hollow fiber membrane; a distribution of pores with radii between 3 and 10 nm was reported. In previous work we reported on the effect of steam and ethylene oxide sterilization treatments on the structure of hemophan® hollow fiber membranes [36,37].

From this introduction it will be clear that the literature concerning water in polymers is extensive and that the interpretation of the experimental data is complex. The aim of the present work is to characterize the structure of different water swollen cellulose membranes rather than to study the structure of the water immobilized in it. We are especially interested in studying the feasibility of thermoporometry for the determination of the pore size distributions of these membranes.

3.2 Calculation procedures

In a liquid filled porous material, e.g. a membrane, the solidification temperature of the liquid depends on the curvature of the liquid-solid interface in the pore. The minimal size of a stable crystal (R_c) is inversely proportional to

the degree of undercooling and in the finely porous material the (frozen) liquid therefore crystallizes or melts at the temperature where the pore radius R_p equals the radius of a stable ice crystal R_c. The melting or solidification thermogram can be monitored in a DSC and translated to a pore size or pore size distribution. A schematic representation of the endothermic heat effect measured from the melting of a frozen liquid in a porous medium is shown in Figure 1.

Brun *et al.* [33] derived simple equations relating R_p and the apparent transition heat effect W_a to the melting point depression $\Delta T = T - T_o$, where T_o is the normal phase transition temperature of the liquid (0 °C for water) and T is the temperature where the phase transition is actually observed when this liquid is contained in pores. For cylindrical pores filled with melting ice, i.e. for a heating run, Brun derived the following equations:

$$R_p = \frac{-32.33}{\Delta T} + 0.68 \qquad [nm] \qquad (1)$$

$$W_a = -0.155\Delta T^2 - 11.39\Delta T - 332 \qquad [J.g^{-1}] \qquad (2)$$

where R_p is the pore radius, W_a the apparent transition energy and ΔT the melting point depression. Eqns. 1 and 2 are somewhat different for pores filled with freezing water, i.e. for a cooling run. Brun *et al.* also derived analogous relations for a spherical pore geometry. In the derivation of the equations Brun accounted for the presence of a 0.8 nm thick transition layer of adsorbed water molecules adjacent to the polymer surface which does not freeze or melt. The transition layer was assumed to be independent of the type of porous material.

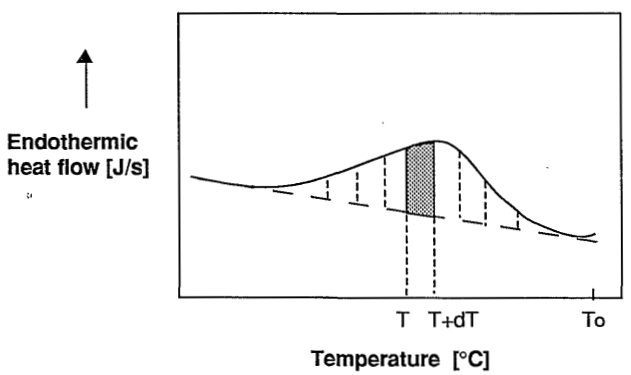

Figure 1 *Schematic representation of the endothermic heat flow from the melting of a frozen liquid in a porous medium as a function of temperature.*

The shaded area under the curve in Figure 1 between T and T+dT represents the transition energy of the melting of ice in pores with corresponding radii in the range between R_p and R_p+dR_p. The temperature interval can be converted to the corresponding temperature interval by means of Eqn. 1. From the transition energy (in Joule) the pore volume of the pores with radii between R_p and R_p+dR_p can be calculated from Eqn. 2.

3.3 Experimental

Materials

For the present studies three different types of hollow-fiber cellulosic hemodialysis membranes were used, i.e. low-flux cuprophan® and hemophan® and high-flux RC-HP400A. The low-flux fibers, with a dry wall thickness of 8 μm, were provided by Organon Teknika, Boxtel, The Netherlands. The high-flux RC-HP400A fibers were provided by Enka, Wuppertal, Germany. The cuprophan and high-flux fibers are made of a regenerated cellulose. The hemophan fibers are made of a regenerated and modified cellulose. In order to improve its biocompatibility the cellulose is modified with a small amount of N,N-di-ethyl-aminoethyl (DEAE) ether groups (degree of substitution 0.01-0.03).

Sample preparation

The fibers were washed with 2-propanol and demineralized water to remove residual substances, i.e. glycerol and isopropyl myristate, from the production process. The effectiveness of the washing procedure was checked by the product control laboratory of Enka in Wuppertal, Germany. No residual substances could be detected. Samples were prepared by cutting the hollow fibers in pieces of about 6 cm. The materials were stored in water containing 200 mg.dm^{-3} formaldehyde to prevent growth of micro organisms.

The samples were wiped with tissues to remove excess water from the fiber wall and lumen as much as possible and then put in a weighed DSC sample capsule. The capsule was immediately closed, weighed and used in the DSC.

For some experiments the water content of the samples was varied by equilibrating the swollen samples with the vapor of different KCl solutions. For that purpose about 20 mg of swollen material was wiped with tissues to remove excess water and put in a weighed DSC sample capsule. Then the samples were equilibrated for two weeks with the vapor of about 20 cm^3 of KCl solution

with one of the following concentrations: 0, 12.5, 25, 50, 75, 100, 150 or 200 $g.dm^{-3}$ KCl. After two weeks the sample capsules were taken from the vapors, closed immediately, weighed and used in the DSC.

Unless stated otherwise, all samples were frozen at maximal speed to a temperature of -40 °C in the DSC apparatus, thermograms were obtained by subsequently heating the sample with a rate of 1 $°C.min^{-1}$ to +10 °C.

After the runs the samples were dried in a vacuum oven at 80 °C till constant weight to determine the dry weight of the samples.

Equipment and data handling

All the experiments were carried out with either a Perkin-Elmer DSC-4 or a Perkin-Elmer DSC-7, both equipped with a data processing unit. The final thermograms (containing 600-1000 data points) were transferred to a spread sheet program for further calculations. Base line correction was performed manually by fitting a second or third order polynomial to the data points between -39 and -30 °C and between +5 and +10 °C. In general no heat evolution was observed at these intervals, otherwise the intervals were adjusted. Peak integration was done numerically using the extended Simpson's rule [38].

Water content of the fibers

The equilibrium swelling water content of the fibers was determined with a centrifuge method based on DIN-53814 [39]. A small centrifuge tube containing a tube provided with a microfiltration membrane in the bottom (Millipore Ultrafree-MC) was filled with pieces of swollen fiber of about 1.5 cm length. The material was centrifuged for 20 minutes at 900 g to remove excess water. The water content of the centrifuged samples was determined from the weight decrease upon drying the fibers overnight in a vacuum oven at 80 °C.

3.4 Results and Discussion

Figure 2 shows a typical thermogram of a water swollen low-flux cellulosic dialysis membrane, two peaks can be distinguished. The apparent jump of the heat flow at -40 °C is caused by a start-up effect. In previous work [36,37] we reported that peak 2 can be explained by the melting of ice which is not present in the pores but in the fiber lumen or adhering to the fiber wall. Because of the experimental procedure that we used to remove excess water from the fiber it appeared reasonable to assume that some water remained in the fiber lumen

giving rise to a melting peak at 0 °C. Peak 1 we explained by the melting of ice in the pores of the membrane. Following this interpretation and using the thermoporometry equations we investigated the effect of ethylene oxide and steam sterilization on the pore size distribution of hollow fiber hemophan membranes. Some of the results are replotted in Figure 3. In particular the applied steam sterilization treatment resulted in a dramatic change of the pore size and porosity of the membranes. A good correlation of the thermoporometry results with the mass transport behavior of the membranes was obtained.

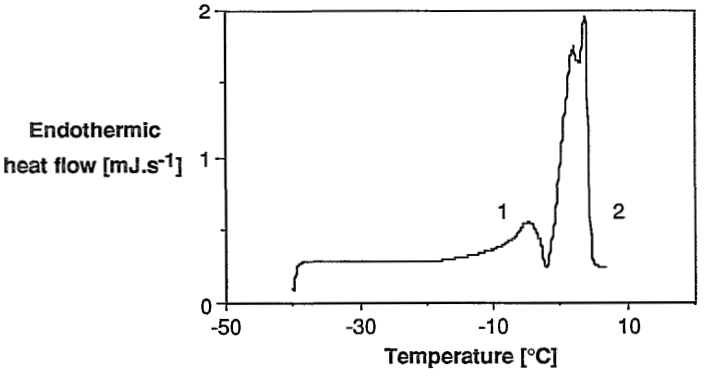

Figure 2 *Typical melting thermogram of a water swollen low-flux cellulosic hollow fiber membrane, 1: pore water; 2: 'adhering water'.*

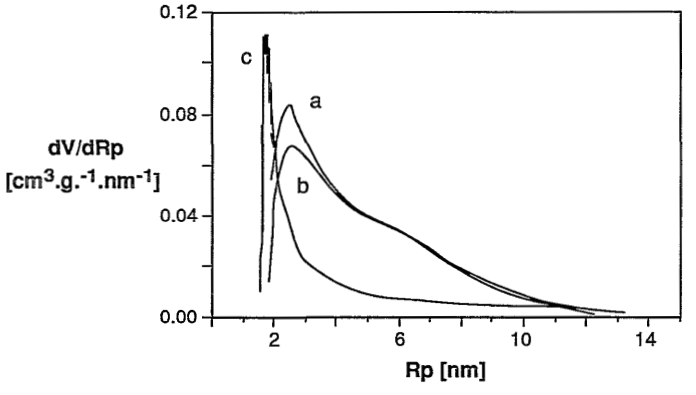

Figure 3 *Differential pore volume distributions of differently sterilized hemophan hollow fiber membranes; a: non-sterilized, b: ethylene oxide sterilized, c: steam sterilized (from Broek et al. [37]).*

As indicated in the introduction to this chapter also different interpretations of the thermograms of water swollen gels are given in literature. Though we

reported a good correlation with the mass transport behavior of the membranes in our interpretation some indistinctness remained as well. We found it therefore necessary to perform a more profound study towards the interpretation of the thermograms. In particular the water content of the samples needed more attention.

For many of the samples investigated we observed a *net exothermic* energy flow at about -2 °C in the melting thermogram. Figure 4 shows three subsequent runs of the same cuprophan sample. The sample was wiped with tissues to remove the excess water before monitoring the thermogram. Only for the first run a (small) net exothermic energy effect is observed. It appears that the position of peak 1 shifts to higher temperatures for the subsequent runs. No changes are observed after the second run.

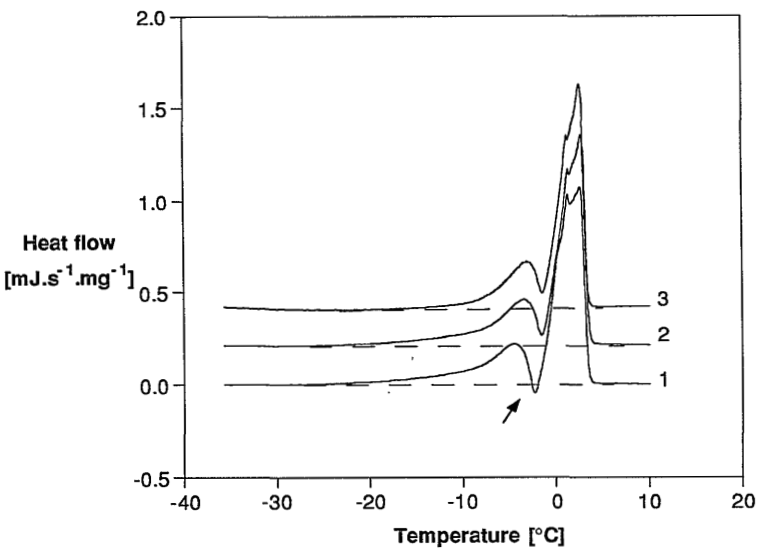

Figure 4 *Stacked curves of three subsequent runs of one cuprophan sample; the sample is cooled in the DSC. Heating rate 1 °C.min-1, water content of the sample 1.38 g.g-1.*

Burghoff and Pusch [12] interpreted the melting peak at 0 °C in the melting thermograms of their cellulose acetate membranes by a freeze drying effect. During the cooling of the samples liquid water is forced out of the fibers by a freeze drying effect so that it freezes at the surface of the membrane. Since this water can not return to the pores during heating, it will melt at a normal temperature of 0 °C. If this explanation holds, a smaller peak at 0 °C is expected when the cooling rate is increased, since this will allow less water migration out of the membrane. Figure 5 shows two subsequent runs of the

same cuprophan sample. The swollen sample was wiped with tissues before putting it into the sample capsules. The sample capsule with the sample was cooled in liquid nitrogen and then transferred to the DSC sample holder which was at a temperature of -40 °C. The second run was monitored after cooling in the DSC. The first run shows again a net exothermic energy effect, peak 1 is broader and smoother compared with the curves shown in Figure 4. Also the exothermic peak is broader. From a comparison of the Figures 4 and 5 no clear difference in the size of the peak at 0 °C is visible. Even when the sample was cooled in nitrogen sludge (mixture of liquid and solid nitrogen) no change in the size of the peak was observed. The observations indicate that a freeze drying effect is not the cause for a melting peak at 0 °C. However, it might be that due to the heat transfer resistance in the sample capsule the effective cooling rate is not high enough.

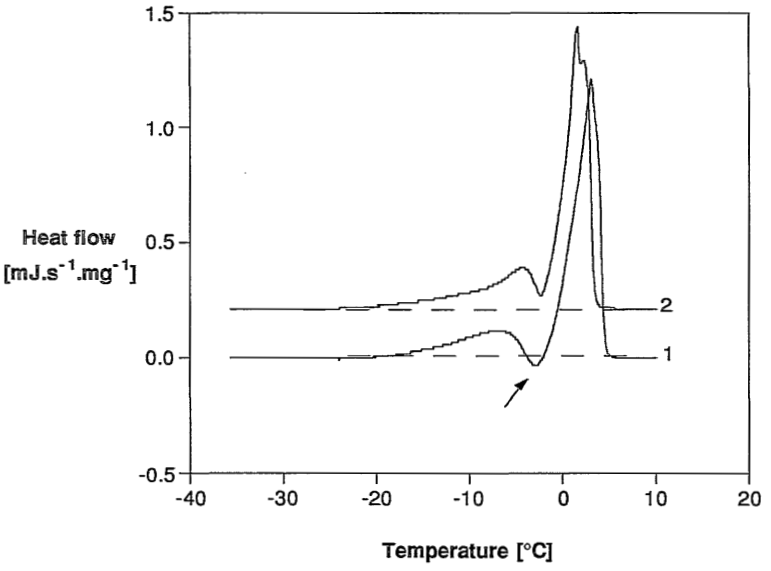

Figure 5 *Stacked curves of two subsequent runs of one cuprophan sample, the sample is cooled in liquid nitrogen for the first run and in the DSC at -40 °C for the second run. Heating rate 1 °C.min-1, water content of the sample 1.41 g.g-1.*

Higuchi *et al.* [17] reported that only for heating rates of 1.25 °C.min-1 or less a net exothermic energy effect could be observed in the melting thermogram of water swollen cellophane. This implies that the occurrence of an exothermic energy effect is influenced by the heat transfer in the sample. It may therefore be expected that also the sample weight is a significant parameter.

Figure 6 shows the effect of sample weight on the thermogram of water swollen cuprophan fibers. The samples were wiped with tissues before freezing. For samples with a dry weight of more than 10 mg a pronounced exothermic peak occurs. For the other samples a net exothermic energy effect does not occur.

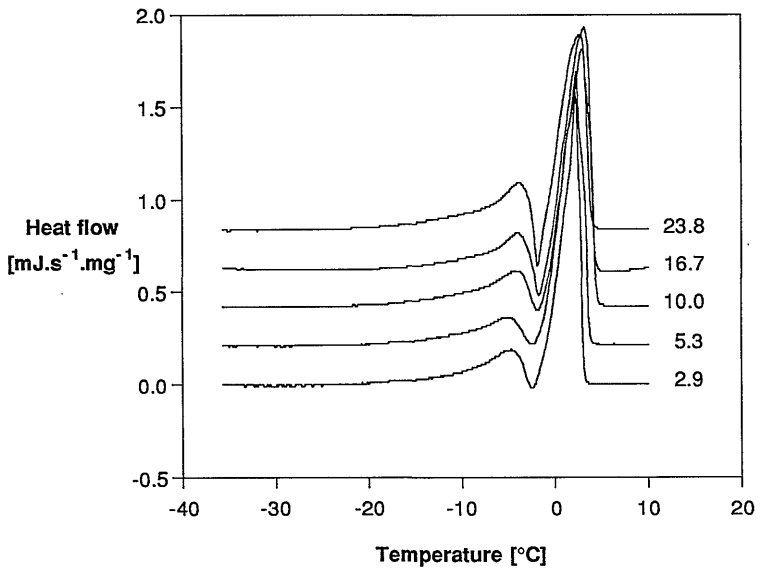

Figure 6 *Effect of dry sample weight on the occurrence of an exothermic heat effect in the thermogram of cuprophan fibers. All runs are first runs, heating rate 1 °C.min-1. Water content of the samples ca. 1.45 g.g-1, dry sample weight 2.9 to 23.8 mg.*

Figure 7 shows the effect of heating rate for cuprophan samples with a (moderate) dry sample weight of about 10 mg. As expected no exothermic peak is observed. The heating rate of 2 °C.min-1 is too high to get a good peak separation between peak 1 and 2.

Figure 8 shows the effect of the heating rate for samples with a high sample weight of about 22 mg. All first runs show a pronounced exothermic energy effect. For curve 2,A the exothermic peak is relatively small, the heating rate of 2 °C.min-1 is too high to get a good peak separation. For the second run with the same sample (curve 2,B) no net exothermic heat flow occurs.

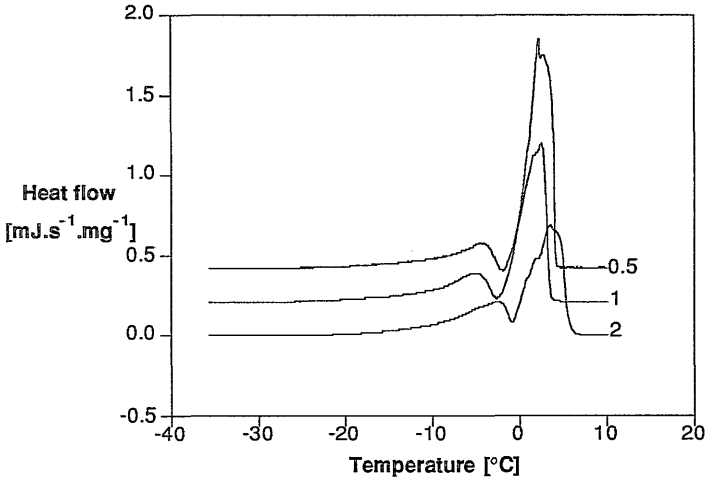

Figure 7 *Effect of the heating rate [°C.min-1] for cuprophan samples with a (moderate) dry sample weight of about 10 mg. All runs are first runs, the numbers indicate the heating rates, the curves are normalized to a heating rate of 1 °C.min-1. Water content of the samples ca. 1.35 g.g-1.*

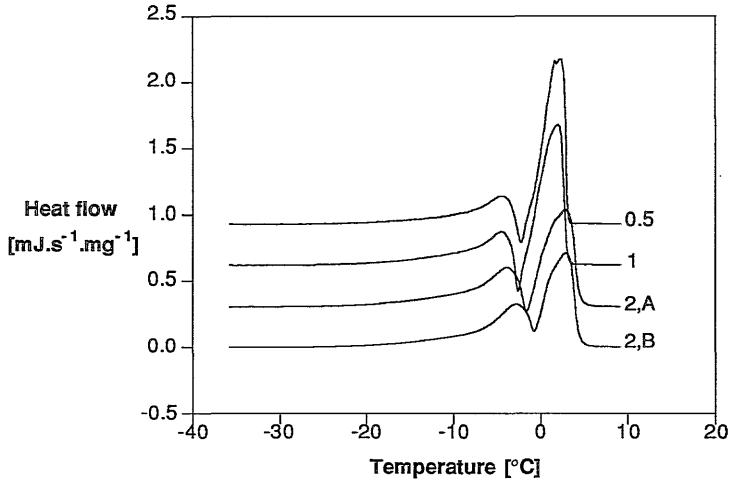

Figure 8 *Effect of the heating rate [°C.min-1] for cuprophan samples with a (high) dry sample weight of about 22 mg. The numbers indicate the heating rates, curve 2,B represents a second run, the curves are normalized to a heating rate of 1 °C.min-1. Water content of the samples ca. 1.42 g.g-1.*

The results presented in the Figures 6-8, indicate that the appearance of the net exothermic heat effect is influenced by the heating rate and by the weight of the sample. This implies that the heat transfer in the sample capsule is an important factor. On the other hand, an exothermic peak is only observed for the first run of each sample, which indicates that the properties of the sample have changed during that first run. Murase *et al.* [15] also found that only for the first DSC run of their sephadex samples an exothermic peak was observed in the melting thermogram. They explained this by changes in the structure of the gels owing to the freezing and melting of the water in the samples. No further explanation was given.

The fact that the appearance of the exothermic peak is influenced by the heating rate is in accordance with the results described by Higuchi *et al.* [17]. At higher heating rates the resolution of the DSC apparatus is not sufficient to make the exothermic peak visible. This could also be an explanation for the fact that this phenomenon is only seldomly reported by other investigators. Most authors apply heating rates of 5 to 10 °C.min^{-1} or even higher.

Higuchi *et al.* [17] and Murase *et al.* [15] did not mention the effect of sample weight on the occurrence of the exothermic peak. The influence of the sample weight shown in the Figures 6-8 can be explained by assuming that the heat transfer in a sample capsule with only a small amount of sample is not sufficient. The main resistance against heat transfer in the sample capsule will be at the interface between capsule wall and sample. The larger the sample, the larger the contact surface between capsule wall and sample will be and only at these contact points the heat can be transported by conduction. At all other places heat has to be transported through a stagnant air layer which may cause a non-equilibrium situation. If the sample weight, and hence the heat capacity of the sample, is too high this will also lead to disbalance of the DSC apparatus.

Murase *et al.* [15] reported that the appearance of an exothermic peak was affected by the water content of their sephadex samples. Figure 9A and 9B show the effect of the water content on the thermogram of the cuprophan fibers. The curves in Figure 9B represent runs of duplicate samples. The duplicate samples were made by equilibrating two different samples in the same vapor. It can be seen that the duplicate samples have comparable water contents. The dashed lines in the figures indicate the positions of the different peak maxima. In Figure 10, these peak maxima are drawn as a function of the water content of the samples.

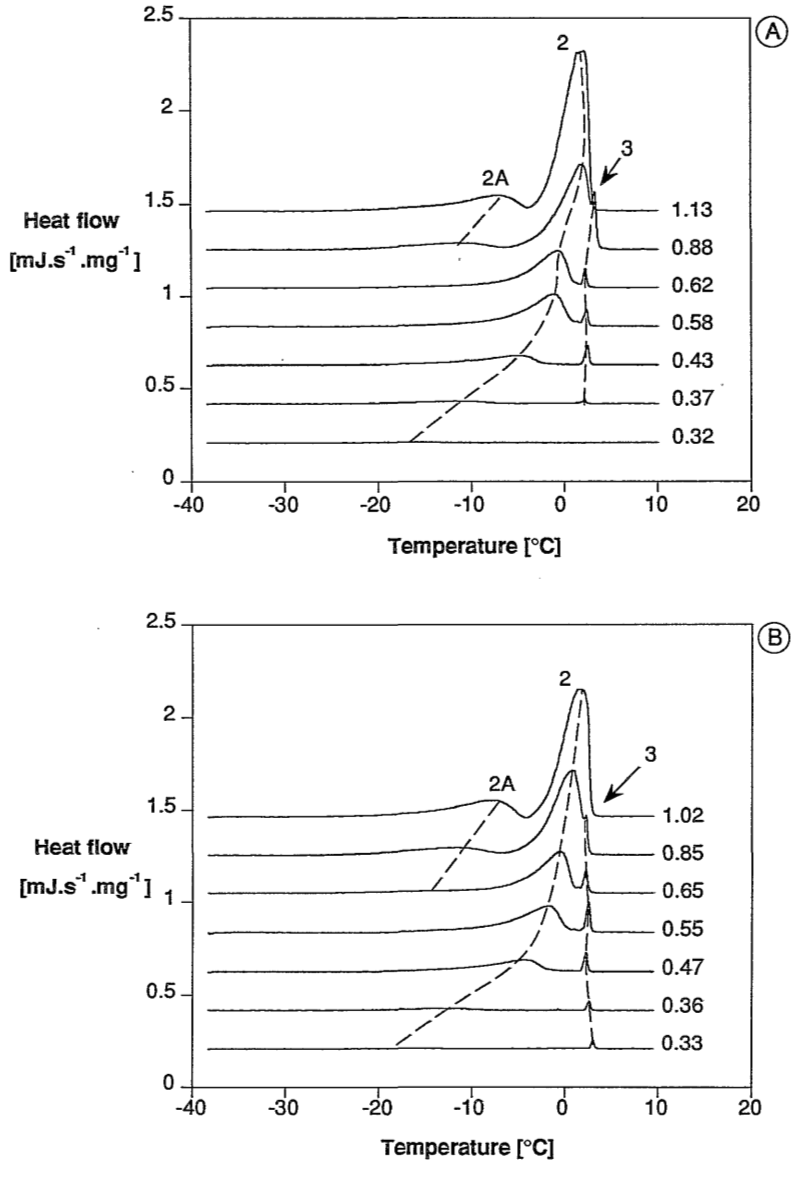

Figure 9A/B *Stacked thermograms of vapor equilibrated cuprophan. All runs are first runs, heating rate 1 °C.min-1, the numbers (1.13, 0.88....) indicate the water content of the samples [g.g-1 dry sample]. The dashed lines indicate the positions of the peak maxima. The curves in Figure 9A and B represent DSC runs of duplicate samples.*

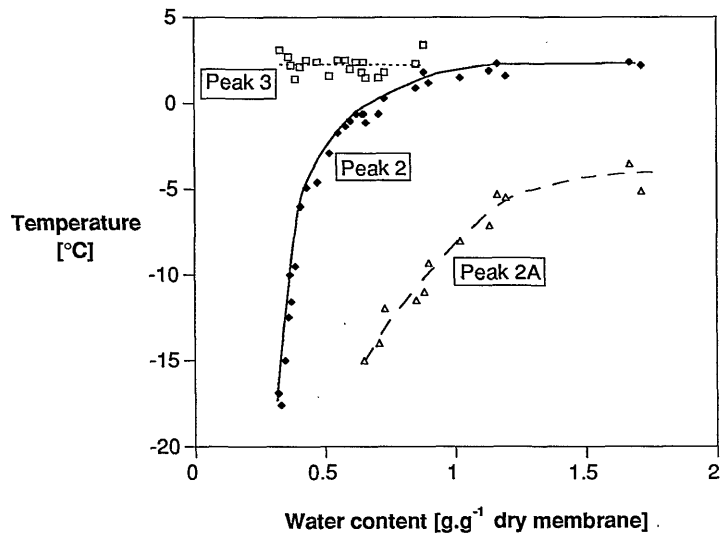

Figure 10 *Positions of the peak maxima in the thermograms of cuprophan shown in Figure 9A/B.*

In the Figures 9A and 9B a sharp peak at about +2 °C (peak 3) is observed at a water content of 0.33 $g.g^{-1}$ and higher. For the sample with a water content of 0.32 $g.g^{-1}$ hardly any energy evolution is observed, hence this value is close to the (lower) limit for the non-freezing water content of the fibers. The position of peak 3 is not dependent on the water content of the samples. For the samples with water contents of more than 1 $g.g^{-1}$ peak 3 is possibly overruled by peak 2. There is no distinct relation between the size of peak 3 and the water content of the sample.

Other authors did not mention the occurrence of a peak like peak 3. The peak might be explained by the melting of ice that has been formed in the lumen of the fiber. This melting process, however, should occur at 0 °C. An apparent shift in melting temperature could be due to either a wrong calibration of the DSC apparatus or to a lack of sufficient heat transfer capacity in the sample capsule. Since the melting temperature of a small amount of pure water was verified to lie at 0 °C the first explanation does not hold. In order to verify the second explanation the following experiment was performed (Figure 11). A normal DSC run was made with a sample showing a clear peak separation between peak 2 and 3. Then a second run was made with the same sample. In this case however, the run was interrupted for 10 minutes at +1 °C to assure equilibrium conditions in the sample. As can be seen from Figure 11 neither the place nor the intensity of peak 3 are changed by this procedure. This indicates that the peak is not due to insufficient heat transfer capacity in

the sample capsule. The equilibrium swelling water content of the fibers was determined with the centrifuge method described in the experimental part. All the samples shown in Figure 9 have a water content which is less than the equilibrium value of 1.48 $g.g^{-1}$. No water is therefore expected at the macroscopic surface of the membrane.

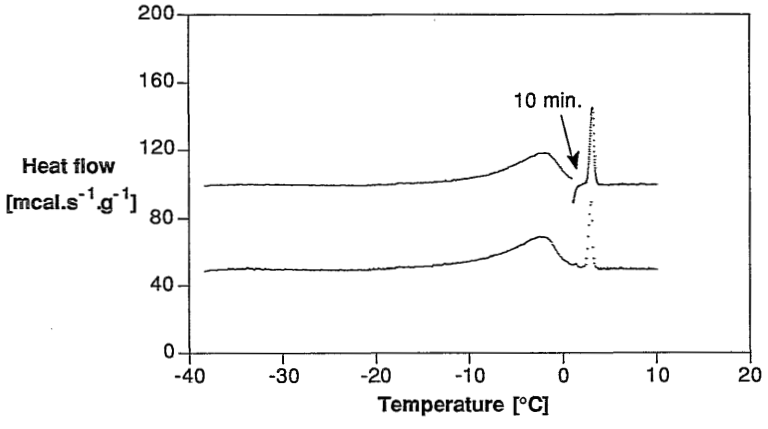

Figure 11 *DSC heating curves for cuprophan containing 0.55 g water/g dry sample; the upper curve was interrupted for 10 minutes at +1 °C to allow equilibrium conditions to be established in the sample. The apparent jump of the heat flow in the upper curve at +1 °C is caused by a start-up effect.*

Other explanations for the occurrence of peak 3 in the thermograms can be a phase transition of a residual substance in the fiber material or a change in the polymer matrix. The samples were analyzed in the laboratory of Enka, Wuppertal: no residues were detected. The concentration of the added formaldehyde in the water swollen samples appears to be too low to be detected and besides no transition is expected for that component at +2 °C.

It might be that the 'drying' of the samples in the vapors causes changes in the structure of the membranes. For instance, the formation of additional domains with a certain ordering which 'melt' at about 2 °C. The domains are formed if the water content is high enough, i.e. above the lower limit for the bound water content. For the validation of this hypothesis additional analytical techniques would be required. Until now we are not able to explain the occurrence of peak 3.

The position of peak 2 in the Figures 9A and 9B is strongly dependent on the water content of the sample. The peak maximum shifts from -18 °C for the

samples with a low water content to an asymptotic value of about 2 °C for the samples with a high water content.

For the samples with a high water content a new peak seems to develop (peak 2A). The maximum of this peak shifts from about -15 °C to -10 °C going from a water content of 0.65 to about 1.2 $g.g^{-1}$. It was this peak that, in our previous work, was interpreted as the pore peak of the thermogram. Other authors used terms as freezing bound water and intermediate water.

It appears from the trends in Figure 9 that peak 2A, which only occurs at high water contents is not caused by the phase transition of a separate water phase. For this reason we named the peak 2A. The apparent peak separation observed between peak 2 and 2A may be the result of an artefact, i.e. the anomalous recrystallization of water.

Figure 12 shows the calculated differential pore volume distributions as a function of the water content of the samples. The curves are calculated from the thermograms shown in Figure 9A using the thermoporometry Eqns. 1 and 2. The integration interval was arbitrarily chosen between -30 and -1 °C. A significant part of the phase transition in the samples with high water content occurs at temperatures above 0 °C. At these temperatures, however, the thermoporometry relations do not have physical significance. According to Eqn. 1 a phase transition temperature of -1 °C corresponds with a pore radius of about 30 nm, -30 °C corresponds with a pore radius of 1.7 nm. Belfort *et al.* [19] and Schultz *et al.* [6] reported a minimal pore radius of 1.6-2.6 and 2.2 nm, respectively, for pores that can contain water with bulk-like properties. The minimum pore radius detected in the cuprophan samples by our measurements is about 2 nm, which is close to the values given by Belfort *et al.* and Schultz *et al.*

The curves shown in Figure 12 reveal a remarkable picture. A dramatic transition is observed between the curves 5 and 6. Going from curve 1 to 5 a gradual increase of the average and maximum pore radius is observed. All curves have their maximum at approximately the same position, the peak height is about 0.015 $cm^3.g.^{-1}.nm^{-1}$. Curve 6 shows a strongly increased pore volume of pores with radii in the range of 2-5 nm. Curve 7 shows the same increased pore volume of small pores but for a somewhat broader pore range (2-7 nm). Both curves have a maximum at a pore radius of about 3 nm. Curves 6 and 7 also reveal a minimum at 6 and 9 nm, respectively. These minima correspond with the peak separation between the peaks 2 and 2A. Curves 4 to 7 all show a comparable pore volume distribution for pores larger than about 18 nm.

The trends shown in Figure 12 may be explained as follows. The curves 1 to 5 of Figure 12 represent a gradual filling of pores in the cuprophan fiber. At a water content somewhere between 0.62 and 0.88 $g.g^{-1}$ the water activity in the sample becomes so high that the water is able to swell the polymer. The water

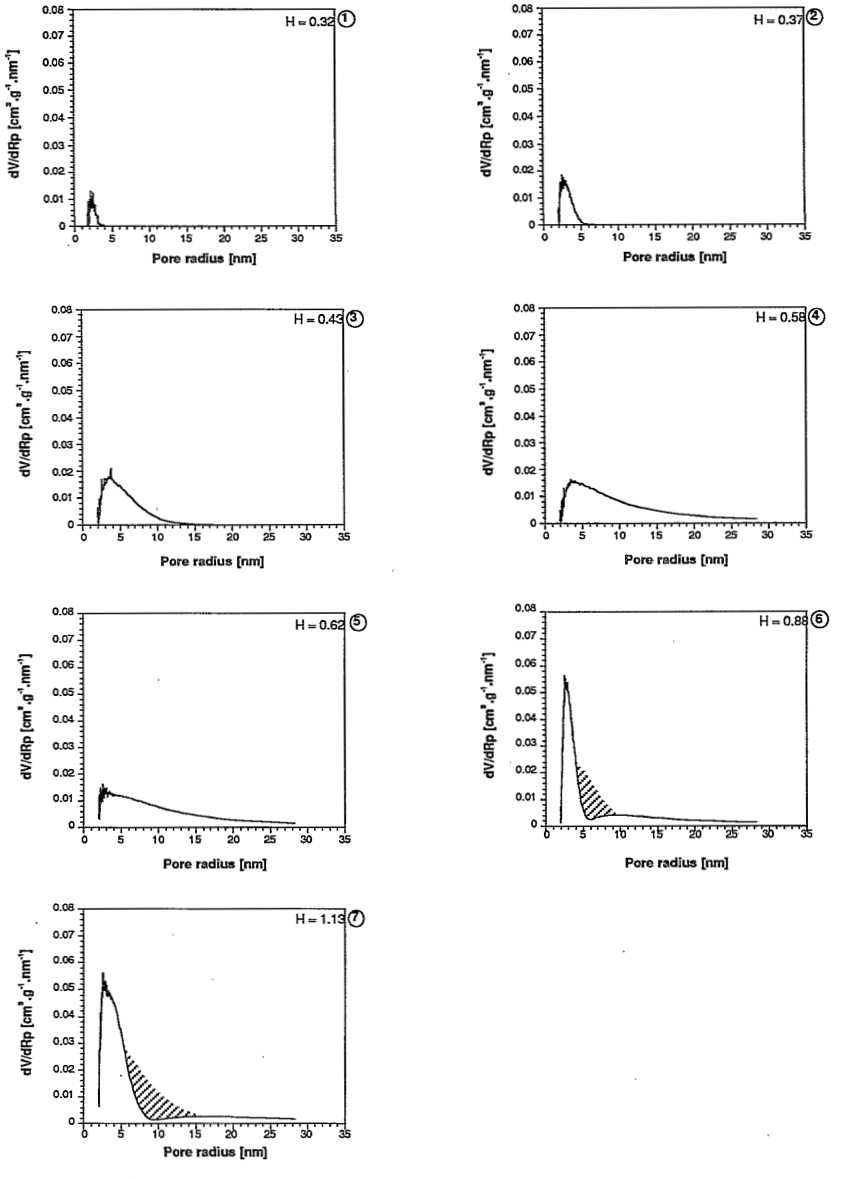

Figure 12 *Differential pore volume distributions of cuprophan calculated from the thermograms of Figure 9A (integration interval -30 to -1 °C). The numbers in the right upper corners indicate the water content of the fibers [g.g-1 dry membrane]. The shaded areas in curves 6 and 7 are caused by the recrystallization phenomena.*

phase is able to disrupt the inter-fibrillar hydrogen bonds of the cuprophan and the inter-fibrillar distance is increased. As a result, many new but small pores are created. The new pores can grow further if the water activity is further increased (curves 6 and 7).

The transition also causes an increased swelling strain in the polymer network. This last point may give a possible explanation for the occurrence of the net exothermic energy evolution in the thermograms. Starting with the melting curve at a temperature of -40 °C all the freezable water in the sample is frozen. By increasing the sample temperature first the water in the smallest pores will melt. In this situation the cuprophan network is strained and only the water in the smallest pores is in the liquid state. The network can relax by allowing the liquid water to move to the larger pores or outside the membrane. There the liquid water will recrystallize because the sample temperature is still below the normal melting-point of water. The recrystallization may give rise to the observed net exothermic energy evolution. The coarsening of the ice crystals may cause changes in the network structure and this could explain why only for the first run of a sample a net exothermic energy effect can be observed.

Peak 2 and 2A in the thermograms are the result of a gradual melting of ice in the pores counter-acted by the recrystallization of melted ice. The apparent peak separation between the peaks is not caused by the existence of two separate types of water but the result of the described recrystallization phenomena. Under certain conditions, this may lead to a temporary net exothermic energy evolution during heating. The exothermic energy effect is only observed between -10 and 0 °C. It might well be, however, that the recrystallization process also takes place at other temperatures. Possibly, this may even lead to a 'massive' melting of water at 0 °C as was suggested by Burghoff and Pusch [12].

The sudden change in membrane morphology at a water content between 0.62 and 0.88 $g.g^{-1}$ may affect the accessible internal polymer surface and thus the amount of non-freezing water in the membrane. Figure 13 shows the amounts of freezing and non-freezing water for all the cuprophan samples investigated as a function of the total water content. The amounts of freezing water were calculated using Eqn. 2 for temperatures below 0 °C and a constant transition energy of 332 $J.g^{-1}$ for temperatures higher than 0 °C. The non-freezing water content was calculated from the difference between the total and the freezing water content. In the Figures 9A and 9B freezing water is observed for water contents of 0.32 $g.g^{-1}$ and more. In Figure 13 the amount of non-freezing water increases from about 0.32 $g.g^{-1}$ to 0.48 $g.g^{-1}$ at the equilibrium water content of 1.48 $g.g^{-1}$. These values correspond with 2.8 and 4.3 water molecules per glucose unit, respectively. The values are not corrected for the crystallinity of the material, the crystalline areas are supposed to be inaccessible to water molecules. As expected the amount of non-freezing water

is dependent on the water content. However, no sudden increase in the non-freezing water content is observed (corresponding with a sudden change in fiber structure). It must be emphasized here that the dependence of the non-freezing water content on the overall water content may also be caused by an artefact which is caused by the recrystallization phenomena.

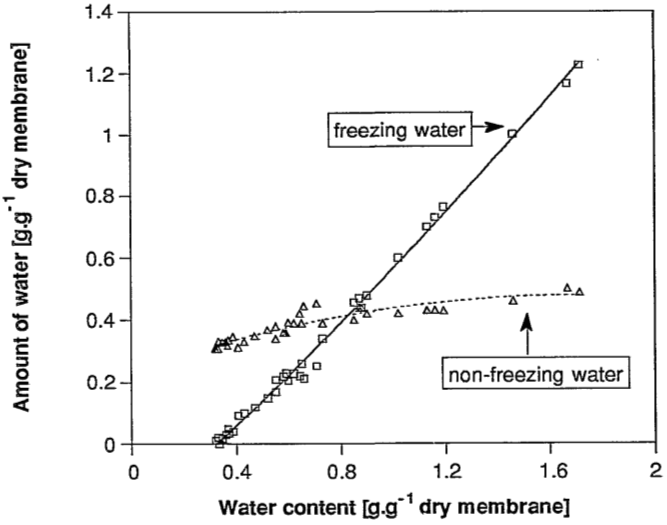

Figure 13 *Calculated amounts of freezing and non-freezing water of cuprophan as a function of the water content.*

In Figure 14 the total phase transition energy is shown as a function of the water content of the sample. The transition energy is calculated by integration of the thermograms over the entire temperature interval. A non-linear relation is found. Several authors extrapolated the upper (linear) part of the curve to the x-axis to estimate the amount of non-freezing water. The slope of the tangent to this curve corresponds with the phase transition energy of the water in the membrane. These procedures for the curve in Figure 14 yield a non-freezing water content of 0.42 $g.g^{-1}$ and a transition energy of 296 $J.g^{-1}$. The phase transition energy of 'ordinary' water is 332 $J.g^{-1}$. Extrapolation of the curve for low water contents yields a bound water content of 0.32 $g.g^{-1}$ and a transition energy of 258 $J.g^{-1}$. The calculated values for the non-freezing water content coincide rather well with the values calculated from Eqn. 2. The intersection of the two lines is found at a water content of 0.69 g. This is in the range between 0.62 and 0.88 $g.g^{-1}$ for which the sudden change in membrane morphology was found.

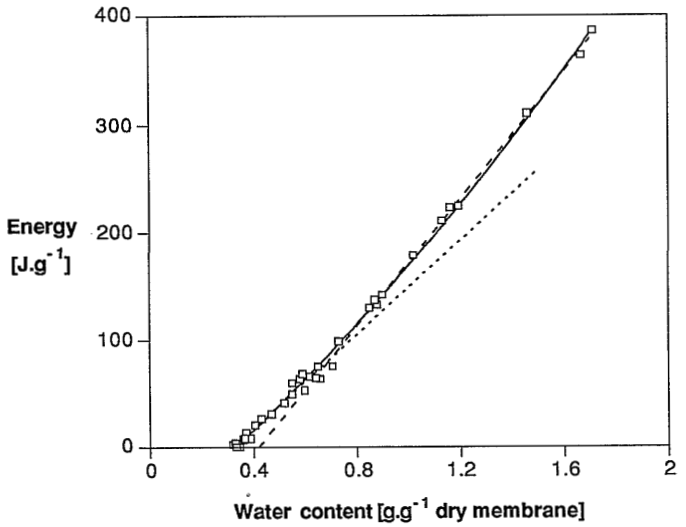

Figure 14 *Calculated transition energy as a function of the water content of cuprophan.*

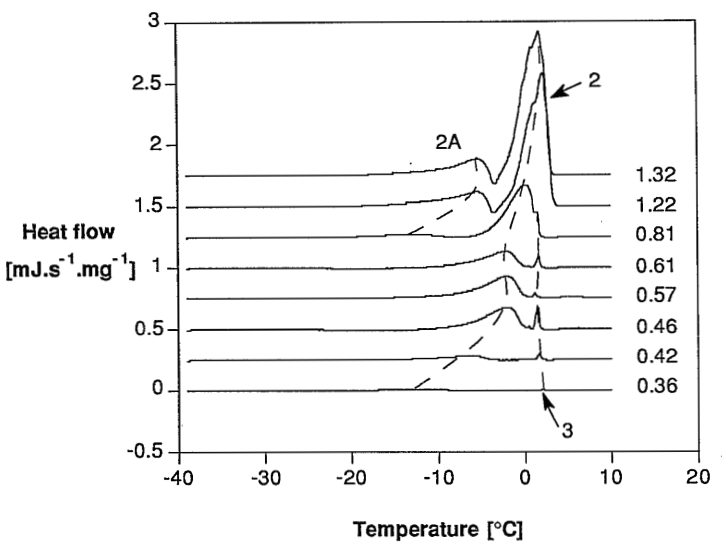

Figure 15 *Stacked thermograms of vapor equilibrated hemophan. All runs are first runs, heating rate 1 °C.min-1. The numbers indicate the water content of the samples [g.g-1 dry sample]. The dashed lines indicate the positions of the peak maxima.*

It is evident that due to the anomalous freezing behavior of water it is doubtful whether the thermoporometry technique is suitable as a characterization method for cellulosic hemodialysis membranes. It might be that at lower temperatures, i.e. smaller pore sizes, the recrystallization effect is only of less or minor importance because in that temperature range most of the water is still frozen. In that case thermoporometry could still be used to detect the smaller pores. It might therefore be worthwhile to compare the thermoporometry results for different membranes.

Figure 15 shows the stacked thermograms of vapor equilibrated hemophan fibers. Also in the thermograms of these hemophan fibers 3 peaks can be distinguished. The curves do not show clear differences with the curves of the cuprophan fibers shown in Figure 9. In the thermograms of the two fibers with the highest water content a small net exothermic energy effect can be observed.

In Figure 16 the differential pore volume distributions of the hemophan fibers are shown. The pore volume distributions of the hemophan fibers are very well comparable with those of the cuprophan fibers shown in Figure 12. The position of the pore distribution maximum is at about 3 nm and rather independent of the water content of the fibers. The results of Figure 16 confirm that at a water content of about 0.6 $g.g^{-1}$ a sudden change in the structure of the water swollen low-flux fibers occurs.

Figure 17 shows the calculated amounts of freezing and non-freezing water in hemophan as a function of the water content of the fibers. The data were calculated using the Eqns. 1 and 2. In Figure 17 the calculated amount of non-freezing water increases from about 0.33 $g.g^{-1}$ at a water content of 0.36 $g.g^{-1}$ to 0.47 $g.g^{-1}$ at the equilibrium water content of 1.57 $g.g^{-1}$.

Figure 18 shows the stacked thermograms of the vapor equilibrated high-flux RC-HP400A fibers and Figure 19 the corresponding pore volume distributions. For the lower water contents the thermograms are comparable with those of the low-flux fibers. For the sample with a water content of 0.52 $g.g^{-1}$ a small and sharp peak (peak 3) at about 2 °C is observed and around -10 °C a broader peak (peak 2). For the sample with a water content of 0.69 $g.g^{-1}$ the same three peaks as for the low-flux fibers are found. From the volume distributions shown in Figure 19 it appears that between a water content of 0.52 and 0.69 $g.g^{-1}$ a sudden change in the structure of the swollen fiber occurs. The same phenomenon was observed for the low-flux fibers. The three peaks, and thus the recrystallization phenomena, are observed for water contents up to 1.40 $g.g^{-1}$. For higher water contents peak 2A apparently disappears again. Up to a water content of 2.4 $g.g^{-1}$ the development of the pore volume distributions of the high-flux fibers is comparable with those of the low-flux fibers. At still higher water contents, however, the pore volume distributions curves appear to collapse.

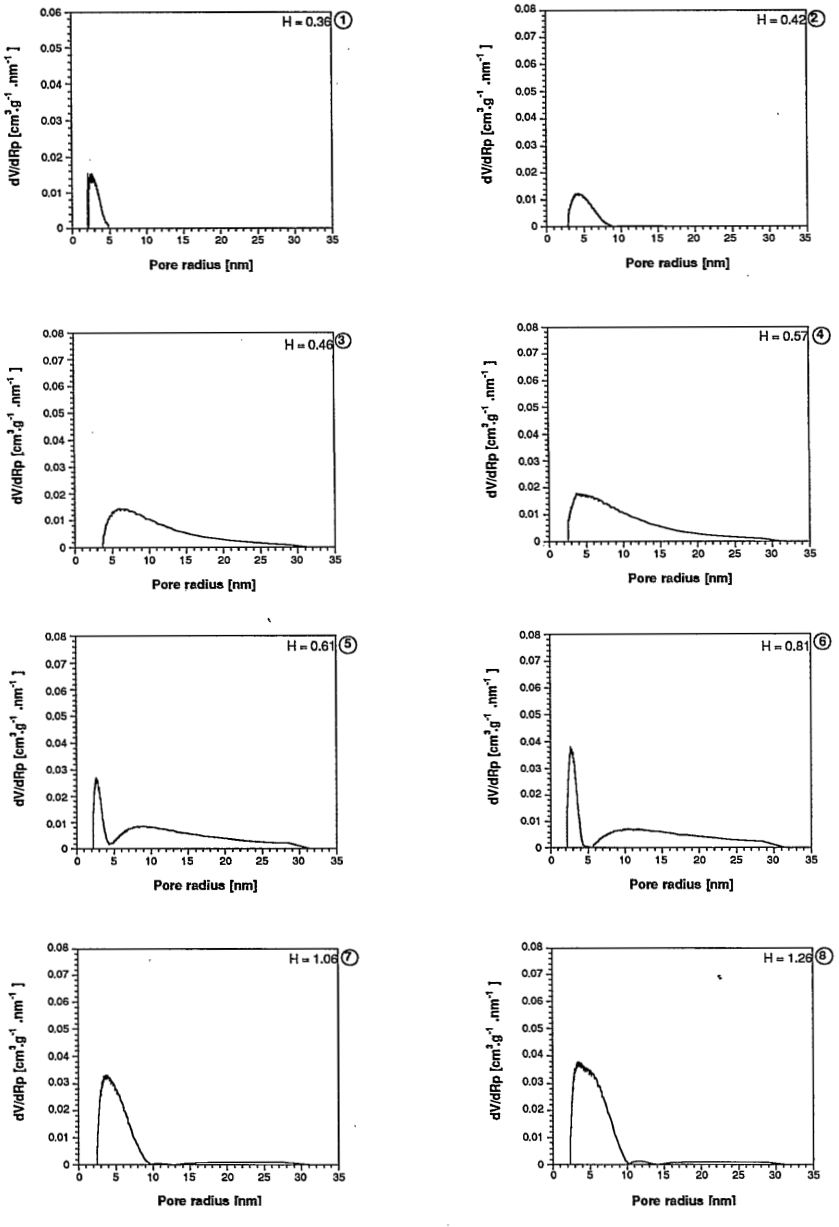

Figure 16 *Differential pore volume distributions of hemophan, numbers in the right upper corners indicate the water content of the fibers.*

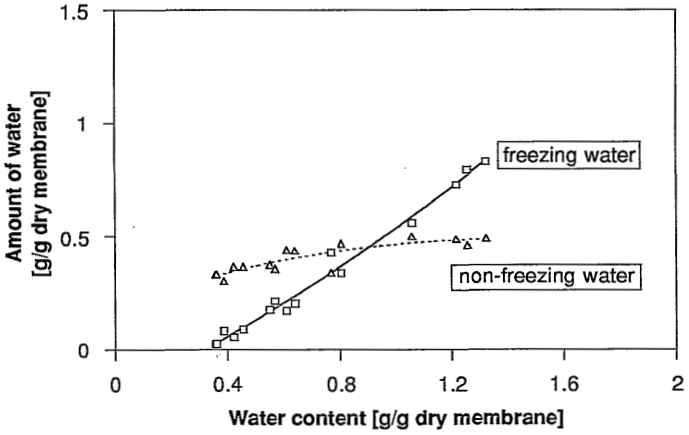

Figure 17 *Calculated amount of freezing and non-freezing water of hemophan as a function of the water content.*

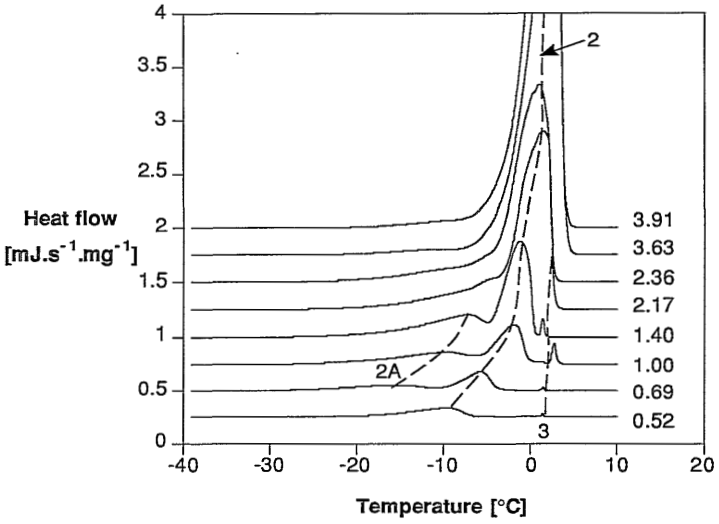

Figure 18 *Stacked thermograms of vapor equilibrated RC-HP400A. All runs are first runs, heating rate 1 °C.min⁻¹. The numbers (0.52, 0.69,...) indicate the water content of the samples [g.g⁻¹ dry sample]. The dashed lines indicate the positions of the peak maxima.*

The equilibrium water content of the RC-HP400A fibers as determined with the centrifuge method is 3.08 $g.g^{-1}$. It can be seen from the Figures 18 and 19 that two samples had a water content which was significantly higher than this equilibrium water content, i.e. the equilibration time had been too short. This means that during the cooling of the samples in the DSC some water *must* be present outside the fiber matrix. During the cooling this water freezes and provides the nuclei for the freezing of water which was present inside the fiber. The water in the fibers is driven out and freezes outside the fiber. This ice will melt at 0 °C and, as a result, the apparent pore volume is found to be smaller. Also for the high-flux fibers the maximum of the pore volume distributions appears to lie at about 3 nm. The measured pore volume, i.e. the area below the curves in Figure 19, is significantly larger for the high-flux fibers. Also the contribution of the larger pores to the pore volume is larger.

Figure 20 shows the calculated amounts of freezing and non-freezing water for the high-flux fibers. The amount of non-freezing water increases from about 0.33 $g.g^{-1}$ to 0.73 $g.g^{-1}$ at the equilibrium water content. The amount of non-freezing water at the equilibrium water content is significantly higher than for the low-flux fibers. In Table 1 the determined membrane parameters are listed. The high-flux fibers are expected to have a lower crystallinity and thus a larger accessible internal polymer surface area and a higher non-freezing water content.

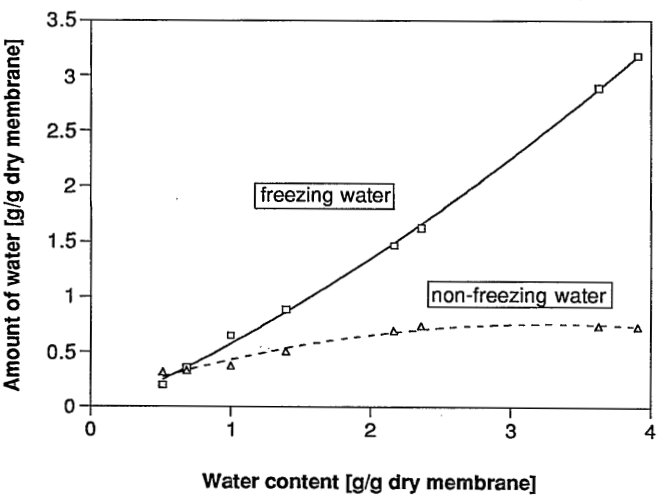

Figure 20 *Calculated amount of freezing and non-freezing water of RC-HP400A as a function of the water content.*

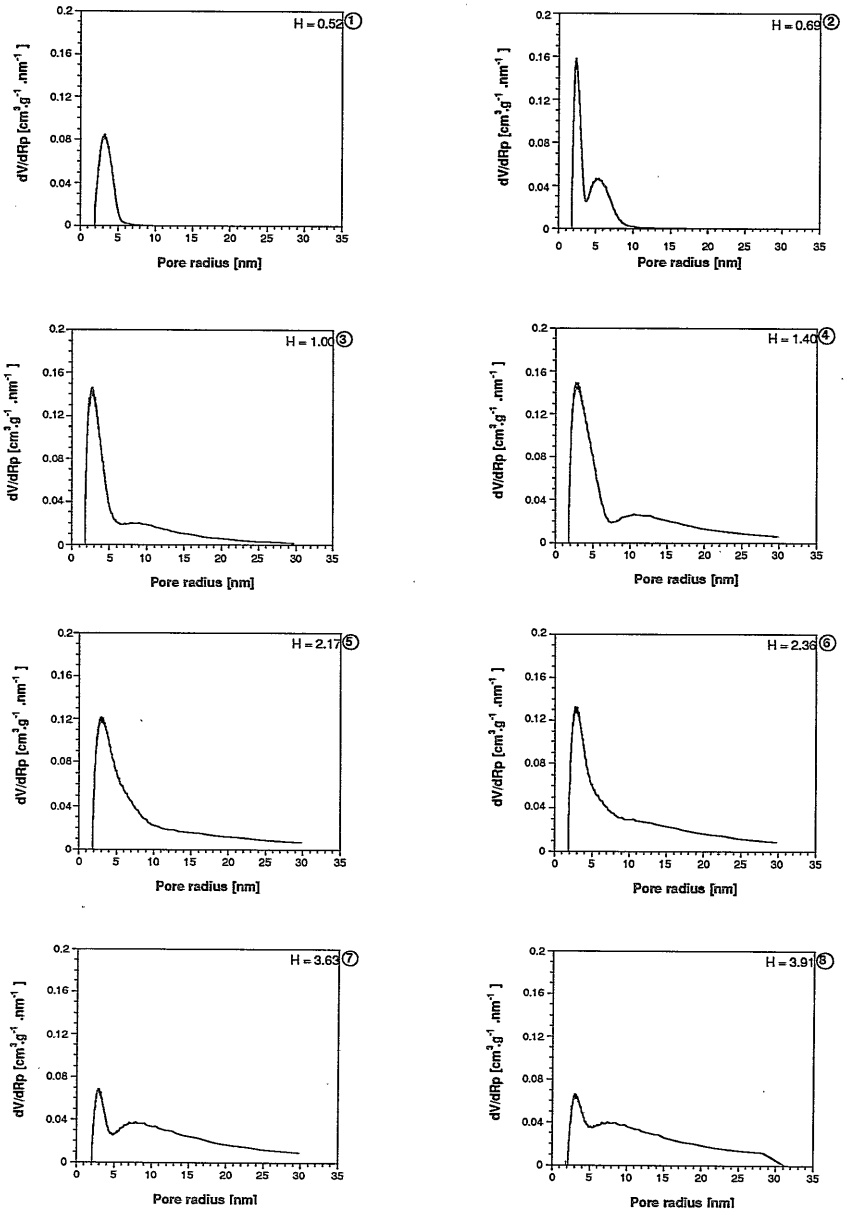

Figure 19 *Differential pore volume distributions of RC-HP400A , numbers in the right upper corners indicate the water contents of the fibers.*

Table 1 *Measured membrane parameters, the column H_2O gives the equilibrium water content as determined with the centrifuge method described in the experimental part. $V_{nf,min}$ and $V_{nf,max}$ are the minimal and maximal non-freezing water content.*

Membrane	H_2O [$cm^3.g^{-1}$]	$V_{nf,min}$ [$cm^3.g^{-1}$]	$V_{nf,max}$ [$cm^3.g^{-1}$]
cuprophan	1.48	0.32	0.48
hemophan	1.57	0.32	0.47
RC-HP400A	3.08	0.33	0.73

3.5 Conclusions

The occurrence of an exothermic peak in the melting thermogram of water swollen cellulosic membranes is very probably caused by the recrystallization of melted ice. During the heating melted ice from the smallest pores is transferred to larger pores or outside the membrane where it can recrystallize giving rise to an exothermic heat evolution. Possibly, this may lead to a 'massive' melting of ice only at 0 °C. For the high-flux RC-HP400A samples with a water content higher than the equilibrium water content, it appears from the calculated pore size distributions that the pores partially collapse. During cooling, the water outside the membrane freezes and provides the nuclei for the freezing of water which was originally present in the pores of the fiber. The water in the fiber is forced out of the fiber and freezes outside the fiber wall. This ice will melt at 0 °C.

The apparent peak separation between the endothermic peaks at 0 °C and below 0 °C is not the result of the existence of two separate types of water. The melting of the ice in the pores is counteracted by the recrystallization of water. Under certain conditions this may even lead to a temporary net exothermic energy evolution during the heating step.

Because of the anomalous freezing behavior of the water in the pores, it appears that the thermoporometry technique is not very suitable as a technique for the characterization of cellulosic hemodialysis membranes. For all 3 membrane types investigated in this study a 'pore volume distribution' with a maximum at about 3 nm is found. For the high-flux RC-HP400A fibers the measured pore volume is higher.

The non-freezing water content of the fibers is dependent on the total water content of the fibers. For the low-flux fibers the non-freezing water content increases from 0.32 $g.g^{-1}$ to about 0.48 $g.g^{-1}$ at the equilibrium water content. For the high-flux fibers the non-freezing water content increases from

0.33 to 0.73 $g.g^{-1}$. For all three fiber types it appears that above a water content of about 0.6 $g.g^{-1}$ a dramatic change in the structure of the fibers takes place.

3.6 References

[1] F.C. Magne, H.J. Portas, H. Wakeham, *A calorimetric investigation of moisture in textile fibers*, J. Am. Chem. Soc., 69 (1947) 1896-1902

[2] Y. Taniguchi, S. Horigome, *The states of water in cellulose acetate membranes*, J. Appl. Polym. Sci., 19 (1975) 2743-2748

[3] M.A. Frommer, D. Lancet, *Freezing and nonfreezing water in cellulose acetate membranes*, J. Appl. Polym. Sci., 16 (1972) 1293-1303

[4] M.A. Frommer, M. Shporer, R.M. Messalem, *Water binding and irreversible dehydration processes in cellulose acetate membranes*, J. Appl. Polym. Sci., 17 (1973) 2263-2276

[5] C. Toprak, J.N. Agar, M. Falk, *State of water in cellulose acetate membranes*, J. Chem. Soc. Faraday Trans. I, 75 (1979) 803-815

[6] R.D. Schultz, S.K. Asunmaa, G.A. Guter, F.E. Littman, *Characterization of ordered water in hydrophylic membrane pores*, Paper 10,247, McDonnell Douglas Corp., Newport Beach California, 1969

[7] S. Sourirajan, *The mechanism of demineralization of aqueous sodium chloride solutions by flow, under pressure, through porous membranes*, Ind. Eng. Chem. Fundamentals, 2 (1963) 51-55

[8] H.S. Frank, W.Y. Wen, *Structural aspects of ion-solvent interaction in aqueous solutions: a suggested picture of water structure*, Discussions Faraday Soc., 24 (1957) 133-140

[9] R.D. Schultz, S.K. Asunmaa, *Ordered water and the ultrastructure of the cellular plasma membrane*, Recent Progr. Surface Sci., 3 (1970) 291-332

[10] W.A.P. Luck, D. Schioeberg, U. Siemann, *Infrared investigation of water structure in desalination membranes*, J. Chem. Soc. Faraday Trans. 2, 76 (1980) 136-147

[11] C.A.J. Hoeve, *The structure of water in polymers*, In: S.P. Rowland (ed.), Water in polymers, ACS Symp. Ser. no. 127, ACS, Washington, 1980, 135-146

[12] H.G. Burghoff, W. Pusch, *Characterization of water structure in cellulose acetate membranes by calorimetric measurements*, J. Appl. Polym. Sci., 23 (1979) 473-484

[13] S. Katayama, S. Fujiwara, *NMR study of the spatial effect of polyacrylamide gel upon the water molecules confined to it*, J. Am. Chem. Soc., 101 (1979) 4485-4488

[14] F.H. Stillinger, *Thermal properties of water in restrictive geometries*, In: S.P. Rowland (ed.), Water in polymers, ACS Symp. Ser. no. 127, ACS, Washington, 1980, 11-22

[15] N. Murase, K. Gonda, T. Watanabe, *Unfrozen compartmentalized water in gels and its anomalous crystallization during warming*, J. Phys. Chem., 90 (1986) 5420-5426

[16] A.D.C. Chan, D.J. Harrison, *NMR study of the state of water in ion-selective electrode membranes*, Anal. Chem., 65 (1993) 32-36

[17] A. Higuchi, J. Komiyama, T. Iijima, *The states of water in gel cellophane membranes*, Polym. Bull., 11 (1984) 203-208

[18] N. Murase, M. Shiraishi, S. Koga, K. Gonda, Cryo-Lett., 3 (1982) 251

[19] G. Belfort, N. Sinai, *Relaxation studies of adsorbed water on porous glass*, In: S.P. Rowland (ed.), Water in polymers, ACS Symp. Ser. no. 127, ACS, Washington, 1980, 323-346

[20] W. Drost-Hansen, *Structure of water near solid interfaces*, Ind. Eng. Chem., 61, 11 (1969) 10-47

[21] K. Nakamura, T. Hatakeyama, H. Hatakeyama, *Studies on bound water of cellulose by differential scanning calorimetry*, Textile Res. J., 51 (1981) 607-613

[22] M.S. Jhon, J.D. Andrade, *Water and hydrogels*, J. Biomed. Mater. Res., 7 (1973) 509-522

[23] T. Hatakeyama, S. Yamamoto, S. Hirose, H. Hatakeyama, *Structural change of water restrained in cellulosic hollow fibres*, In: C. Schuerch (ed.), Cellulose and Wood - Chemistry and Technology, Proceedings of the 10th cellulose conference, Syracuse, New York, May 39 - June 2, 1988, 431-446

[24] T. Hatakeyama, *Structure and properties of the amorphous region of cellulose*, In: J.F. Kennedy, G.O. Phillips, P.A. Williams (eds.), Cellulose structural and functional aspects, Ellis Horwood, Chichester, 1989, 45-52

[25] R. Wycisk, W.M. Trochimczuk, *Water states in PE-poly(MA-co-DVB) inter-polymer type carboxylic ion-exchange membranes*, J. Membrane Sci., 66 (1992) 89-96

[26] N. Nishioka, S. Yoshimi, T. Iwaguchi, K. Kosai, *Permeability through cellulose membranes grafted with vinyl monomers in homogeneous system II. States of water in acrylonitrile grafted cellulose membranes*, Polym. J., 16 (1984) 877-885

[27] N. Nishioka, T. Kuromatsu, T. Takahashi, M. Uno, K. Kosai, *Permeability through cellulose membranes grafted with vinyl monomers in a homogenous system III. Methyl Acrylate grafted cellulose membranes*, Polym. J., 18 (1986) 131-140

[28] N. Nishioka, O. Fujimoto, M. Tachibana, M. Uno, K. Kosai, *Permeability through cellulose membranes grafted with vinyl monomers in a homogenous system IV. Methyl methacrylate grafted cellulose membranes*, Polym. J., 19 (1987) 1341-1350

[29] N. Nishioka, H. Yamaguchi, K. Kosai, *Permeability through cellulose membranes grafted with vinyl monomers in a homogenous system VI. States of water in membranes swollen in solutions*, J. Appl. Polym. Sci., 40 (1990) 2007-2014

[30] S. Deodhar, P. Luner, *Measurement of bound (nonfreezing) water by differential scanning calorimetry*, In: S.P. Rowland (ed.), Water in polymers, ACS Symp. Ser. no. 127, ACS, Washington, 1980, 273-286

[31] T. Kobayashi, M. Todoki, M. Kimura, Y. Fujii, T. Takeyama, H. Tanzawa, *Permeability and structure of PMMA stereocomplex hollow fiber membrane for hemodialysis*, In: E. Drioli, M. Nakayaki (eds.), Membranes and membrane processes, New York, Plenum Press, 1986, 507-513

[32] T. Tatsuguchi, K. Sakai, *Determination of structure and permeability of drawn hollow fibers dialysis membranes of regenerated cellulose*, In: N.N. Li (ed.), Ext. Abstr. ICOM'90, Chigago, NAMS, 1990, 1238-1239

[33] M. Brun, A. Lallemand, J.F. Quinson, C. Eyraud, *A new method for the simultaneous determination of the size and the shape of pores: the thermoporometry*, Thermochim. Acta, 21 (1977) 59-88

[34] J. Desbrieres, M. Rinaudo, M. Brun, J.F. Quinson, *Relation entre le taux de rétention et la distribution de pores dans une membrane d'ultrafiltration*, J. Chim. Phys., 78 (1981) 187-191

[35] F.P. Cuperus, D. Bargeman, C.A. Smolders, *Critical points in the analysis of membrane pore structures by thermoporometry*, J. Membrane Sci., 66 (1992) 45-53

[36] A.P. Broek, D. Bargeman, E.D. Sprengers, C.A. Smolders, *Characterization of hemophan hemodialysis membranes by thermoporometry*, Int. J. Artificial Organs, 15 (1992) 25-28

[37] A.P. Broek, H.A. Teunis, D. Bargeman, E.D. Sprengers, C.A. Smolders, *Characterization of hollow fiber hemodialysis membranes: pore size distribution and performance*, J. Membrane Sci., 73 (1992) 143-152

[38] W.H. Press, B.P. Flannery, S.A. Teukolsky, W.T. Vetterling, *Numerical recipes in pascal*, Cambridge etc., Cambridge University Press, 1990, p. 122

[39] DIN 53814, *Bestimmung des Wasserrückhaltevermögens von Fasern und Faden-abschnitten*, October 1974

4

CHARACTERIZATION OF HEMODIALYSIS MEMBRANES BY INVERSE SIZE EXCLUSION CHROMATOGRAPHY

4.1 Introduction

For the characterization of cellulosic hemodialysis membranes only a limited number of characterization techniques for porous structures are useful [1]. Because the pores in these membranes develop upon swelling in water wet-state characterization techniques are essential. Besides, dialysis membranes are typically used to separate low and high molecular weight solutes in a solution, which means that the characteristic or average pore size is just a few nanometers. For low-flux cuprophan membranes pore radii of 2-3 nm are reported in literature [2]. The characterization technique(s) to be used for a reliable evaluation of cellulosic hemodialysis membranes should be capable of determining such small pores in the wet state.

Size exclusion chromatography (SEC) is a widely employed technique for the separation of solutes according to their size. It is also applied as a standard technique for the determination of the size and molecular weight of (macro)molecules. If well-defined tracer molecules are taken instead, inverse size exclusion chromatography (i-SEC) can be used to study the morphology of porous materials.

Several authors studied the structure of cellulose used in the paper and textile industry by means of i-SEC techniques. Stone and Scallan [3] developed a static method based on depletion measurements with a range of standard molecules. The method was shown to be very time consuming and susceptible to disturbances. Especially for the hollow fiber geometry it is difficult to get accurate results because it is difficult to remove water from the lumen of the fiber. Rowland *et al.* [4,5] performed i-SEC measurements with preparative chromatography columns packed with ball-milled decrystallized cotton. Only with these ball-milled materials homogeneous and stable columns could be obtained. The grounding procedure, however, affected the structure of the cellulose. Recently Bredereck *et al.* [6-8] and Grünwald *et al.* [9] reported on i-SEC studies with packed HPLC-columns. By packing the columns with pieces of material cut to small size, stable columns and reproducible results could be obtained. Bredereck *et al.* reported good correlations between their i-SEC results and, e.g., iodide sorption, BET internal surface area and dyeing characteristics [6].

The i-SEC technique has several advantages compared to other membrane characterization techniques such as retention or diffusion measurements. I-SEC measurements are not disturbed by concentration polarization, and because the membrane material is cut into small pieces the method is not hampered by the geometry of the hollow fiber. An additional advantage is that only very small amounts of tracer are needed. Finally, i-SEC measurements allow the discrimination between adsorption and geometrical effects: by comparing the elution volume of a certain substance with a standard elution curve interaction effects can be studied. The i-SEC technique is probably not suitable for studying the structure of anisotropic membranes.

4.2 Theoretical

Principle

Size exclusion chromatography is based on the principle that dependent on its size a molecule is more-or-less able to enter the pores of a porous material. When a column is packed with a porous material and an eluent is forced through, injected molecules that are too large to enter the pores will be eluted in the so-called 'void volume' of the column. Very small tracer molecules are able to penetrate into (almost) all the pores of the material and the measured elution volume corresponds accordingly with the sum of the total pore volume and the void volume of the column. The measured elution volume of a tracer is a function of the distribution coefficient of the tracer in the material:

$$V_e = V_o + K.V_p^t \qquad (1)$$

where V_e is the elution volume of the tracer, V_o the void volume of the column, K the distribution coefficient of the tracer and V_p^t the total volume of the pores in the column.

The distribution coefficient of non-adsorbing molecules is only determined by the size and shape of the tracer and the size distribution and the shape of the pores. For a reliable characterization of a porous structure the following basic experimental conditions should be satisfied:

- no adsorption interaction between tracer molecules and porous material
- the elution rate should be sufficiently slow to allow equilibrium distribution of the tracers in the pores
- low tracer concentrations to avoid intermolecular interactions between tracer molecules in the eluent
- the tracer molecules should be well defined (shape, size) and should

not deform due to the pressure drop over the column

For the characterization of water swollen cellulosic materials lower alcohols, mono- and oligosaccharides, dextranes and polyethylene glycols are reported to be suitable tracers [7-9].

Equilibrium partitioning of molecules in pores

The i-SEC technique uses a wide range of tracer molecules with largely different dimensions. The smallest tracer molecules can be considered as rigid spheres. The large macromolecules do behave as flexible random-coil polymer chains. Essentially two classes of solute partitioning models have been proposed, i.e. for rigid and for flexible molecules.

The partitioning of rigid molecules in inert porous networks is described by Giddings *et al.* [10]. Following a statistical mechanical approach they obtained relations for the partitioning of solutes of different shapes, in pores of different shapes and for different pore size distributions. The partitioning of rigid spherical solutes in pores of different shapes is given by:

$$K = (1-q)^{\alpha} \qquad q \leq 1 \qquad (2)$$
$$K = 0 \qquad q > 1$$

where K is the distribution coefficient of the tracer, q is the ratio of the solute radius r and the pore radius R_p and α is the pore shape factor. For slit-shaped pores α=1, for cylindrical pores α=2 and for spherical pores α=3.

The partitioning of random-coil macromolecules in pores of various shapes was analyzed by Casassa *et al.* [11-13]. Their theory is based on the calculation of the change of entropy of a macromolecule as it leaves the mobile phase (solution) to enter the sorbent pores. Casassa assumed a flexible chain macromolecule in a thermodynamically ideal solvent and a low polymer concentration. The result is a relation for the distribution coefficient of a macromolecule with a radius of gyration r_g in a pore with radius R_p:

$$K^{(\alpha)} = \sum_{m=1}^{\infty} \frac{2\alpha}{\left[\beta_m^{(\alpha)}\right]^2} \cdot \exp\left[-\left(\beta_m^{(\alpha)} \cdot \frac{r_g}{R_p}\right)^2\right] \qquad (3)$$

For slit-shaped pores α=1 and $\beta_m^{(\alpha=1)} = \pi(m-0.5)$, for cylindrical pores α=2 and $\beta_m^{(\alpha=2)}$ is the m^{th} root of the Bessel function $J_o(\beta)$, for spherical pores α=3 and $\beta_m^{(\alpha=3)}=\pi m$. In narrow pores, i.e. $R_p<r_g$:

$$K^{(\alpha)} \approx \frac{2\alpha}{\left[\beta_1^{(\alpha)}\right]^2} \cdot \exp\left[-\left(\beta_1^{(\alpha)} \cdot \frac{r_g}{R_p}\right)^2\right] \qquad (4)$$

In wide pores, i.e. $R_p \gg r_g$:

$$K^{(\alpha)} \approx 1 - \frac{2\alpha}{\sqrt{\pi}} \cdot \frac{r_g}{R_p} \qquad (5)$$

Eqn. 5 indicates that for wide pores the initial course of the SEC curve is linear. Casassa's results are valid in the limit of an infinite number of chain segments of vanishingly small length. Davidson *et al.* [14] confirmed the results of Casassa by means of Monte Carlo simulations and examined the effect of finite segment number and length. The work of Giddings *et al.* [10] was included as the limiting case for a molecule with one rod shaped segment. It was found that the partition coefficient of a chain with finite segment length can be substantially higher than that of a chain with an infinite number of infinitesimally short segments but with the same radius of gyration. Davidson *et al.* derived the following approximating function for the cylindrical pore geometry:

$$\ln\left[K(q_g)\right] = \ln\left[K\left(l/R_p=0\right)\right] + \left(l/R_p\right)\left(0.49 + 1.09q_g + 1.79q_g^2\right) \qquad (6)$$

where K is the distribution coefficient, q_g is the ratio of the gyration radius of the tracer and the pore radius and l the length of a segment of the random coil molecule. In Eqn. 6 the factor $K(l/R_p=0)$ represents the limiting value of Casassa calculated from Eqn. 3 with $\alpha=2$.

Figure 1 shows for the cylindrical pore geometry the relations of Giddings (Eqn. 2), Casassa (Eqn. 3) and Davidson (Eqn. 6) for chains of different length.

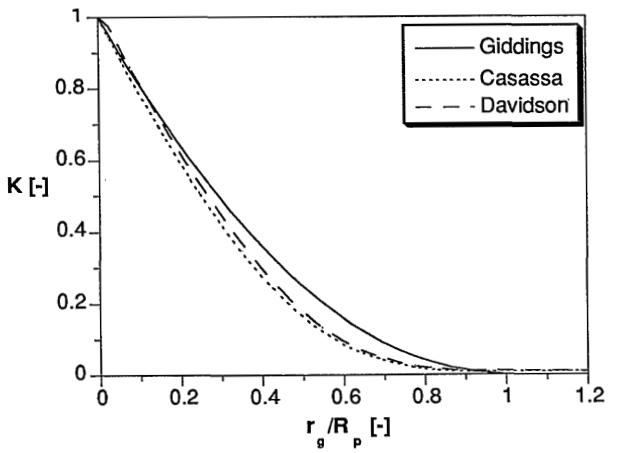

Figure 1 *Distribution coefficients calculated according to the cylindrical pore models of Giddings (Eqn. 2), Casassa (Eqn. 3) and Davidson (Eqn. 6); (parameters assumed R_p=5 nm, l=0.3 nm).*

An important result of Casassa's work is that with large macromolecules and narrow pores at $r_g > R_p$, the distribution coefficient is not equal to zero. This means that a number of larger macromolecules penetrate into narrow pores, assuming elongated conformations that are different from the equilibrium conformation of the macromolecules in solution (figure 2).

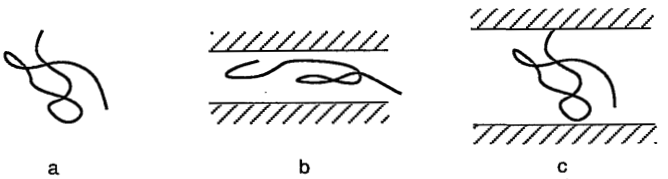

Figure 2 *Typical macromolecular conformations; a: in solution, b: in narrow pores, c: in wide pores, after Gorbunov [15].*

Eqn. 5 acquires the most universal and model-independent form for the distribution coefficient in wide pores if a transition is made from the radius of gyration of the macromolecule to its effective chromatographic radius $s = \frac{2r_g}{\sqrt{\pi}}$. This means that the effective radius is about 13% larger than the radius of gyration. Gorbunov *et al.* [15] introduced the parameter $\Sigma = \frac{\alpha}{R_p} = \frac{S_p}{V_p}$, the ratio of pore surface S_p to pore volume V_p instead of the pore radius R_p:

$$K^{(\alpha)} \approx 1 - s\Sigma \qquad (7)$$

The $K^{(\alpha)}$ versus $s\Sigma$ relationships for different pore shapes are shown in Figure 3. The curves show a linear dependence of K for small values of $s\Sigma$. Plotted in these coordinates, the three different curves are rather close to one another and at $s\Sigma<0.4$ they almost coincide. Consequently, i-SEC measurements cannot be used to obtain reliable information about the pore form of the sorbent.

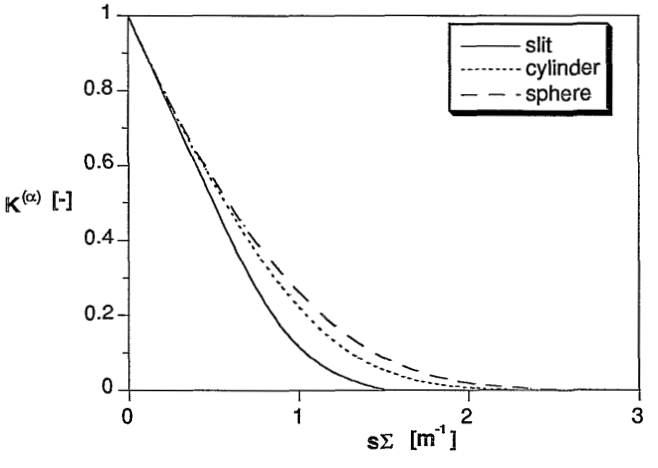

Figure 3 *The $K^{(\alpha)}$ versus $s\Sigma$ relationships for the different pore geometries, after Gorbunov [15].*

Determination of pore volume distributions from SEC curves

In an excellent paper Gorbunov *et al.* [15] reviewed different methods of calculating pore volume distributions from SEC curves. The relative pore volume distribution function $f_v(R_p)$ is defined by:

$$f_v(R_p) = \frac{1}{V_p} \cdot \frac{dV}{dR_p} \qquad (8)$$

where V is the volume of pores with a radius between R_p and R_p+dR_p and V_p is the total pore volume of the membrane.

The first method to calculate pore volume distributions from i-SEC data is of Halász and Martin [16]. The method has been, and still is, used extensively by other authors. The model is based on the assumption that the distribution coefficient K=1 for all tracer molecules smaller than the pore and that K=0 if the tracer size exceeds the pore size, hence a step function is assumed. By definition then, a plot of K versus tracer dimension directly represents the (cumulative)

pore volume distribution of the porous material. Knox and Scott [17] were the first[1] to point out that this assumption is incorrect, as is accepted generally nowadays. The model leads to an underestimation of pore sizes by a factor of 2 to 3, whereas the width of the pore size distribution is largely overestimated.

Knox and Scott [17] proposed a different method for cylindrical shaped pores. The method was extended by Nikolov [19] to pores of other geometries using the partitioning theory for rigid spherical particles of Giddings *et al.* (Eqn. 2). The equations for the pore volume distributions can be written in the following general form:

$$f_v^{(\alpha)}(R_p) = (-1)^{(\alpha+1)} \frac{R_p^{\alpha}}{\alpha!} \left[\frac{d^{(\alpha+1)}K}{dR^{(\alpha+1)}} \right]_{R=R_p} \qquad (9)$$

where $f_v(R_p)$ is the relative pore volume distribution, R_p the pore radius, α the pore shape factor and K is the distribution coefficient.

Eqn. 9 is valid for rigid spherical particles. In the original studies of Knox and Scott and Nikolov, however, flexible macromolecules were used as tracers. Applying Eqn. 9 for cylindrical pores (α=2) means that the i-SEC curve has to be differentiated 3 times to obtain the pore volume distribution which makes the method extremely sensitive to experimental inaccuracy. Gorbunov *et al.* [15] showed that the procedure easily leads to erroneous and even unrealistic results.

Gorbunov [20] introduced differential functions for the pore volume distribution $f_v(R_p)$ and for the pore surface distribution $f_s(R_p)$, normalized for the total pore volume V_p and for the total pore surface area S_p. The mean radii R_v and R_s corresponding to these functions are defined by the following relationships:

$$R_v = V_p^{-1} \int_0^{\infty} R f_v dR = R_s^{-1} . S_p^{-1} \int_0^{\infty} R^2 f_s(R) dR \qquad (10)$$

$$R_s = S_p^{-1} \int_0^{\infty} R f_s dR = V_p \left[\int_0^{\infty} R^{-1} f_v(R) dR \right]^{-1} = \alpha \frac{V_p}{S_p} \qquad (11)$$

Gorbunov [20] showed that also for polydisperse sorbents the initial course of the $\overline{K}(r)$ relationship is described by a simple universal equation:

[1] Actually already in 1936 Ferry [18] showed that the sieve constant of an ultrafiltration membrane for a certain solute changes gradually (and not by a step function) from 0 to 1 as the pore size is progressively increased.

$$\overline{K}(r) \approx 1 - \frac{2\alpha}{\sqrt{\pi}} \cdot \frac{r}{R_s} = 1 - s\Sigma \qquad r \ll R_s \qquad (12)$$

where $\overline{K}(r)$ is the mean distribution coefficient for a polydisperse sorbent. The initial slope of the $\overline{K}(r)$ relationship depends only on the specific surface area of the sorbent Σ (or mean pore radius R_s), and is independent of the width and type of the pore size distribution function. Eqn. 12 can be rewritten to allow calculation of the mean pore radius R_s from the initial slope of the $\overline{K}(r)$ curve:

$$R_s = \alpha \cdot \frac{V_p}{S_p} \cdot 10^3 \qquad [nm] \qquad (13)$$

Bredereck [21] used this Eqn. 13 to calculate the pore radii of differently treated cellulosic materials.

When the sizes of the tracer molecules are comparable to the pore radius R_s the distribution coefficient becomes dependent on the width and type of the function $f_v(R_p)$. Gorbunov *et al.* [15] calculated SEC curves for different pore size distribution functions. The final result of their calculations was that the SEC curves depend mainly on two parameters, the mean pore radius R_s and the width of the pore size distribution function U. The type of distribution function has only little effect.

For a polydisperse sorbent the distribution coefficient function $\overline{K}(r)$ is calculated as:

$$\overline{K}(r) = \frac{1}{V_p} \int_0^\infty K(r/R_p) \cdot f_v(R_p) dR_p \qquad (14)$$

Eqn. 14 is a so-called first-kind Fredholm equation and the problem of using this equation to find an unknown function $f_v(R_p)$ is classed among the 'ill-posed' mathematical problems. This implies that for all practical purposes minor errors in the initial data will have a considerable effect on the calculated results. The same problem is encountered for the determination of pore volume distributions from sieving coefficients or retention data [22,23]. Mason *et al.* [22] and Leypoldt [24] concluded that there is not a single solution to the problem unless some assumption is made about the shape of the pore volume distribution.

Gorbunov proposed a procedure which consists of approximating the experimental $\overline{K}^{(i)}(r_i)$ relationship obtained by using a series of tracer molecules of known radii r_i, by means of the theoretical Eqn. 14. The kernel of the procedure is the $K(r/R_p)$ function of the form of Eqn. 3, whereas the desired

distribution function $f_v(R_p)$ is specified by a 'logarithmic normal law' (Eqn. 16) with varying parameters R_s and U. A set of parameters (V_p, R_s, U) is searched to find those which minimize the function:

$$T(V_p,R_s,U) = \sum_i \left(K_i^{exp} - K_i\right)^2 \qquad (15)$$

where R_s is the mean pore size (Eqn. 11), U the pore volume distribution width, K_i^{exp} the experimentally observed distribution coefficient and K_i the calculated distributed coefficient. The logarithmic normal distribution function is given by:

$$f_v(R_p) = \frac{V_p}{R_p\sqrt{2\pi\ln(U)}} \cdot \exp\left[-\frac{\left(\ln\left(\frac{R_p}{R_s\sqrt{U}}\right)\right)^2}{2\ln(U)}\right] \qquad (16)$$

A comparable procedure was proposed by Knox and Ritchie [25]. They fitted logarithmic normal distribution functions to i-SEC curves using the SEC theory for rigid spherical particles. They reported that the i-SEC curves could only moderately be fitted with logarithmic normal distribution functions. As an alternative they proposed a method in which they selected an optimum single pore size and then built around that a distribution of pores whose sizes fall in geometrical progression. The method was implemented by a microcomputer using up to seven pore contributions, or in a more powerful procedure by a mainframe computer which can also allow for incomplete penetration of the smallest sample probe and incomplete exclusion of the largest sample probe.

4.3 Experimental

Tracers

A critical point in the i-SEC analysis is the size assessment of the tracer molecules. Various methods are described in literature to determine the dimensions of the tracer molecules. Characteristic sizes were derived for instance from diffusion and sedimentation coefficients and from viscosity and turbidity measurements. The different methods all give a characteristic dimension but it is rather uncertain which parameter gives the best results with size exclusion chromatography. Furthermore, changes in the actual size of the tracer can (easily) arise because of the flow-induced deformation of the flexible tracer molecules. Several authors reported on this phenomenon [26-28]. Squire [29] mentioned that especially polyethylene glycols are susceptible to

deformation.

For the size determination of dextranes Bredereck [21] used an equation of Haller [30] based on viscosimetric data:

$$r = 0.027M^{0.5} \quad [nm] \qquad (17)$$

where r is the tracer radius and M is the molecular weight of the tracer.

For the polyethylene glycols a relation of Squire [29] based on SEC data was used:

$$r = 0.087M^{0.4} \quad [nm] \qquad (18)$$

For sugars and oligosaccharides Bredereck used data of Brown and Johnsen [31] based on Stokes radii. For our work we used mono- and oligosaccharides (n=1 to 7) of glucose. The radii of these molecules were calculated from an equation which was obtained by fitting the data of Bredereck to a power-law:

$$r = 0.037M^{0.47} \quad [nm] \qquad (19)$$

The radii of methanol and D_2O were taken from Bredereck and Klein *et al.* [32], respectively. Data for creatinine and vitamin B12 are based on Stokes radii, the diffusion coefficients were measured using a Taylor capillary dispersion technique in a set-up described by Snijder *et al.* [33]. The characteristics of the tracers used for this study are listed in Table 1. The dextranes were purchased from Pharmacia, the polyethylene glycols from Fluka and all other tracers from Merck. Tracer concentrations of 1 $g.dm^{-3}$ (0.1%) in water were used and a volume of 50 mm^3 was injected. For the determination of the elution volumes of D_2O and methanol 5 mm^3 and 3 mm^3 of the pure substance were injected, respectively. To prevent growth of micro organisms 200 $mg.dm^{-3}$ formaldehyde was added to the samples. Small quantities of the filtered tracer solutions were stored separately at -18 °C.

HPLC system

The HPLC system consisted of a Waters 610 HPLC pump with a 600E pump controller, a 410 refractive index detector, a column oven and a 746 integrator.

Column material

For the studies three different types of hollow-fiber cellulosic hemodialysis membranes were used, i.e. low-flux cuprophan® and hemophan® and high-

flux RC-HP400A. The low-flux fibers, with a dry wall thickness of 8 μm, were provided by Organon Teknika, Boxtel, The Netherlands. The high-flux RC-HP400A fibers were provided by Enka, Wuppertal, Germany. The cuprophan and RC-HP400A fibers are made of a regenerated cellulose. The hemophan fibers are made of a regenerated and modified cellulose. In order to improve its biocompatibility the cellulose of hemophan has been modified with a small amount of (positively charged) N,N-di-ethyl-aminoethyl (DEAE) ether groups.

Table 1 *Characteristics of the tracers used.*

Tracer	M [g.mole^{-1}]	r [nm]
creatinine	113	0.28
vitamin B12	1355	0.78
D_2O	20	0.11
methanol	32	0.23
D-glucose	180	0.36
maltose	342	0.49
maltotriose	504	0.58
maltotetraose	667	0.66
maltopentaose	824	0.72
maltohexaose	991	0.79
maltoheptaose	1153	0.84
PEG 200	200	0.73
PEG 400	400	0.96
PEG 600	600	1.12
PEG 1000	1,000	1.41
PEG 1500	1,500	1.63
PEG 2000	2,000	1.82
PEG 3000	3,000	2.20
PEG 4000	4,000	2.40
PEG 6000	6,000	2.83
Dextran T10	10,000	2.68
Dextran T40	40,000	4.86
Dextran T70	70,000	6.35
Dextran T500	500,000	14.5
Dextran T2000	2,000,000	37.5

Column preparation

The fibers were cut into pieces of about 0.5-1 mm using scissors. Unless stated otherwise, the fibers were swollen in water and the water was decanted several times to remove impurities as much as possible. The column (300 x 7.5 mm internal diameter, stainless steel) was filled with the swollen fibers by pressing manually with a suitable piston. After closing, the column was eluted overnight

with the eluent. The eluent was degassed and filtered over a 0.2 μm filter before use. To prevent the growth of micro organisms 200 mg.dm^{-3} formaldehyde was added to the eluent. In general, a stable detector signal was obtained after running overnight with eluent. The void volume of each column was determined from the elution volume of dextran T2000 (M=2,000,000 g.mole^{-1}). The elution volumes were determined from the peak maxima.

After the runs, the columns were dried in a vacuum oven at 80 °C till a constant weight was reached and the weight of the column material was determined.

Water content of the fibers

The equilibrium water content of the swollen fibers was determined with a centrifuge method based on DIN-53814 [34]. In a small centrifuge tube, a tube provided with a microfiltration membrane in the bottom was mounted (Millipore Ultrafree-MC); this tube was filled with swollen fiber pieces of about 1.5 cm. The material was centrifuged for 20 minutes at 900 g to remove excess water. The water content of the samples was determined from the weight decrease upon drying the centrifuged fibers overnight in a vacuum oven at 80 °C.

Pore size modelling

The pore size distributions were determined by minimizing Eqn. 15 using the Eqns. 14 and 16. A cylindrical pore geometry was assumed. Since for the measurements both small rigid and large flexible tracers have been used the partitioning models were arbitrarily chosen as follows:

$r < R_p$: rigid exclusion model of Giddings (Eqn. 2)
$r \geq R_p$: flexible exclusion model of Casassa (Eqn. 3)

The fitting procedure was implemented in the spreadsheet program Excel using a minimization routine of Newton. The accessible pore volumes of all tracers with water as the eluent, except vitamin B12 and creatinine, were used in the fitting procedure.

4.4 Results and Discussion

Packing of the column

The packing of the column is an important parameter. When the column is packed to loose channelling, i.e. irregular flow of the eluent, occurs. On the other hand, when the packing is too tight this will result in incomplete swelling of the column material and hence in a membrane structure which deviates from the structure under normal dialysis conditions. Figure 4 shows two elution curves of columns packed with cuprophan fibers. The first curve is of a column packed with swollen cuprophan as described in the experimental section. The second curve is of a column which is packed with dry cuprophan and then eluted to allow swelling of the fiber material. It is obvious that the latter procedure does not allow the membrane to swell completely. For one of the columns tested it was not even possible to obtain any flow of eluent through the column.

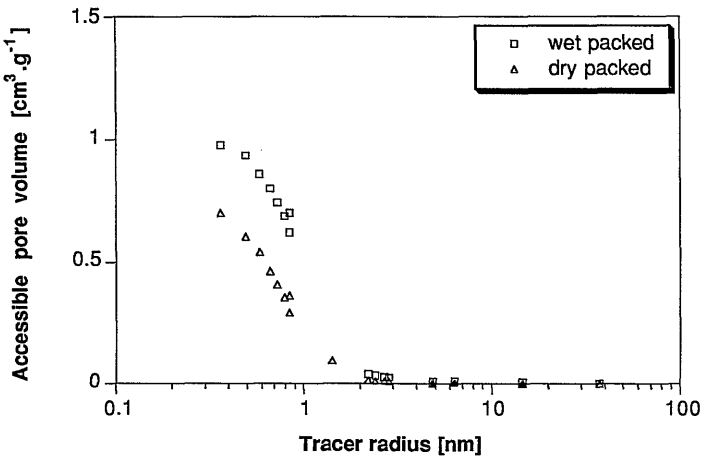

Figure 4 *Elution curves of differently packed cuprophan columns.*

For the low-flux fibers reproducible results could be obtained by packing the column with wet fiber material. For the high-flux fiber, however, special care had to be taken to obtain columns with a completely swollen matrix. Only by packing the swollen fibers very carefully and without pressing also for the high-flux fibers reproducible results could be obtained. Figure 5 shows the effect of column packing on the calculated membrane parameters.

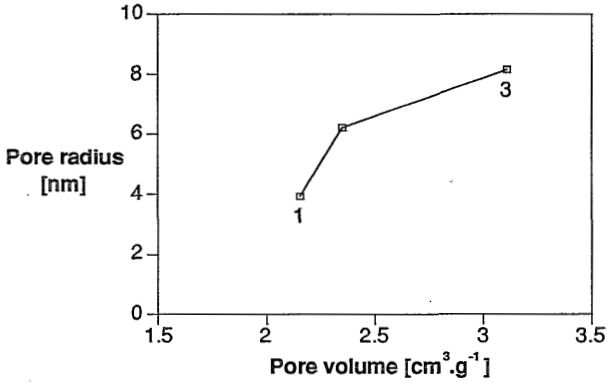

Figure 5 *Relation between pore radius and pore volume of three different columns filled with high-flux RC-HP400A; the packing density of the columns was varied, 1: high packing density, 3: low packing density.*

Choice of the experimental conditions

The elution rate in an i-SEC column should be sufficiently low to obtain equilibrium partitioning of the tracers between the pores and eluent. Figure 6 shows the effect of the elution rate on the elution volume of several tracers. In particular the elution volumes of maltose and maltoheptaose are dependent on the flow rate. The dashed parts of the curves indicate the estimated elution volumes extrapolated to elution rate zero. The curves were extrapolated by fitting second order polynomials to the measured data.

Since the time needed to obtain equilibrium partitioning is expected to decrease with increasing temperature the elution volumes of the tracers were also determined at elevated temperatures. In Table 2 the elution volumes are listed as a percentage of the estimated elution volume at elution rate zero and for various temperatures. For all the tracers shown a flow rate of 0.25 $cm^3.min^{-1}$ and a column temperature of 50 °C are sufficient to approach equilibrium conditions reasonably well (≥95 %). For the following measurements a flow rate of 0.25 $cm^3.min^{-1}$ and a temperature of 70 °C were chosen. The temperature of 70 °C is probably not too high for the column material; as shown in Table 2 only small differences between 50 and 70 °C are found. Grünwald *et al.* [9] reported that no changes of the column material occurred at temperatures up to 90 °C.

Bredereck *et al.* [21] and Grünwald *et al.* [9] reported that linear flow velocities of maximal 4.4 $cm.min^{-1}$ at 20 °C gave acceptable results for most

column materials and tracers. The columns used in this study all have a void volume of at least 2.5-3 cm^3. A linear flow velocity of 4.4 $cm.min^{-1}$ thus corresponds to an elution rate of about 0.4 $cm^3.min^{-1}$. The flow rates used in this study (0.25 $cm^3.min^{-1}$) are therefore sufficiently small.

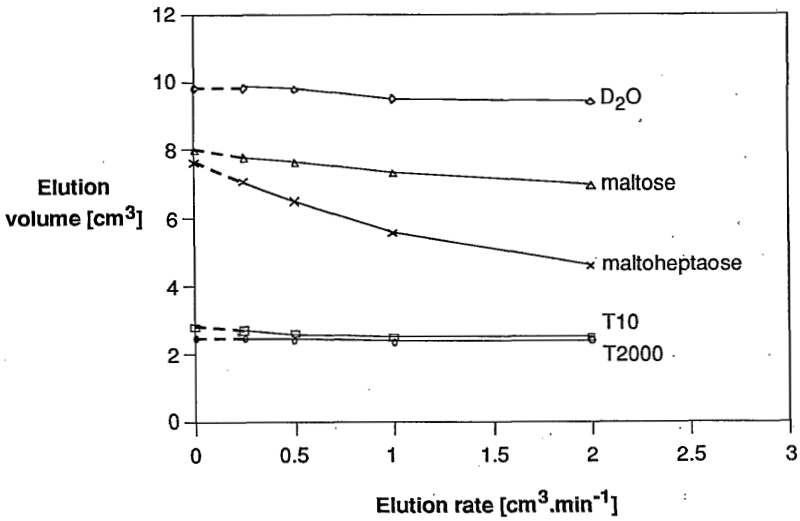

Figure 6 *Relation between the elution volume and the elution rate for several tracers, T=37 °C, cuprophan.*

Elution curves

The elution curves of the different membrane materials are shown in the Figures 7-9. The most remarkable result is the difference in total accessible pore volume between the high- and low-flux fibers. The set of chosen tracer molecules cover the complete range of relevant tracer radii. Most of the tracers shown do fit a smooth S-shaped curve, as was expected. It appears therefore that the tracer dimensions were estimated adequately and that no deformation of the tracers occurred. Some tracers, however, deviate from the curve indicating that adsorption effects may be present.

The tracer indicated with number 1 in the figures represents D_2O. This molecule seems to have a somewhat larger elution volume than expected. The same phenomenon was also reported by Bredereck *et al.* [21] and other authors [35] for different kinds of cellulosic materials. They suggested that an adsorption effect, probably because of -OD/-OH exchange is present. Bredereck *et al.* found a slight decrease of the elution volume of D_2O when the temperature of the column was increased (3% when the temperature was

increased from 20 to 80 °C). An increased temperature is expected to reduce the extent of adsorption. The decrease of 3%, however, was insufficient to explain the deviating elution volume of D_2O. Bredereck also found that the difference in elution volume of D_2O and methanol (no adsorption) was strongly fluctuating for different kinds of samples. They suggested that a small part of the total pore volume is excluded from tracer penetration and accessible only to water or D_2O. Only the very small and polar water or D_2O molecule is able to penetrate into the narrowest pores between some cellulose chains (disordered crystallite surfaces). Bredereck *et al.* found that when water was replaced by methanol as eluent, both deuterated methanol (MeOD) and D_2O approximately had the same elution volume. Apparently the change in eluent resulted in a disappearance of the very small pores that exist in water swollen cellulose. Although Bredereck did not use the term bound water, it might be that these pores are filled with so-called bound or non-freezing water and therefore they are not accessible to other molecules than water. Bredereck reported a good agreement between the accessible pore volume of D_2O and the water content of the membrane as determined with the centrifuge method according to DIN-53814.

Table 2 *Estimated elution volumes as a percentage of the extrapolated values for elution rate zero at different elution rates and column temperatures.*

Tracer	Rate [$cm^3.min^{-1}$] / T [°C]	0.25	0.5	1.0	2
T2000	37	98	97	95	96
	50	100	100	100	100
	70	100	100	100	100
T10	37	97	93	90	89
	50	99	97	95	93
	70	100	100	98	96
PEG600	37	-	-	-	-
	50	97	95	91	89
	70	99	98	94	90
Maltoheptaose	37	92	84	73	60
	50	96	93	87	78
	70	97	96	91	87
Maltose	37	97	96	91	87
	50	98	95	92	90
	70	97	93	90	82
D2O	37	100	100	97	96
	50	100	100	98	98
	70	99	99	98	97

The test molecules creatinine and vitamin B12 both appear to adsorb to the cellulosic membranes, the apparent accessible pore volumes are higher than expected on the basis of their size. For the cuprophan and RC-HP400A fibers no elution peak of creatinine can be observed using pure water as eluent. With an eluent containing 0.6 g.dm^{-3} NaCl the accessible pore volume is somewhat higher than expected. Figure 10 shows the effect of the NaCl concentration on the elution volume of creatinine and dextran T2000 on a cuprophan column. The elution volume of creatinine is a strong function of the NaCl concentration in the eluent. For very low concentrations creatinine is strongly adsorbing to the cuprophan matrix. Colton *et al.* [36] determined the distribution coefficient of creatinine for a cuprophan flat sheet membrane by depletion measurements. They reported no adsorption of the creatinine, there results, however, were obtained from depletion measurements in an isotonic NaCl solution (9 g.dm^{-3} NaCl).

The adsorption behavior of creatinine on hemophan is opposite. Using water as the eluent the apparent accessible pore volume of creatinine is somewhat smaller than expected, the creatinine is partly excluded. For eluentia with a higher ionic strength the accessible pore volume for creatinine increases. For the highest NaCl concentration the accessible pore volume is higher than expected indicating that additionally an other adsorption mechanism may be present. The adsorption effects are much less dependent on the NaCl concentration.

These results indicate that an electrostatic interaction is responsible for the adsorption behavior of creatinine. The creatinine molecule is a weak base and can adapt a positive charge [37]. Regenerated celluloses contain a small amount of carboxylic groups which cause a negative charge [38]. The hemophan fibers have been modified with positively charged DEAE groups. From the curves in Figure 8 it appears that the hemophan has a net positive charge although the net amount of charge is smaller than for the cuprophan and RC-HP400A fibers.

The accessible pore volume for vitamin B12 is hardly influenced by the ionic strength of the eluent indicating that no electrostatic interaction is responsible for its adsorption behavior.

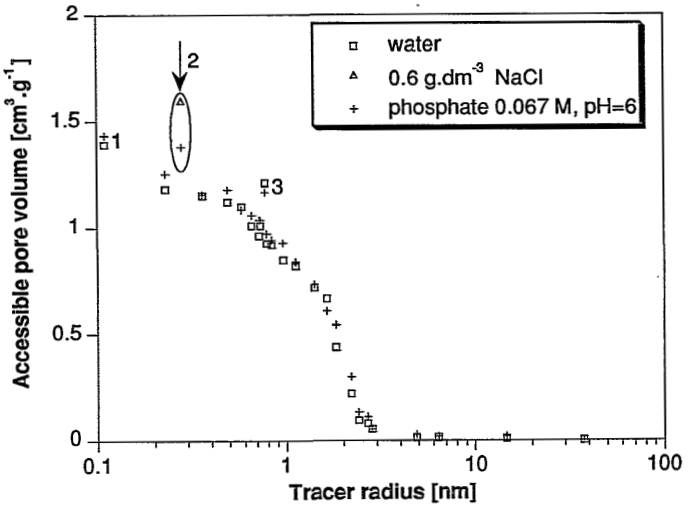

Figure 7 *Elution curves of cuprophan, T = 70 °C, elution rate 0.25 $cm^3.min^{-1}$ (1: D_2O, 2: creatinine, 3: vitamin B12).*

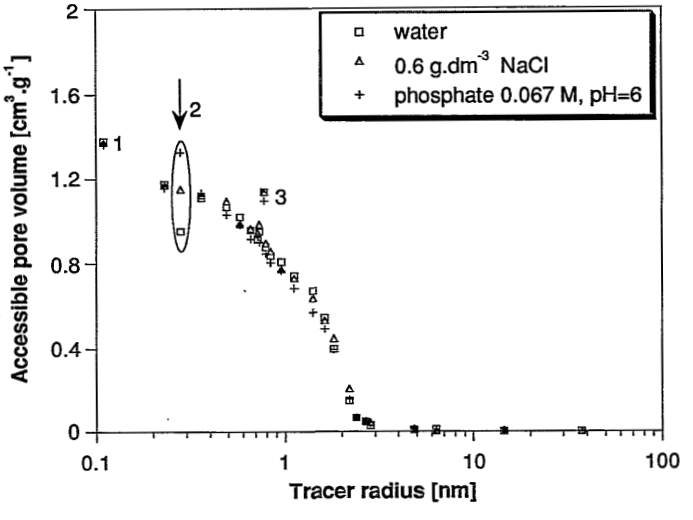

Figure 8 *Elution curves of hemophan, T = 70 °C, elution rate 0.25 $cm^3.min^{-1}$ (1: D_2O, 2: creatinine, 3: vitamin B12).*

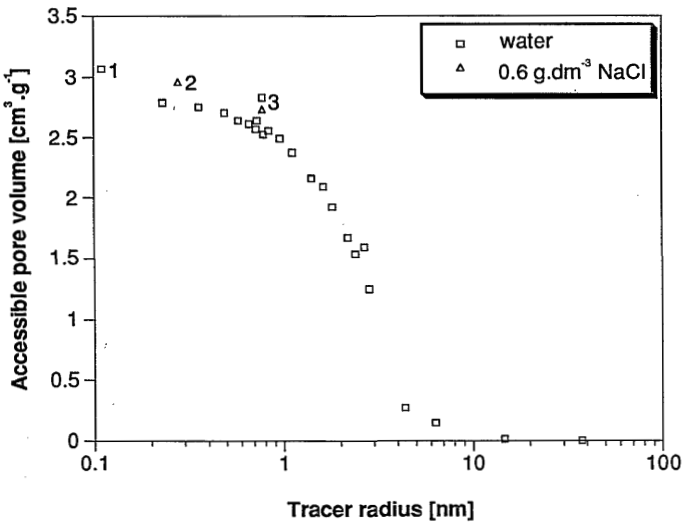

Figure 9 *Elution curve of RC-HP400A, T = 70 °C, elution rate 0.25 $cm^3.min^{-1}$ (1: D_2O, 2: creatinine, 3: vitamin B12).*

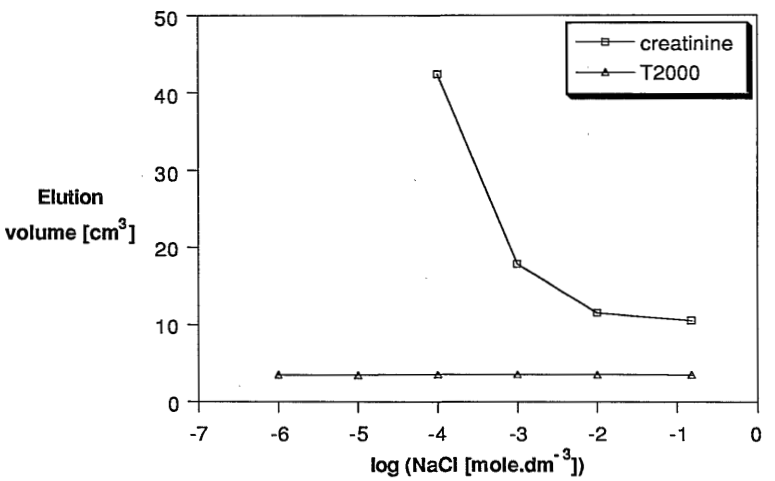

Figure 10 *Elution volumes of creatinine and T2000 as a function of the NaCl concentration for a cuprophan column.*

Pore size determination

The calculated and measured membrane parameters are shown in Table 3. For all the membranes it is found that the elution curves are best described by a homoporous pore size distribution, i.e. U=1. In Figure 11 the measured and calculated elution curves of the different membranes are shown. The lines represent the calculated curves based on the membrane parameters, V_p, U and R_p, shown in Table 3. All curves are well described with a homoporous pore volume distribution. In the fitting procedure the sum of the absolute differences between experimental and calculated distribution coefficients is minimized. This means that especially the small solutes contribute to the sum of errors. The distribution coefficient of small solutes is relatively insensitive towards a distribution of pores. Still, also fitting of the curves by minimizing the sum of relative errors resulted in a homoporous pore volume distribution function.

Figure 12 shows the sensitivity of the model towards its parameters. The model is most sensitive to the pore volume parameter. It is rather insensitive to the distribution width and this may also explain why homoporous pore volume distributions are found. Although actually no pore size (volume) distributions of regenerated cellulose membranes are reported in literature also other authors got indications that the pore size distributions in these membranes must be very narrow indeed [2,39].

In Table 3 four different estimates for the total pore volume of the membranes are given. The first column (H_2O) gives the equilibrium water content as measured with the centrifuge method described in the experimental part. The second column (V_p) contains the optimal fit for the pore volume. The third (V_{D2O} meas.) and fourth column (V_{D2O} calc.) represent the measured and calculated accessible pore volume for D_2O, respectively. Since the D_2O molecule has a finite dimension this value is somewhat smaller than the fitted pore volume V_p.

Table 3 *Calculated and measured membrane parameters, assuming a cylindrical pore shape.*

Membrane	H_2O [$cm^3.g^{-1}$]	V_p [$cm^3.g^{-1}$]	V_{D2O} meas. [$cm^3.g^{-1}$]	V_{D2O} calc. [$cm^3.g^{-1}$]	R_p [nm]	U [-]
cuprophan	1.48	1.48	1.41	1.40	4.1	1
hemophan	1.57	1.45	1.38	1.36	3.7	1
RC-HP400A	3.08	3.11	3.07	3.03	8.2	1

The listed estimates for the total pore volume coincide very well indicating that

the membranes were completely swollen. Only for the hemophan columns the obtained value for V_p appears to be somewhat low. The measured and calculated data for the accessible pore volume for D_2O are about 5% smaller than the H_2O content and V_p, respectively. This may be explained by the different temperatures used for the determination of the water content and the i-SEC measurements.

The accessible pore volume of the high-flux fiber is more than twice the pore volume of the low-flux fibers. Also the pore radius of the high-flux fiber appears to be about twice as large. For low-flux cuprophan membranes cylindrical pore radii of 2-3 nm are reported in literature [2]. The radius of 4.1 nm given in Table 3 is (somewhat) larger.

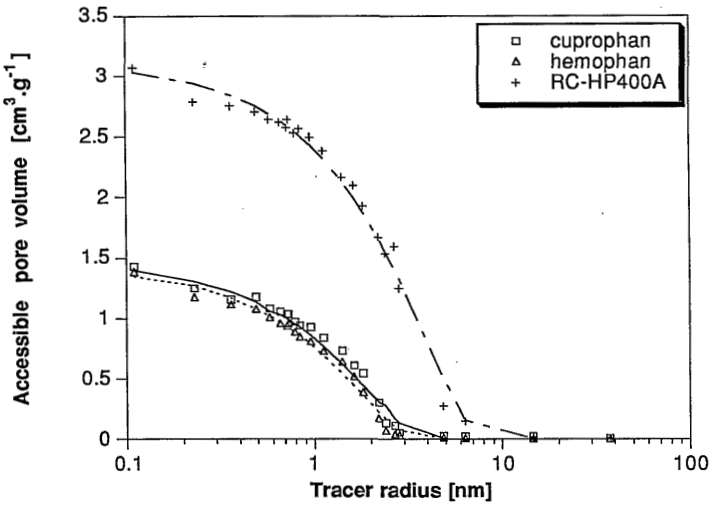

Figure 11 *Measured and calculated elution curves. The lines represent the calculated curves based on the parameters V_p and R_p of Table 3.*

From the curves in Figure 11 it appears that some of the smaller tracers do not fit the calculated curves. For all three curves methanol and glucose have a measured accessible pore volume which is smaller than the calculated values. The D_2O data points do fit the calculated curves. The observations may be explained partly by assuming, as Bredereck *et al.* did, that some of the pores in the membranes are so small that they can only contain a water or D_2O molecule. It might be that these water molecules form the non-freezing or bound water of the membrane. The non-freezing water content of these membranes was determined as 0.48 $g.g^{-1}$ for the low-flux membranes and

0.73 g.g^{-1} for the high-flux membrane [40]. These values were determined with a calorimetric method at temperatures below 0 °C. The i-SEC measurements are performed at a (much) higher temperature. It may be that for these higher temperatures the amount of bound water is different. Bound or non-freezing water is often assumed to be inaccessible to solutes. The differences between the accessible pore volume for D_2O and methanol are only about 0.2 and 0.28 g.g^{-1} for the low- and high-flux membrane, respectively. These values are much smaller than the values determined with the calorimetric method suggesting that at least some of the non-freezing water may be accessible for other molecules. If a part of the water in the membranes is present as inaccessible bound water then it may be expected that the fitted parameter V_p is smaller than the measured pore volume from the water content. From Table 3 it appears that this is not the case, both parameters coincide very well.

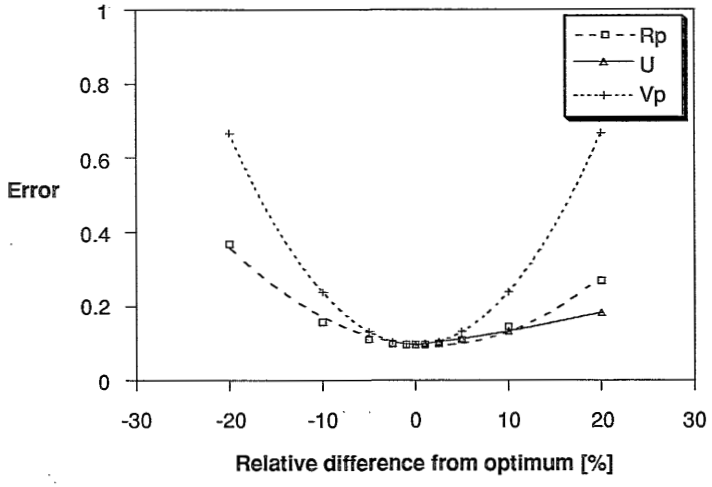

Figure 12 *Sensitivity of the model to its parameters. Data were calculated for a cuprophan column.*

4.5 Conclusions

The i-SEC technique is an elegant and, for the purpose of membrane characterization, very useful technique. The pore size distribution of a membrane can be determined and adsorption phenomena can be studied.

The membranes used in this study show clear differences in pore size and porosity. The high-flux RC-HP400A membrane has a larger pore size as well as a larger porosity than the two low-flux membranes. For all the membranes it is found that the elution curves are best described by a

homoporous pore volume distribution. It appears that at least some of the bound or non-freezing water in the membranes is accessible to the tracer molecules.

The adsorption behavior of the test molecule creatinine is influenced by the NaCl concentration of the eluent, indicating that an electrostatic interaction is present. The observations can be explained by assuming that the cuprophan and RC-HP400A fibers are negatively charged and the hemophan fiber is positively charged due to its modification with DEAE. The net charge of the hemophan fiber, however, is smaller.

4.6 Symbols

f_v	differential pore volume distribution function [$m^3.kg^{-1}.m^{-1}$]
H	equilibrium water content of the swollen fiber [$cm^3.g^{-1}$]
K	distribution coefficient of the tracer [-]
$\overline{K}$	mean distribution coefficient for a polydisperse sorbent [-]
l	segment length random coil molecule [m]
M	molecular weight tracer [$g.mole^{-1}$]
q	ratio of tracer radius and pore radius [-]
q_g	ratio of gyration radius of the tracer and the pore radius [-]
r	tracer radius [m]
r_g	gyration radius [m]
R_p	pore radius [m]
R_v	the volume mean pore radius defined by Eqn. 10 [m]
R_s	the surface mean pore radius defined by Eqn. 11 [m]
s	effective chromatographic radius [m]
S_p	specific pore surface area of the membrane [$m^2.kg^{-1}$]
T	minimization function defined by Eqn. 15
U	pore volume distribution width [-]
V_e	elution volume of the tracer [m^3]
V_o	void volume of the column [m^3]
V_p	pore volume of the membrane [$m^3.kg^{-1}$]
V_p^t	total volume of the pores in the column [-]
α	pore shape factor [-]
β_m	parameter defined by Eqn. 3 [-]
Σ	ratio of pore volume and pore surface area [m^{-1}]

4.7 References

[1] Chapter 2 of this thesis

[2] R.P. Wendt, E. Klein, E.H. Bressler, F.F. Holland, R.M. Serino, H. Villa, *Sieving properties of hemodialysis membranes*, J. Membrane Sci., 5 (1979) 23-49

[3] J.E. Stone, A.M. Scallan, *Structural model for the cell wall of water swollen pulp fibers*, Cell. Chem. Technol., 2 (1968) 343-358

[4] S.P. Rowland, N.R. Bertoniere, *Chemical methods of studying supramolecular structure*, In: T.P. Nevell, S.H. Zeronian (eds.), Cellulose chemistry and its

application, Chichester, Ellis Horwood, 1985, p. 112-137

[5] L.F. Martin, S.P. Rowland, *Gel permeation properties of decrystallized cotton cellulose*, J. Chromatogr., 28 (1967) 139-142

[6] K. Bredereck, A. Blüher, *Die Ammoniak-Vorbehandlung und ihre Auswirkung auf die Veredlung*, Melliand Textilber., 72 (1991) 446-454

[7] K. Bredereck, A. Blüher, A. Hoffmann-Frey, *Die Bestimmung der Porenstruktur von Cellulosefasern durch Ausschlußmessung*, Das Papier, 44 (1990) 648-656

[8] K. Bredereck, E. Bader, U. Schmitt, *Die Bestimmung der Porenstruktur wassergequollener Zellulosefasern*, Textilveredlung, 24 (1989) 142-150

[9] M. Grünwald, E. Burtscher, O. Bobleter, *HPLC determination of the pore distribution and chromatographic properties of cellulosic textile materials*, J. Appl. Polym. Sci., 39 (1990) 301-317

[10] J.C. Giddings, E. Kucera, C.P. Russell, M.N. Myers, *Statistical theory for the equilibrium distribution of rigid molecules in inert porous networks, Exclusion Chromatography*, J. Chem. Phys., 72 (1968) 4397-4408

[11] E.F. Casassa, *Equilibrium distribution of flexible polymer chains between a macroscopic solution phase and small voids*, J. Polym. Sci.: Polym. Lett., 5 (1967) 773-778

[12] E.F. Casassa, Y. Tagami, *Equilibrium model for gel permeation chromatography of flexible polymer chains*, Macromol., 2 (1969) 14-26

[13] E.F. Casassa, *Comments on exclusion of polymer chains from small pores and its relation to gel permeation chromatography*, Macromol., 9 (1976) 182-185

[14] M.G. Davidson, U.W. Suter, W.M. Deen, *Equilibrium partitioning of flexible macromolecules between bulk solution and cylindrical pores*, Macromol., 20 (1987) 1141-1146

[15] A.A. Gorbunov, L.Y. Solovyova, V.A. Pasechnik, *Fundamentals of the theory and practice of polymer gel permeation chromatography as a method of chromatographic porosimetry*, J. Chromatogr., 448 (1988) 307-322

[16] I. Halász, K. Martin, *Porengrößen von Festkörpern*, Angew. Chem., 90 (1978) 954-961

[17] J. H. Knox, H.P. Scott, *Theoretical models for size-exclusion chromatography and calculation of pore size distribution from size-exclusion chromatography data*, J. Chromatogr., 316 (1984) 311-332

[18] J.D. Ferry, *Statistical evaluation of sieve constants in ultrafiltration*, J. Gen. Physiol., 20 (1936) 95-104

[19] R.N. Nikolov, *Theoretical aspects of the pore distribution and its determination by size-exclusion chromatography*, J. Chromatogr., 364 (1986) 163-182

[20] A.A. Gorbunov, L.Y. Solovyova, V.A. Pasechnik, *Determination of the characteristics of the porous structure of sorbents using gel permeation chromatography of polymers*, Vysokomol. Soedin. Ser. A., 26 (1984) 967-973

[21] K. Bredereck, A. Blüher, *Porenstrukturbestimmung von Cellulosefasern durch Ausschlußchromatographie. Grundlagen und Anwendungsbeispiele für Quellbehandlungen und Hochveredlung von Baumwollgewebe*, Melliand Textilber., 73 (1992) 652-662

[22] E.A. Mason, R.P. Wendt, E.H. Bressler, *Similarity relations (dimensional analysis) for membrane transport*, J. Membrane Sci., 6 (1980) 283-298

[23] K.D. Knierim, E.A. Mason, *Heteroporous sieving membranes: rigorous bounds on pore size distribution and sieving curves*, J. Membrane Sci., 42 (1989) 87-107

[24] J.K. Leypoldt, *Determining pore size distributions of ultrafiltration membranes by solute sieving - Mathematical limitations*, J. Membrane Sci., 31 (1987) 289-305

[25] J.H. Knox, H.J. Ritchie, *Determination of pore size distribution curves by size exclusion chromatography*, J. Chromatogr., 387 (1987) 65-84

[26] W.M. Deen, *Hindered transport of large molecules in liquid-filled pores*, Am. Inst.

Chem. Eng. J., 33 (1987) 1409-1425

[27] Q.T. Nguyen, J. Neel, *Characterization of ultrafiltration membranes. Part IV. Influence of the deformation of macromolecular solutes on the transport through UF-membranes*, J. Membrane Sci., 14 (1983) 111-128

[28] S. Daoudi, F. Brochard, *Flows of flexible polymer solutions in pores*, Macromol., 11 (1978) 751-758

[29] P.G. Squire, *Calculation of hydrodynamic parameters of random coil polymers from size exclusion chromatography and comparison with parameters by conventional methods*, J. Chromatogr., 210 (1981) 433-442

[30] W. Haller, *Critical permeation size of dextran molecules*, Macromol., 10 (1977) 83-86

[31] W. Brown, R.M. Johnsen, *Transport from an aqueous phase through cellulosic gels and membranes*, J. Appl. Polym. Sci., 26 (1981) 4135-4148

[32] E. Klein, F.F. Holland, K. Eberle, *Comparison of experimental and calculated permeability and rejection coefficients for hemodialysis membranes*, J. Membrane Sci., 5 (1979) 173-188

[33] E.D. Snijder, M.J.M. te Riele, G.F. Versteeg, W.P.M. van Swaay, *Diffusion coefficients of several aqueous alkanolamine solutions*, J. Chem. Eng. Data, 38 (1993) 475-480

[34] DIN 53814, *Bestimmung des Wasserrückhaltevermögens von Fasern und Fadenabschnitten*, October 1974

[35] S.P. Rowland, C.P. Wade, N.R. Bertoniere, *Pore structure analysis of purified, sodium hydroxide-treated and liquid ammonia-treated cotton celluloses*, J. Appl. Polym. Sci., 29 (1984) 3349-3357

[36] C.K. Colton, K.A. Smith, E.W. Merrill, P.C. Farrell, *Permeability studies with cellulosic membranes*, J. Biomed. Mater. Res., 5 (1971) 459-488

[37] H. Yasuda, L.D. Ikenberry, C.E. Lamaze, *Permeability of solutes through hydrated polymer membranes. II Permeability of water soluble organic solutes*, Makromol. Chem., 125 (1969) 108-118

[38] H. Krässig, R.G. Steadman, K. Schliefer, W. Albrecht, *Cellulose*, In: W. Gerhartz et al. (eds.), Ullmann's Encyclopedia of Industrial Chemistry, Weinheim, VCH, 5th edition, vol. A5, 1986, p. 375-418

[39] A. Hoffmann-Frey, K. Bredereck, unpublished results

[40] Chapter 3 of this thesis

5

CHARACTERIZATION OF HEMODIALYSIS MEMBRANES BY MASS TRANSPORT MEASUREMENTS

5.1 Introduction

The ultimate aim of membrane characterization is to predict the performance, i.e. the mass transport properties of a membrane or membrane device from its characteristic structure. In practice, however, it is often found that the performance of a membrane is not only dependent on its structure. Also external factors such as process conditions and device configuration in combination with phenomena such as membrane fouling and concentration polarization play a role. In some cases the contribution of the typical membrane features to the overall performance is completely overruled by these external factors. Many of the process affecting phenomena, such as fouling and concentration polarization, are closely related to the characteristic structure of the membrane surface. Also in the artificial kidney these phenomena have a significant effect on the performance of the final device. For the characterization of membranes it is important to exclude the influence of these external factors as much as possible. In an artificial kidney device with hollow fibers this is hard to achieve. The devices are therefore not suitable for a reliable characterization of the membranes.

Stevenson *et al.* [1-4] developed experimental methods for the determination of the permeability of hollow fiber membranes. The set-ups are suitable to determine the diffusive and hydraulic permeabilities of one single hollow fiber. The influence of the boundary layer at the outside of the fiber is diminished by rapidly rotating the fiber in the dialysate.

Klein *et al.* [5] described a set-up to measure the diffusive and hydraulic permeabilities of small bundles of hollow fibers. The boundary layer at the outside of the fibers is minimized by pumping dialysate with a high velocity at the outside of the fibers.

Artificial kidney manufacturers often specify their devices with so-called 'clearance rates' and the 'ultrafiltration capacity'. The clearance rate represents the volume of feed stream which is cleared completely of a certain solute. Normally, the clearance rate for urea or creatinine is given to represent the low-molecular weight solutes and the vitamin B12 clearance rate to represent the molecules with a middle-molecular weight. The ultrafiltration capacity is related to the hydraulic membrane permeability.

The data in specification sheets, are in general determined from *in vitro* model studies. The circumstances under which these data are obtained are seldom completely specified in the brochures of the manufacturers. There are several examples in literature which show that the performance of a cellulosic artificial kidney membrane can be affected by the composition of the feed (blood) and dialysate. Okada *et al.* [6] found that the transport of phosphate was strongly dependent on the ionic strength in the dialysate. They showed that higher ionic strengths resulted in higher clearance rates. The results were explained by a Donnan exclusion mechanism. Colton *et al.* [7] found that the transport of NaCl was also affected by the overall ionic strength. In Chapter 4 of this thesis it is shown that both creatinine and vitamin B12 adsorb to cellulosic membranes. The adsorption behavior of creatinine is strongly dependent on the ionic strength of the system which indicates that an electrostatic interaction effect is responsible. Celluloses always contain a small number of carboxyl groups which give the material a negative charge. Typical values for cotton cellulose are 1 carboxyl group per 100-500 glucose units [8].

The objective of this chapter is to measure and to compare the diffusive and hydraulic permeabilities of different cellulosic hollow fiber hemodialysis membranes and to study the effect of feed and dialysate composition. Furthermore, the objective is to obtain information about the structure of the membranes.

5.2 Theoretical

According to the tortuous capillary pore model the solute and hydraulic permeabilities of a membrane can be expressed by:

$$P_m = \frac{\varepsilon f(q) K(q) D}{\tau^2 \Delta x} \qquad (1)$$

$$L_p = \frac{\varepsilon R_p^2}{8\eta\tau^2\Delta x} \qquad (2)$$

with:

$$f(q) = \frac{1-2.105q+2.087q^3-1.707q^5+0.726q^6}{1-0.759q^5} \qquad (3)$$

$$K(q) = (1-q)^2 \qquad (4)$$

$$q = \frac{r}{R_p} \qquad (5)$$

and where P_m is the diffusive membrane permeability coefficient, ε the volume porosity of the membrane, D the solute diffusion coefficient in solution, τ the tortuosity factor, Δx the membrane thickness, L_p the hydraulic permeability coefficient, R_p the pore radius, r the solute radius and η the viscosity. Eqn. 1 is based on an equation originally derived by Verniory *et al.* [9]. The factor f(q) in Eqn. 1 and expressed in Eqn. 3 is a wall correction factor as derived by Pappenheimer *et al.* [10] and Renkin [11]. The factor K(q) in Eqn. 1 and expressed in Eqn. 4 is the steric hindrance factor derived by Giddings *et al.* [12]. Eqn. 2 is a modification of the Hagen-Poiseuille equation. The equations are valid for spherical non-interacting solutes in cylindrical pores. Because in the Eqns. 1 and 2 the volume porosity ε is used instead of the surface porosity the tortuosity factor τ has to be taken squared.

Klein *et al.* [13] and Sakai *et al.* [14,15] used the tortuous capillary pore model to evaluate the pore morphology of their membranes. Combination of Eqns. 1 and 2 leads to:

$$\frac{P_m}{L_p} = \frac{f(q)K(q)D8\eta}{R_p^2} \qquad (6)$$

Introduction of measured P_m and L_p data and known values for D and η into Eqn. 6 will yield the pore radius of the membrane by iteration. The equation does not allow the determination of a pore size distribution. Using the calculated pore radius the tortuosity factor τ for cylindrical pores can be calculated assuming that the volume porosity of the membrane is equal to the volume fraction of water. Klein *et al.* [13] pointed out that the method is only valid if the ε/τ^2 term used in the Eqns. 1 and 2 are equal which is true if L_p and P_m can be measured for the same solute, i.e. water and/or tritiated water. Sakai *et al.* [14,15], however, also used other solute/solvent pairs. Their results were found to be only slightly dependent on the solutes used. Typical values reported for low-flux regenerated cellulose membranes are a pore radius of 2-3 nm, a surface porosity of 32% and a tortuosity factor of 2 [13-15].

The tortuosity factor τ is a complex parameter and in practical situations it is often used as a fitting parameter. Wolf and Strieder [16] calculated tortuosity factors for a random fiber bed of overlapping cylinders. A lower-bound for the void tortuosity factor can be calculated from:

$$\tau \geq 1 - \ln(\varepsilon) \qquad (7)$$

5.3 Experimental

Membranes

For the present studies three different types of hollow-fiber cellulosic hemodialysis membranes were used, i.e. low-flux cuprophan® and hemophan® and high-flux RC-HP400A. The low-flux fibers, with a dry wall thickness of 8 μm, were provided by Organon Teknika, Boxtel, The Netherlands. The high-flux RC-HP400A fibers were provided by Enka, Wuppertal, Germany. The cuprophan and high-flux fibers are made of regenerated cellulose. The hemophan fibers are made of a regenerated and modified cellulose. In order to improve its biocompatibility the cellulose has been modified with a small amount of positively charged N,N-di-ethyl-aminoethyl (DEAE) ether groups (1 DEAE group per 100-300 glucose units) [17].

Membrane modules were prepared by potting 150 fibers of 25 cm at both ends in polyurethane (potting length 3 cm). The fiber ends were opened by cutting the potted parts with a scalpel.

Diffusive permeability

For the determination of the diffusive permeabilities the set-up shown in Figure 1 was used [5]. The feed solution was pumped in single-pass through the lumen of the fibers with a Masterflex peristaltic pump (model 7550-62, Masterflex Norprene tubing) with a flow rate of about 0.3 $cm^3.min^{-1}$ (corresponding with a linear flow velocity of about 0.11 $cm.s^{-1}$). For every measurement the exact feed flow rate was determined. The dialysate was pumped with a Verder gear pump with a maximal flow rate of 5 $dm^3.min^{-1}$. The volume of the dialysate container (100 dm^3) was large enough to regard it as 'infinitely large'. For the larger solutes a total feed volume of 0.1 dm^3 was recirculated through the fiber lumen and the concentration change in the feed was followed as a function of time.

The dialysate was heated to 37 °C and left overnight to let dissolved air escape. The feed solution was prepared from the dialysate by dissolving the solute(s) of interest. The feed solution was pre-filtered through a 0.2 μm membrane before use.

A pre-swollen membrane module was mounted in the diffusion cell and the feed was pumped through the module for at least 20 minutes to remove air and to obtain steady-state diffusion. Fibers that were not open were clearly visible and a correction was made for calculation of the total available membrane surface area. All diffusion experiments were performed at 37 °C, the dialysate flow rate was set at 4.2 $dm^3.min^{-1}$. The transmembrane pressure was adjusted to zero by pinching off the tubings.

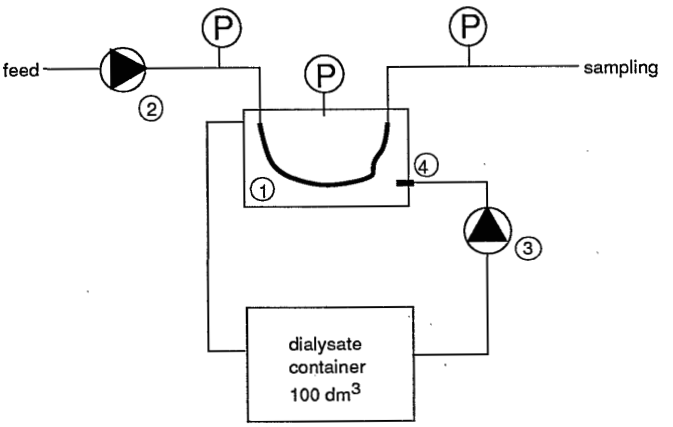

Figure 1 *Experimental set-up for diffusion experiments, 1: diffusion cell (about 1 dm³) with fiber bundle, 2: peristaltic feed pump, 3: gear pump dialysate, 4: dialysate injection nozzle.*

Hydraulic permeability

The hydraulic permeabilities were determined with the set-up shown in Figure 2. The pre-swollen bundle was installed into the set-up and eluted with water to remove air from the fibers and to obtain equilibrium swelling. Then the open end of the bundle was closed and the pressure was adjusted to 20 kPa. The flux was determined from the volume change observed in the buret which was measured after 20 min. All measurements were performed at 37 °C. The deionized water was pre-filtered through a reverse osmosis membrane before use.

Analytical methods

The concentrations of creatinine and vitamin B12 were determined photospectrometrically (Philips, PU 8720 UV/VIS), at 234 and 550 nm, respectively. The concentrations of NaCl were determined with a conductivity meter (Radiometer Copenhagen, CDM3). All other concentrations (polyethylene glycols (PEG), methanol) were determined with an HPLC system consisting of a Waters 610 HPLC pump, a 600E pump controller, a 410 R.I. detector, a column oven and a 746 integrator. A 2 cm³ void loop was used to increase the residence time of the samples.

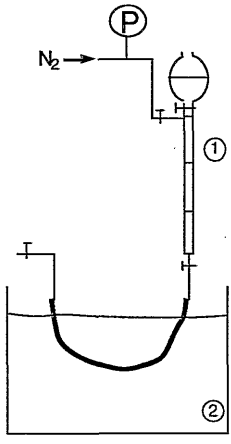

Figure 2 *Experimental set-up for hydraulic permeability measurements, 1: buret, 2: thermostated waterbath with fiber bundle.*

Membrane dimensions

For the determination of the membrane cross-sectional dimensions the water swollen membranes were frozen in a nitrogen slush (mixture of liquid and solid nitrogen) prepared in an Emscope SP2000A system. After breaking the fiber water was sublimated at 193 K for 30 min. Then the sample was sputtered using argon at a pressure of 7 Pa and an electronic current of 20 mA. The sample was transferred under vacuum to the scanning electron microscope (JEOL JSM-T220A) and kept at a temperature of 113 K. Micrographs of the fibers were made at 15 kV and a magnification of 15,000. Membrane dimensions were determined from the micrographs.

Water content of the fibers

The equilibrium water content of the swollen fibers was determined with a centrifuge method based on DIN-53814 [18]. In a small centrifuge tube, a tube provided with a microfiltration membrane in the bottom was mounted (Millipore Ultrafree-MC); this tube was filled with swollen fiber pieces of about 1.5 cm. The material was centrifuged for 20 minutes at 900 g to remove excess water. The water content of the samples was determined from the weight decrease upon drying the centrifuged fibers overnight in a vacuum oven at 80 °C.

Diffusion coefficients

Diffusion coefficients of creatinine and vitamin B12 were determined with a Taylor capillary dispersion technique in a set-up described by Snijder [19]. Diffusion coefficients of the polyethylene glycols were taken from data of Brown and Johnsen [20]. The diffusion coefficient of methanol was taken from Bredereck and Blüher [21]. The diffusion coefficients and the calculated Stokes radii of the solutes are listed below. The viscosity of water at 37 °C is $6.95*10^{-4}$ Pa.s [22]

Table 1 *Diffusion coefficients at 37 °C and Stokes radii of the solutes.*

Solute	D $[m^2.s^{-1}]*10^9$	r_s [nm]
creatinine	1.171 ±0.005	0.28
vitamin B12	0.419 ±0.011	0.78
methanol	1.42	0.23
PEG 200	0.84	0.39
PEG 400	0.57	0.57
PEG 600	0.46	0.71
PEG 1000	0.36	0.90
PEG 1500	0.29	1.12
PEG 2000	0.25	1.30
PEG 3000	0.20	1.60
PEG 4000	0.17	1.90
PEG 6000	0.14	2.29

Carboxyl and DEAE determination

The fiber material was cut into pieces of about 1 mm and washed with water and ethanol to remove residual substances, e.g. glycerol, from the production process. After washing the material was dried in air. The carboxyl group content of the fibers was determined by titration according to the alkalimetric method of Samuelson and Wennerblom [23]. The DEAE content of the hemophan fibers was calculated from the N content as determined by micro element analysis [24]. The N content of the cuprophan and RC-HP400A fibers was used as a blank.

Data reduction

With a single-pass feed flow the overall diffusive permeability is calculated as [5]:

$$P = \frac{Q_b}{A} \cdot \ln\left(\frac{c_{f,i}}{c_{f,o}}\right) \qquad (8)$$

where P is the overall membrane permeability and Q_b the feed flow rate, $c_{f,i}$ and $c_{f,o}$ are the feed concentrations at the feed inlet and outlet and A is the membrane surface area.

The membrane surface area is calculated as the logarithmic mean surface area [25]:

$$A = NL\pi \frac{d_o - d_i}{\ln(d_o/d_i)} \qquad (9)$$

where N is the total number of fibers, L is the wet effective fiber length and d_o and d_i are the wet outer and inner fiber diameter.

With a recirculating feed the overall diffusive permeability is calculated from [5]:

$$\ln(c_{f,t}) = \ln(c_{f,0}) - \frac{P.A.t}{V} \qquad (10)$$

where $c_{f,t}$ and $c_{f,0}$ are the feed concentrations at time t=t and time t=0, respectively, and V is the volume of the feed circuit.

If the dialysate flow velocity is sufficiently high the boundary layer outside the fiber can be neglected and the true membrane permeability is calculated from:

$$\frac{1}{P_m} = \frac{1}{P} - \frac{1}{P_b} \qquad (11)$$

where P_m is the true membrane permeability and P_b the permeability of the boundary layer in the fiber lumen.
The permeability of the boundary layer in the fiber lumen is calculated as [5]:

$$P_b = \frac{4D_b}{d_i} \qquad (12)$$

where D_b is taken as the free diffusion coefficient of the solute in the feed.

Eqn. 12 may be used provided that the following condition is fulfilled [26,27]:

$$Gz_b = \frac{\bar{v}_b d_i^2}{LD_b} < 2.5\text{-}10 \qquad (13)$$

where Gz_b is the Graetz number for the fiber lumen and $\bar{v}_b$ the average liquid velocity in the fiber lumen.

The hydraulic permeability coefficient L_p is calculated as:

$$L_p = \frac{W}{A.\Delta t.\Delta p} \qquad (14)$$

where W is the volume of the collected permeate, Δt the time interval and Δp the applied pressure difference.

5.4 Results and Discussion

Figure 3 shows the overall 'diffusive' resistance (reciprocal permeability) related to the diffusive transport of NaCl through a cuprophan membrane as a function of the dialysate flow rate. For high dialysate flow rates the resistance reaches a plateau value indicating that the influence of the boundary layer at the outside of the fibers is constant. The relative contribution of the boundary layers to the diffusive resistance is most significant for solutes with a high permeability. Since the permeability of the small NaCl is relatively high it appears that also for the other (larger) solutes a flow rate of about 4 $dm^3.min^{-1}$ is high enough to obtain a minimized boundary layer.

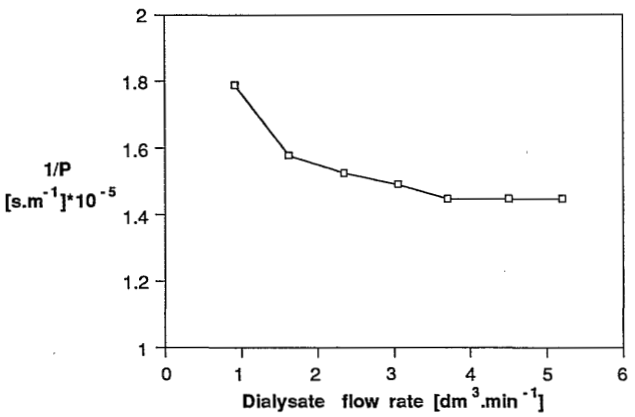

Figure 3 *Overall 'diffusive' resistance (reciprocal permeability) related to the diffusive transport of NaCl through a cuprophan membrane as a function of the dialysate flow rate.*

In Table 2 the dimensions and water content of the swollen fibers are listed. The porosity of the fibers is calculated as the volume fraction of water assuming that the specific density of the cellulose is 1520 kg.m^{-3} [7].

Table 2 *Fiber dimensions, water content and volume porosity of the swollen fibers; data are given ± standard deviation.*

Membrane	d_o [μm]	d_i [μm]	Δx [μm]	H [cm^3.g^{-1}]	ε [-]
cuprophan	244.2 ±2.3	202.2 ±3.2	21.0 ±1.9	1.48 ±0.02	0.692
hemophan	245.6 ±3.6	201.7 ±2.7	21.9 ±2.2	1.57 ±0.02	0.704
RC-HP400A	282.9 ±2.1	215.3 ±2.1	33.7 ±1.1	3.08 ±0.03	0.824

d_o outer fiber diameter
d_i inner fiber diameter
Δx membrane wall thickness
H equilibrium water content
ε volume porosity

In Table 3 the measured diffusive membrane permeabilities for creatinine are given for three different NaCl concentrations in the feed and dialysate. Figure 4 shows the permeability of cuprophan for creatinine as a function of the NaCl concentration. The permeability of cuprophan is strongly dependent on the NaCl concentration. For an isotonic NaCl concentration of 9 g.dm^{-3} the permeabilities of the cuprophan and hemophan fibers are about equal (Table 3). Without NaCl the cuprophan permeability is about three times as high. Also the permeability of the RC-HP400A fibers for creatinine is (somewhat) dependent on the NaCl concentration.

The permeability of the fibers for vitamin B12 is hardly dependent on the NaCl concentration as shown in Table 4.

Table 3 *Measured membrane permeabilities for creatinine as a function of the NaCl concentration [g.dm^{-3}] in the feed and dialysate; data are given ± standard deviation.*

	P_m creatinine [m.s^{-1}]*10^6		
NaCl conc. [g.dm^{-3}]	0	0.6	9
Membrane			
cuprophan	23.8 ±0.71	8.4 ±0.26	8.5 ±0.10
hemophan	8.6 ±0.13	8.9 ±0.22	8.6 ±0.08
RC-HP400A	12.7 ±0.92	10.2 ±0.22	10.3 ±0.17

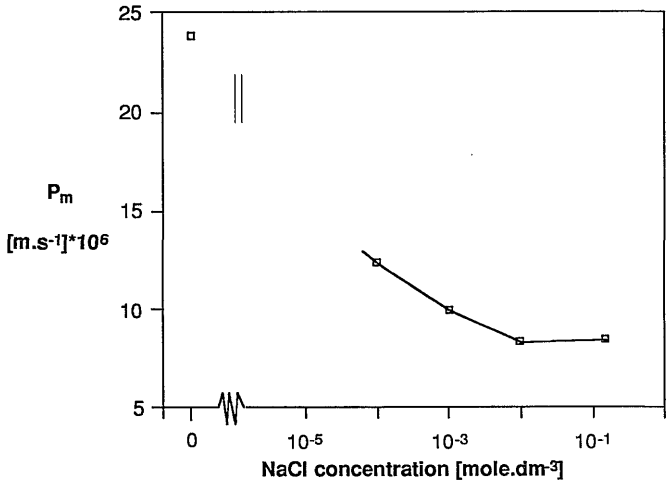

Figure 4 *Permeability of cuprophan to creatinine as a function of the NaCl concentration.*

Table 4 *Measured membrane permeabilities for vitamin B12 as a function of the NaCl concentration [g.dm-3] in the feed and dialysate; data are given ± standard deviation.*

	P_m vitamin B12 [m.s-1]*10^6		
NaCl conc. [g.dm-3]	0	0.6	9
Membrane			
cuprophan	1.03 ±0.00	1.02±0.01	0.95 ±0.01
hemophan	1.11 ±0.02	1.14 ±0.03	1.12 ±0.05
RC-HP400A	2.16 ±0.06	2.13 ±0.03	2.23 ±0.06

In Chapter 4 of this thesis it has been shown that both creatinine and vitamin B12 adsorb to the cellulosic membranes. The adsorption of vitamin B12 is not influenced by the ionic strength. The adsorption of the positively charged creatinine, however, is clearly dependent on the NaCl concentration. For low NaCl concentrations creatinine is strongly adsorbing to the cuprophan and RC-HP400A fibers whereas it is somewhat excluded from the hemophan fibers. On the basis of the adsorption phenomena we concluded that the cuprophan and RC-HP400A fibers are negatively charged and the hemophan due to its modification with DEAE ether groups is positively charged. The net charge of the hemophan fibers is smaller than that of the other fibers. The permeability data of Table 3 confirm these conclusions. It appears that the cuprophan fibers have the highest (negative) charge density. The permeability of hemophan for

creatinine is hardly influenced by the NaCl concentration indicating that it has a low net charge density.

Table 5 gives the measured carboxyl and DEAE group contents of the fibers. These values are in the ranges reported in literature. The cuprophan and RC-HP400A fibers have an almost identical carboxyl group content. The difference is not enough to explain the difference in permeation behavior of creatinine. The hemophan fibers appear to have a lower carboxyl group content, possibly due to the chemical modification treatment. The net charge of the hemophan fibers is about 1 positive charge per 746 glucose units which is indeed significantly less.

Table 5 *Measured carboxyl and DEAE content of the fibers.*

Membrane	COOH [μmole.g^{-1}]	glucose:COOH	N [% w/w]	glucose:DEAE
Cuprophan	33.8	183:1	0.034	-
Hemophan	15.3	403:1	0.067	262:1
RC-HP400A	30.9	200:1	0.034	-

In Table 6 the measured hydraulic permeabilities of the fibers are listed. As expected the high-flux RC-HP400A fibers have a substantially higher permeability than both low-flux fibers.

Table 6 *Measured hydraulic membrane permeabilities; data are given ± standard deviation.*

Membrane	L_p [m^3.m^{-2}.s^{-1}.Pa^{-1}]*10^{11}
cuprophan	1.22 ±0.04
hemophan	1.32 ±0.05
RC-HP400A	7.53 ±0.43

Pore size determination

Table 7 shows the calculated membrane structure parameters based on Eqn. 6 and the permeability data for creatinine in a solution of 9 g.dm^{-3} NaCl and the vitamin B12 permeability data in a solution without NaCl. In particular the parameters of the low-flux fibers are reasonably consistent. The parameters of the low-flux fibers are close to the data reported in literature for regenerated cellulose membranes. The high-flux fiber has a larger pore radius and a smaller tortuosity factor as may be expected for a more swollen network. The

last column of Table 7 gives the lower limit values for the tortuosity factors calculated from Eqn. 7. This equation indeed predicts smaller values for the tortuosity factor than the ones calculated on the basis of Eqn. 6 and the water content.

Table 7 *Calculated structure parameters obtained by fitting hydraulic and diffusive permeability data for creatinine and vitamin B12 to Eqn. 6.*

Membrane	creatinine			vitamin B12			
	R_p [nm]	τ [-]	ε/τ [-]	R_p [nm]	τ [-]	ε/τ [-]	τ (Eqn. 7)
cuprophan	2.49	1.74	0.40	2.73	1.90	0.36	1.37
hemophan	2.57	1.70	0.41	2.72	1.80	0.39	1.37
RC-HP400A	5.61	1.36	0.61	4.68	1.13	0.73	1.19

In order to study the relation between membrane permeability and the size of the solute molecules, solutes are needed which do not adsorb. Since both creatinine and vitamin B12 adsorb to the cellulosic membranes these are in fact not suitable for this purpose. In Chapter 4 of this thesis it has been shown that polyethylene glycols, dextranes and (oligo)saccharides are suitable for application in the inverse size exclusion chromatography technique. Figure 5 shows the membrane permeabilities of the fibers for a range of polyethylene glycols and for methanol. Permeabilities for creatinine (9 $g.dm^{-3}$ NaCl) and vitamin B12 (0 $g.dm^{-3}$ NaCl) are also included. Most solutes do fit a smooth curve. Only vitamin B12 clearly deviates which may be an indication for adsorption. The permeabilities of the low-flux fibers are almost identical. The differences between the low- and high flux fibers are most prominent for the larger solutes.

In principle the permeability data of Figure 5 can give information about the pore morphology of the membranes. The problem, however, is that two parameters are unknown, i.e. the pore size (distribution) and the tortuosity factor. In Figure 6 the factors $f(q).K(q)/\tau^2$ are drawn as a function of the Stokes radii of the solutes. The lines in Figure 6 indicate the calculated values based on the structure parameters for creatinine of Table 7. For the larger solutes and low-flux membranes the pore model predicts too low values. Two explanations may be given for this deviation. It may be that the flexible polyethylene glycol molecules deform in the smaller pores so that the effective size of the polyethylene glycol molecules is smaller. Casassa [28] has shown that flexible macromolecules can penetrate pores that are smaller than the equilibrium size of the macromolecule in solution. The other possibility is that the effective pore size is dependent on the molecular size of the solute. This may be an indication for the existence of a distribution of pores instead of one single

pore size. Large molecules can only permeate through the larger pores of the membranes while small molecules can permeate through both the small and the large pores. Small pores do not contribute to the transport of large molecules which means that the effective pore size (and the overall porosity) obtained from permeation experiments must depend on the dimensions of the solute molecule. The effect will be most prominent when the solute size approaches the pore size.

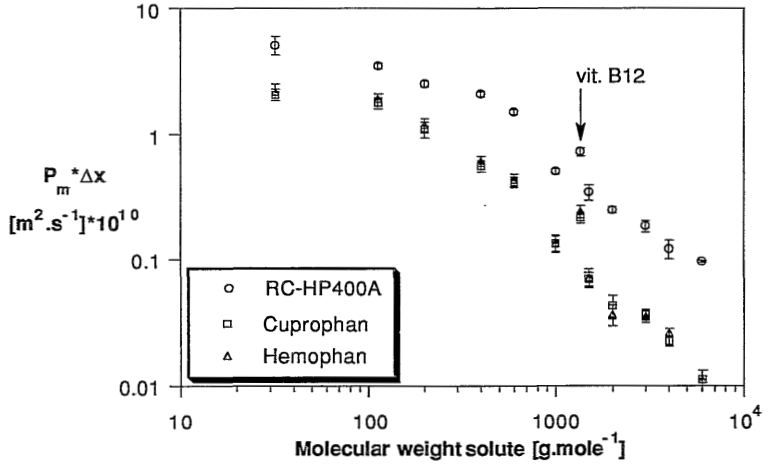

Figure 5 *Permeabilities of the membranes (corrected for membrane thickness) for different molecules as a function of the molecular weight. Error bars indicate the standard deviations.*

By providing the tortuosity values of Eqn. 7 (Table 7, last column) lower bound values for the pore sizes of the membranes can be calculated from the data of Figure 6. Figure 7 shows the calculated pore radii as a function of the Stokes radii of the tracer molecules. It appears indeed that the calculated pore radius is *not* independent of the Stokes radius of the solute. The apparent pore size increases with the size of the solute indicating that the membranes may have a distribution of pores. The pore radii of Figure 7 are somewhat smaller than the pore radii shown in Table 7. This can be explained by the fact that lower bound values for the tortuosity factor were assumed.

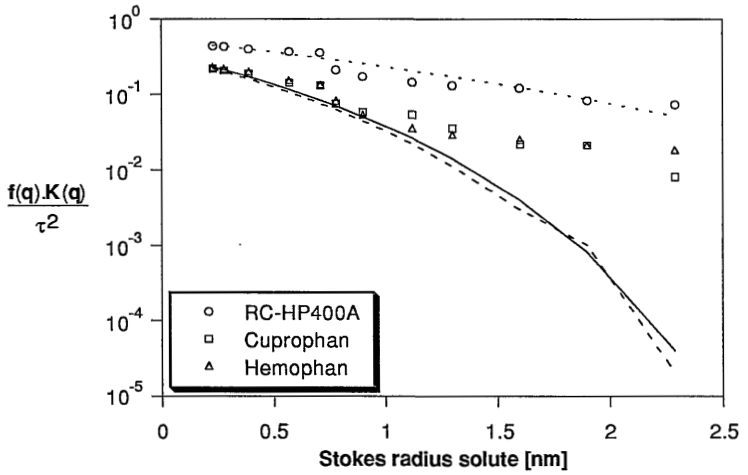

Figure 6 *Factor f(q).K(q) / τ² as a function of the Stokes radii of the solutes. The lines indicate the calculated values based on the parameters for creatinine from Table 7.*

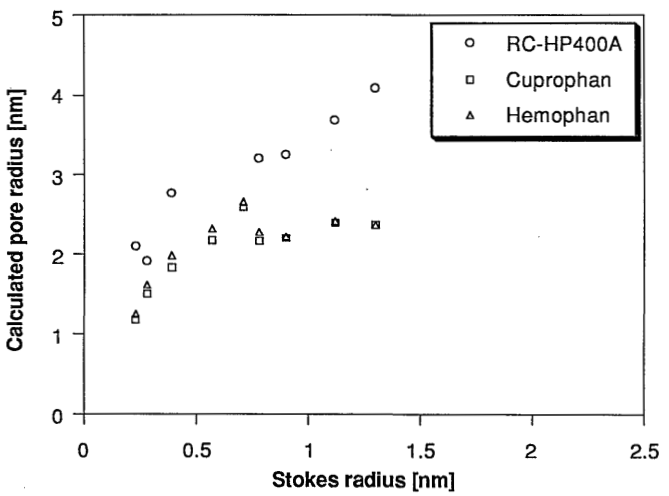

Figure 7 *Calculated pore radii as a function of the Stokes radii of the solutes.*

5.5 Conclusions

The membranes used in this study show clear differences in permeability. The more swollen high-flux RC-HP400A fiber has a higher diffusive and hydraulic permeability. The permeation of creatinine through cuprophan (and to a lesser extent through RC-HP400A) is strongly dependent on the NaCl concentration in feed and dialysate. It appears that the cuprophan fibers have the highest (negative) charge density whereas the hemophan fibers have a slightly positive charge.

The permeation data can be used to obtain information about the pore sizes of the membranes. Fitting of the permeability data to the tortuous capillary pore model as proposed by Klein *et al.* yields values for the membrane parameters which are close to data reported in literature. The RC-HP400A fibers have a larger pore size and a smaller tortuosity.

Permeability data for several polyethylene glycols are also fitted to the tortuous capillary pore model. Lower bound values for the tortuosity factor are provided. It appears that the calculated pore size increases with the size of the solute molecules which may be an indication for the existence of a distribution of pores.

5.6 Symbols

A	total membrane surface area defined by Eqn. 9 [m^2]
$c_{f,i}$	feed concentration at inlet [$mole.m^{-3}$]
$c_{f,o}$	feed concentration at outlet [$mole.m^{-3}$]
$c_{f,0}$	feed concentration at time zero [$mole.m^{-3}$]
$c_{f,t}$	feed concentration at time t [$mole.m^{-3}$]
D	diffusion coefficient in solution [mole.m-3]
D_b	diffusion coefficient in the feed [$m^2.s^{-1}$]
d_o	outer fiber diameter [m]
d_i	inner fiber diameter [m]
f(q)	wall correction factor defined by Eqn. 3 [-]
Gz_b	Graetz number for the fiber lumen [-]
K(q)	steric hindrance distribution coefficient defined by Eqn. 4 [-]
L	effective fiber length [m]
L_p	hydraulic membrane permeability [$m^3.m^{-2}.s^{-1}.Pa.^{-1}$]
N	number of fibers in the bundle [-]
P_b	permeability boundary layer in the fiber lumen [$m.s^{-1}$]
P	overall membrane permeability [$m.s^{-1}$]
P_m	true membrane permeability [$m.s^{-1}$]
Δp	applied pressure difference [Pa]
Q_b	feed flow rate [$m^3.s^{-1}$]
q	ratio of solute radius and pore radius [-]
R_p	pore radius [m]
r	solute radius [m]

r_s	Stokes radius solute [m]
Δt	time interval [s]
v_b	average liquid velocity in the fiber lumen [-]
V	volume of the feed circuit [m^3]
W	collected volume of permeate [m^3]
Δx	membrane thickness [m]
ε	membrane volume porosity [-]
η	viscosity [Pa.s]
τ	membrane tortuosity factor [-]

5.7 References

[1] J.F. Stevenson, *Unsteady mass transfer in a long composite cylinder with interfacial resistances*, Am. Inst. Chem. Eng. J., 20 (1974) 461-466

[2] J.F. Stevenson, M.A. von Deak, M. Weinberg, R.W. Schuette, *An unsteady state method for measuring the permeability of small tubular membranes*, Am. Inst. Chem. Eng. J., 21 (1975) 1192-1199

[3] J.F. Stevenson, J.S. Parry, K.M. Gupta, *Hydraulic permeability of hollow-fiber membranes*, J. Biomed. Mater. Res., 12 (1978) 401-419

[4] S.M. Dinh, J.F. Stevenson, *A transient experiment to measure the diffusive permeability of hollow fiber membranes*, J. Membrane Sci., 11 (1982) 127-145

[5] E. Klein, F. Holland, A. Lebeouf, A. Donnaud, J.K. Smith, *Transport and mechanical properties of hemodialysis hollow fibers*, J. Membrane Sci., 1 (1976) 371-396

[6] M. Okada, T. Watanabe, K. Imamura, T. Tsurumi, Y. Suma, K. Sakai, *Ionic strength affects diffusive permeability to an organic phosphate ion of negatively charged dialysis membranes*, Trans. Am. Soc. Artif. Internal Organs, 36 (1990) 324-327

[7] C.K. Colton, K.A. Smith, E.W. Merrill, P.C. Farrell, *Permeability studies with cellulosic membranes*, J. Biomed. Mater. Res., 5 (1971) 459-488

[8] H. Krässig, R.G. Steadman, K. Schliefer, W. Albrecht, *Cellulose*, In: W. Gerhartz et al. (eds.), Ullmann's encyclopedia of industrial chemistry, Weinheim, VCH, 5th edition, vol. A5, 1986, p. 375-418

[9] A. Verniory, R. Du Bois, P. Decoodt, J.P. Gassee, P.P. Lambert, *Measurement of the permeability of biological membranes*, J. Gen. Physiol., 62 (1973) 489-507

[10] J.R. Pappenheimer, E.M. Renkin, L.M. Borrero, *Filtration, diffusion, and molecular sieving through capillary membranes. The pore theory of capillary permeability*, Am. J. Physiol., 167 (1951) 13-46

[11] E.M. Renkin, *Filtration, diffusion, and molecular sieving through porous cellulose membranes*, J. Gen. Physiol., 38 (1954) 225-243

[12] J.C. Giddings, E. Kucera, C.P. Russell, M.N. Myers, *Statistical theory for the equilibrium distribution of rigid molecules in inert porous networks. Exclusion chromatography*, J. Phys. Chem., 72 (1968) 4397-4408

[13] E. Klein, F.F. Holland, K. Eberle, *Comparison of experimental and calculated permeability and rejection coefficients for hemodialysis membranes*, J. Membrane Sci., 5 (1979) 173-188

[14] K. Sakai, S. Takesawa, R. Mimura, H. Ohashi, *Structural analysis of hollow fiber dialysis membranes for clinical use*, J. Chem. Eng. Jpn., 20 (1987) 351-356

[15] K. Sakai, H. Chiba, A. Naitoh, *Determination of the pore radius of regenerated cellulose membranes by a dyeing technique*, J. Membrane Sci., 37 (1988) 101-112

[16] J.R. Wolf, W. Strieder, *Surface and void tortuosities for a random fiber bed: overlapping, parallel cylinders of several radii*, J. Membrane Sci., 49 (1990) 103-115

[17] Enka, manufacturer information

[18] DIN 53814, *Bestimmung des Wasserrückhaltevermögens von Fasern und Fadenabschnitten*, October 1974

[19] E.D. Snijder, M.J.M. te Riele, G.F. Versteeg, W.P.M. van Swaay, *Diffusion coefficients of several aqueous alkanolamine solutions*, J. Chem. Eng. Data, 38 (1993) 475-480

[20] W. Brown, R.M. Johnsen, *Transport from an aqueous phase through cellulosic gels and membranes*, J. Appl. Polym. Sci., 26 (1981) 4135-4148

[21] K. Bredereck, A. Blüher, *Porenstrukturbestimmung von Cellulosefasern durch Ausschlußchromatographie. Grundlagen und Anwendungsbeispiele für Quellbehandlungen und Hochveredlung von Baumwollgewebe*, Melliand Textilber., 73 (1992) 652-662

[22] R.C. Weast (ed.), *Handbook of Chemistry and Physics*, Cleveland OH, Chemical Rubber Co., 52 edn., 1971

[23] O. Samuelson, *Determination of carboxyl groups*, In: R.L. Whistler (ed.), Methods in carbohydrate chemistry, volume 3: Cellulose, New York etc., Academic Press, 1963, p. 31

[24] E. Pella, B. Colombo, *Simultaneous C-H-N and S microdetermination by combustion and gas chromatography*, Mikrochimica Acta I, (1978) 271-286

[25] J.E. Sigdell, *Calculation of combined diffusive and convective mass transfer*, Int. J. Artif. Organs, 5 (1982) 361-372

[26] J.E. Sigdell, *A mathematical theory for the capillary artificial kidney*, Stuttgart, Hippokrates Verlag, 1974

[27] W.J. Beek, K.M.K. Muttzall, *Transport phenomena*, London, Wiley, 1975, Chapter 3

[28] E.F. Casassa, *Equilibrium distribution of flexible polymer chains between a macroscopic solution phase and small voids*, J. Polym. Sci.: Polym. Lett., 5 (1967) 773-778

6

CHARACTERIZATION OF CELLULOSIC HEMODIALYSIS MEMBRANES: MEMBRANE STRUCTURE AND FUNCTION

6.1 Introduction

The characterization of membranes may serve two goals. Firstly, to get a detailed knowledge about the membrane structure and its relation to the production process. Secondly, to obtain a firm basis for the development of consistent membrane performance theories.

Both goals would benefit from the existence of fast, effective characterization techniques that give relevant and detailed information about the structure of the membranes. Preferably, at least some of the techniques should *not* be based on performance measurements to obtain structure parameters which are not performance related as well. In the ideal case the combination of several characterization techniques will yield a consistent set of data describing the structure of the membrane.

Nowadays various membrane characterization techniques based on different principles are available. The specific features of a certain membrane will determine which of the characterization techniques may be applied. When a dry cellulosic membrane is brought in contact with water it swells, thereby increasing the inter-fibrillar distance of the cellulose chains. As a result, water filled channels or pores are formed through which mass transport can occur. For the characterization of cellulosic membranes it is essential to use wet-state characterization techniques since otherwise misleading information, i.e. information about the non- or partly swollen membrane, will be obtained. The characteristic size of the pores in swollen cellulosic dialysis membranes is a few nanometers. For low-flux cuprophan membranes typical data reported are a pore radius of 2-3 nm, a surface porosity of 32% and a tortuosity factor of 2 [1-3]. These data were derived from mass transport measurements. The choice for a specific characterization technique is further restricted by the minimal and maximal pore size that can be measured. Cellulosic hemodialysis membranes are often isotropic, i.e. these membranes have no densified skin layer. For the purpose of characterization this is advantageous since the properties of the membrane are achieved over the complete membrane cross-section. In short, owing to the specific features of cellulosic dialysis membranes only a limited number of the existing characterization techniques can be used [4].

The aim of this chapter is to discuss the results of three different

membrane characterization techniques: (1) calorimetry/ thermoporometry, (2) inverse size exclusion chromatography (i-SEC) and (3) mass transport measurements.

6.2 Experimental

For the studies presented here three different hollow-fiber cellulosic membranes were used: low-flux cuprophan® and hemophan® and high-flux RC-HP400A. The cuprophan and RC-HP400A fibers are made of regenerated cellulose. The hemophan fibers are made of regenerated and modified cellulose. Here the cellulose has been modified with a small amount of positively charged N,N-di-ethyl-aminoethyl (DEAE) ether groups (1 DEAE group per 100-300 glucose units).

The characterization techniques used are described extensively in Chapter 3 (thermoporometry), Chapter 4 (i-SEC) and Chapter 5 (mass transport measurements).

6.3 Results and discussion

Figure 1 shows the elution curves of the membranes obtained with the i-SEC technique. The dashed horizontal lines indicate the contents of non-freezing water of the membranes as measured with calorimetry/ thermoporometry. Though the i-SEC and calorimetry measurements are performed at different temperatures (70 °C and ≤0 °C, respectively), it appears from Figure 1 that a substantial part of the non-freezing water in the membranes is accessible to solutes. The dashed horizontal lines and arrows in the figures indicate the amount of non-freezing water in the membranes. The smaller tracers have an accessible pore volume which is larger than the freezing water content, thus the non-freezing water of the membranes is at least partly accessible to solutes. In literature, it is often assumed that the non-freezing or bound water does not, or to a lesser extent, contribute to the transport of permeants [5-7].

The curved lines in Figure 1 represent the i-SEC curves calculated on the basis of the determined pore radius R_p and the pore volume V_p as listed in Table 1. Most data points do fit the calculated curves. In Chapter 4 of this thesis we reported that the pore volume distributions of the membranes are probably very narrow. The elution curves of Figure 1 are in fact best described by a homoporous pore volume distribution. The pore radii in Table 1 are (somewhat) larger than the values reported in literature. It can be seen from Figure 1 that vitamin B12 adsorbs to the membranes. The accessible pore volumes for vitamin B12 are 10-25% larger than expected on the basis of its size.

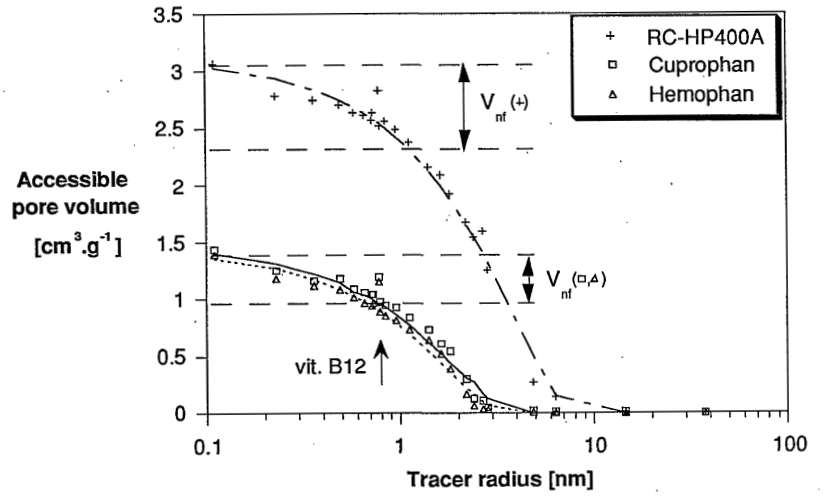

Figure 1 *Inverse size exclusion elution curves. The dashed horizontal lines (V_{nf}) indicate the non-freezing water content of the membranes. The curves through the data points indicate the calculated i-SEC curves based on the pore volume V_p and the pore radius R_p shown in Table 1.*

Table 1 *Measured membrane structure parameters.*

Membrane	H [cm³.g⁻¹]	V_p [cm³.g⁻¹]	V_{nf} [cm³.g⁻¹]	R_p [nm]
cuprophan	1.48	1.48	0.48	4.1
hemophan	1.57	1.45	0.47	3.7
RC-HP400A	3.08	3.11	0.73	8.2

H equilibrium water content per g dry polymer, centrifuge method
V_p pore volume per g dry polymer, i-SEC
V_{nf} non-freezing water content from thermoporometry
R_p pore radius from i-SEC

In Chapter 3 of this thesis it has been shown that the thermoporometry technique is not suitable for the determination of the pore size distributions of cellulosic hemodialysis membranes due to the anomalous recrystallization of water. Some information on the pore structure, however, can be obtained using DSC measurements. Figure 2 shows the pore volume distributions for samples with a water content of about 30% below the equilibrium water content of the membranes. The equilibrium water content of the membranes was determined from the weight decrease upon drying of centrifuged samples as described in

the Chapters 3-5. Water contents below the equilibrium value were obtained by equilibrating water swollen samples with the vapor of KCl solutions with different concentrations. Figure 2 shows clearly the differences between the pore size distributions of the low- and the high-flux membranes, i.e. between cuprophan or hemophan and RC-HP400A. The maximum of the pore volume distribution curves is at a pore radius of about 3 nm for all the membranes investigated. The low-flux fibers appear to have pores with radii between 2 and 10 nm. The high-flux RC-HP400A membrane also has larger pores. The maximum of the pore volume distribution at 3 nm is higher for the high-flux fibers. The pore radii determined with the i-SEC technique fall within the ranges for the pore radii obtained with thermoporometry. The thermoporometry results do not confirm the hypothesis that the pore size distributions of the membranes are very narrow or homoporous. It seems as if the high-flux membrane has a substantial amount of large pores. This result, however, is probably caused by the anomalous freezing of the pore water during the thermoporometry measurements (Chapter 3).

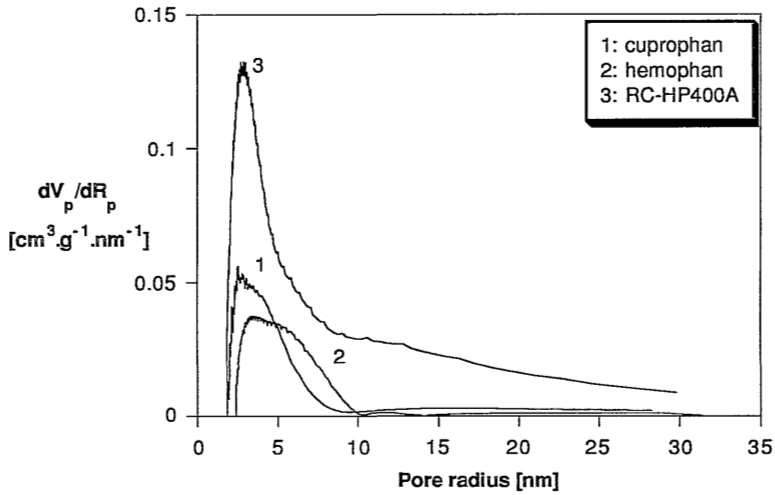

Figure 2 *Differential pore volume distributions determined with thermoporometry.*

Integration of the curves in Figure 2 yields values for the 'DSC' pore volume of the membrane. Because the non-freezing water of the membranes is accessible to solutes it is reasonable to add the non-freezing water content to the pore volume determined by DSC for calculation of the total pore volume of the membranes. The calculated pore volumes, shown in Table 2, are clearly smaller than the values given in Table 1. The difference can be explained partly

by the fact that the water content of the thermoporometry samples is about 30% below the equilibrium water content of a fully swollen sample. The rest of the difference can be explained by the fact that a substantial amount of water in the membranes melts (according to the DSC measurements) at temperatures ≥0 °C. As described in Chapter 3 the melting of ice at these temperatures is very probably caused by an artefact that can be attributed to the anomalous freezing and melting of water in cellulosic membranes. As a consequence, this melting of ice can not be attributed to the melting of ice in pores of a certain size because the thermoporometry relations are only valid for temperatures below 0 °C. This is the reason that the thermoporometry technique can not be applied for the determination of the pore size distributions of swollen cellulosic membranes.

Table 2 *Membrane structure parameters measured by thermoporometry.*

Membrane	V_{pf} [$cm^3.g^{-1}$]	$V_{pf}+V_{nf}$ [$cm^3.g^{-1}$]	V_s [$cm^3.g^{-1}$]	H [$cm^3.g^{-1}$]
cuprophan	0.23	0.71	1.13	1.48
hemophan	0.21	0.68	1.26	1.57
RC-HP400A	0.86	1.59	2.36	3.08

V_{pf} water content of water melting below -1 °C
V_{nf} non-freezing water content from thermoporometry
V_s water content of the thermoporometry sample used
H equilibrium water content for fully swollen sample

Table 3 shows the calculated membrane structure parameters obtained by fitting diffusive and hydraulic permeability data to the tortuous capillary pore model as described in Chapter 5 of this thesis. The data of Table 3 agree rather well with data reported in literature which were obtained in the same way. The calculated pore radii are smaller than the values obtained from the i-SEC technique. The listed parameters are based on the assumption that an average effective pore size exists. This is only reasonable if the pore size distributions are relatively narrow or if the mass transport is not too sensitive towards the membrane structure. In Chapter 5 we have shown that the parameters of Table 3 can not predict the diffusive permeation behavior of the larger solutes. This may be an indication for the existence of a distribution of pores. With a pore size distribution the average effective pore size will be dependent on the size of the permeant.

Table 3 *Calculated pore radius, tortuosity and surface porosity obtained by fitting hydraulic and diffusive permeability data for creatinine to the tortuous capillary pore model.*

Membrane	R_p [nm]	τ [-]	ε/τ [-]
Cuprophan	2.49	1.74	0.40
Hemophan	2.57	1.70	0.41
RC-HP400A	5.61	1.36	0.61

τ tortuosity factor
ε/τ surface porosity

Figure 3A shows the measured diffusive permeabilities of the membranes for various polyethylene glycols, methanol, creatinine and vitamin B12. The permeabilities are plotted versus the size of the permeants, as estimated for the i-SEC technique (Chapter 4, Table 1). The size of the permeants was determined using a calibrated SEC column. The results do not fit smooth curves as expected on the basis of the i-SEC data shown in Figure 1. Figure 3B shows the measured permeabilities as a function of the Stokes radii of the permeants (Chapter 5, Table 1). In this case the measured permeabilities do fall on smooth curves. It appears from Figures 3A and 3B that the effective size of the permeants, i.e. the polyethylene glycols (PEG), is different for the i-SEC and the diffusive permeation process. With i-SEC the effective radii of the polyethylene glycols are 24-87% larger than the Stokes radii. The discrepancy is most significant for the smaller PEG molecules. The radii of the polyethylene glycols are estimated from an equation of Squire [8] based on data for a calibrated, commercially available, SEC column. Squire reported already the existence of a discrepancy between the Stokes radii and the radii based on SEC data. He explained this by deformation (owing to the pressure drop over the column) of the PEG molecules during the size exclusion process. However, as mentioned, the discrepancy is most prominent for the smaller PEG molecules while especially large molecules will be sensitive to deformation. Furthermore, deformation will most likely result in an effective solute size which is smaller.

The discrepancy in the radii of the PEG molecules may explain why larger pore radii are found with the i-SEC technique. The average PEG radius calculated from the equation of Squire is roughly 50% larger than the corresponding Stokes radii. If this ratio is taken into account the calculated pore radii shown in Table 1 will be about 2.6 nm for the low-flux membranes and 5.5 nm for the high-flux membranes. These values correspond very well with the data shown in Table 3. It is obvious that the correction procedure is only qualitative since for the i-SEC measurements also other tracer molecules, e.g. dextrans and oligosaccharides, were used.

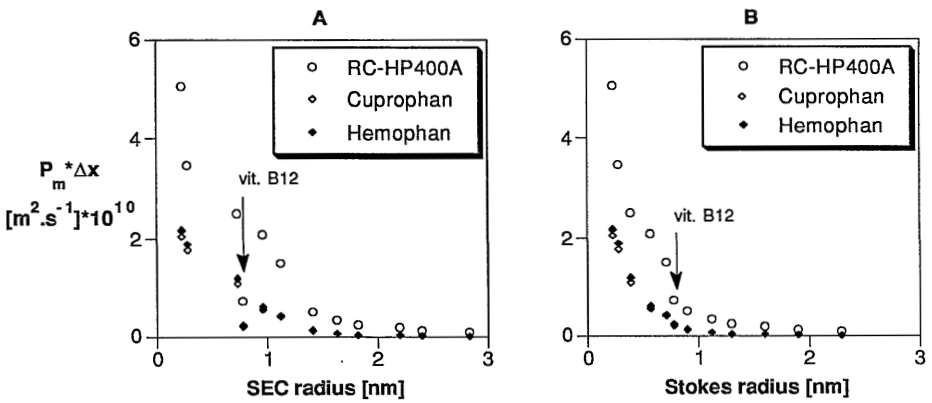

Figure 3A/B *Diffusive membrane permeabilities (corrected for the membrane thickness) as a function of the SEC radii (A) and of the Stokes radii (B) of the solutes.*

With the measured membrane parameters it is possible to predict the retention behavior of the membranes. The calculations are shown in appendix A. These calculations show that the estimated cut-off of the RC-HP400A membrane is significantly larger than 100 kg.mole^{-1}. This implies that the membrane should show a significant extent of protein leakage. According to the specifications of Enka the high-flux membranes have a retention for the protein Bovine Serum Albumine (M=69 kg.mole^{-1}) of more than 95%. As one realizes, a substantial leakage of protein during the blood purification process would be highly undesirable. The explanation for non-leakage may be that the RC-HP400A membrane is not isotropic but has a thin densified skin layer. Such a skin would probably not be detected by the used techniques because the pore volume of the skin is negligible. In appendix A it is shown that *with* a skin the cut-off of the RC-HP400A membrane drops to values comparable with those of the low-flux membranes whereas the diffusive permeability of the membrane is hardly affected.

Although it was shown in Figure 1 that vitamin B12 adsorbs to the membranes, no increased permeability to B12 can be observed from the Figures 3A or 3B. Adsorption of a solute may result in an enhanced permeability of the solute because its average concentration in the membrane is higher. If, however, the interaction energy of solute and membrane is very high the transport of the solute will be hindered until the membrane becomes saturated with the solute. If, because of the adsorption, pore blocking occurs the transport of solutes may be irreversibly hindered.

Figure 4 shows the permeability of cuprophan to creatinine and the elution volume of creatinine for a cuprophan i-SEC column as a function of the

NaCl concentration. The trend in creatinine permeability follows the dependence of the elution volume on the NaCl concentration. Hence, the decrease in permeability is caused by a decrease in adsorption. In Chapters 4 and 5 we have shown that the salt dependence of the permeability to creatinine is caused by an electrostatic interaction effect. If a Donnan exclusion mechanism is assumed, the extent of interaction can be predicted from the charge density of the membranes (see appendix B). Figure 5 shows the calculated adsorption factors together with some measured data (i-SEC). In the calculations we did not consider non-ideality. It appears that the trends in adsorption behavior are predicted reasonably well.

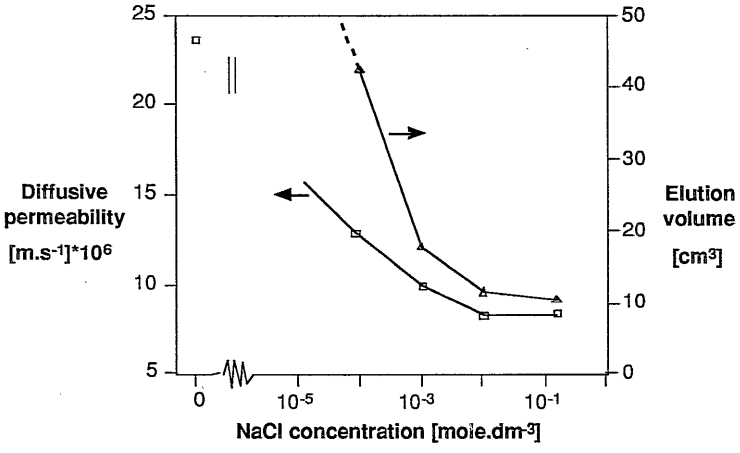

Figure 4 *Permeability of cuprophan to creatinine and the elution volume of creatinine for a cuprophan i-SEC column as a function of the NaCl concentration.*

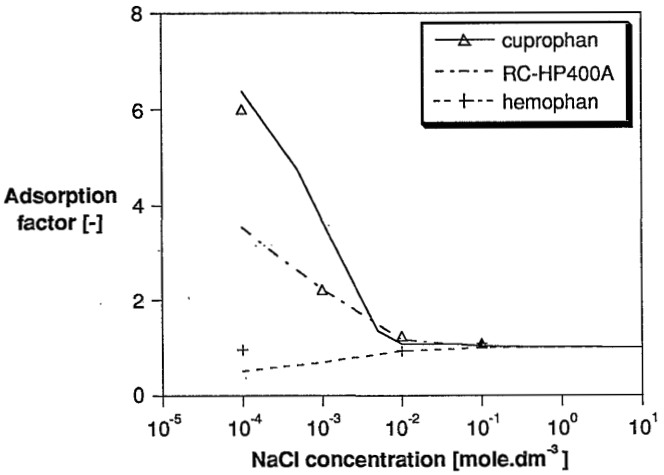

Figure 5 *Adsorption factors of the membranes as a function of the NaCl concentration. The lines indicate the calculated adsorption factors based on a Donnan exclusion mechanism (see appendix B).*

6.4 Conclusions

The applied characterization techniques all give relevant information about the structure of swollen cellulosic membranes. There is, however, some discrepancy between the results of the methods.

With the i-SEC technique very sharp, i.e. homoporous, pore volume distributions are found. Thermoporometry and the mass transport measurements do not confirm this. Thermoporometry gives too small values for the porosity of the membranes.

The i-SEC yields somewhat larger values for the pore radii of the membranes than the mass transport measurements. The difference can be explained by the difference in characteristic size of the PEG molecules for the size exclusion and diffusion process.

From a combination of the thermoporometry and i-SEC results it is shown that the non-freezing water of cellulosic membranes is at least partly accessible to solutes.

Both test molecules creatinine and vitamin B12 adsorb to the membranes. Despite the fact that the accessible pore volume to vitamin B12 is about 10-25% higher than expected on the basis of its size no enhanced diffusive permeability was found. The adsorption and the transport of vitamin B12 are

not dependent on the NaCl concentration.

Creatinine is strongly adsorbing at the cuprophan membranes at low NaCl concentration. The trends in adsorption can be explained qualitatively by a Donnan exclusion mechanism.

It is shown that the performance of the cellulosic membranes is dependent on the morphology as well as on the interaction with the membranes. For the purpose of characterization it is therefore important to specify the conditions under which the results were obtained.

6.5 References

[1] E. Klein, F.F. Holland, K. Eberle, *Comparison of experimental and calculated permeability and rejection coefficients for hemodialysis membranes*, J. Membrane Sci., 5 (1979) 173-188

[2] K. Sakai, S. Takesawa, R. Mimura, H. Ohashi, *Structural analysis of hollow fiber dialysis membranes for clinical use*, J. Chem. Eng. Jpn., 20 (1987) 351-356

[3] K. Sakai, H. Chiba, A. Naitoh, *Determination of the pore radius of regenerated cellulose membranes by a dyeing technique*, J. Membrane Sci., 37 (1988) 101-112

[4] Chapter 2 of this thesis

[5] T. Hori, *The role of water in the dyeing process*, Text. Chem. Colorist, 18 (1986) 19-25

[6] N. Nishioka, S. Yoshimi, T. Iwaguchi, K. Kosai, *Permeability through cellulose membranes grafted with vinyl monomers in homogeneous system II States of water in acrylonitrile grafted cellulose membranes*, Polym. J., 16 (1984) 877-885

[7] S. Wisniewski, S.W. Kim, *Permeation of water-soluble solutes through poly(2-hydroxyethyl methacrylate) and poly(2-hydroxyethylmethacrylate) crosslinked with ethylene glycol dimethacrylate*, J. Membrane Sci., 6 (1980) 299-308

[8] P.G. Squire, *Calculation of hydrodynamic parameters of random coil polymers from size exclusion chromatography and comparison with parameters by conventional methods*, J. Chromatogr., 210 (1981) 433-442

6.6 Appendix A. Effect of membrane structure on solute retention

On the basis of the measured membrane structure parameters it is possible to estimate the retention behavior of the membranes using the capillary pore model [1-3].

The retention coefficient R is related to the Staverman reflection coefficient σ and the trans-membrane Peclet number β by the Spiegler-Kedem equation.

$$R = \frac{\sigma(\exp(\beta) - 1)}{\exp(\beta) - \sigma} \qquad \text{(A1)}$$

When the solute transport is convective, i.e., the transmembrane Péclet number is high, the retention coefficient approaches the Staverman reflection coefficient.
The transmembrane Péclet number is given by:

$$\beta = J_v(1 - \sigma)/P_m \qquad \text{(A2)}$$

where J_v is the solvent flux through the membrane and P_m is the diffusive permeability coefficient.
The solvent flux J_v is calculated from:

$$J_v = \frac{\varepsilon . R_p^2 . \Delta p}{8\eta . \tau^2 . \Delta x} \qquad \text{(A3)}$$

where ε is the volume porosity of the membrane, R_p the pore radius of the membrane, Δp the applied pressure difference, η the solvent viscosity, τ the tortuosity factor and Δx the membrane thickness.
The solute permeability P_m is calculated as:

$$P_m = \frac{\varepsilon . D . f(q) . S_d(q)}{\tau^2 . \Delta x} \qquad \text{(A4)}$$

with:

$$f(q) = \frac{1 - 2.105q + 2.0865q^3 - 1.7068q^5 + 0.72603q^6}{1 - 0.75857q^5} \qquad \text{(A5)}$$

$$S_d(q) = (1 - q)^2 \qquad \text{(A6)}$$

$$q = \frac{r}{R_p} \qquad \text{(A7)}$$

where r is the solute radius and D is the diffusion coefficient of the solute in the solvent.
The Staverman reflection coefficient is given by:

$$\sigma = 1 - g(q) . S_f(q) \qquad \text{(A8)}$$

with:

$$g(q) = \frac{1 - 0.67q^2 - 0.20217q^5}{1 - 0.75857q^5} \qquad \text{(A9)}$$

$$S_f(q) = 2(1-q)^2 - (1-q)^4 \qquad \text{(A10)}$$

The diffusion coefficient in solution D and the radius r of the solutes are related to the molecular weight M of the solutes:

$$r = \sqrt[3]{\frac{3M}{4\pi . \rho . N_a}} \qquad \text{(A11)}$$

$$D = \frac{RT}{6\pi . \eta . N_a . \rho} \qquad \text{(A12)}$$

where ρ is the density of the solute, N_a is Avogadro's number, R the gas constant and T the temperature.

Figure A1 shows the calculated retention curves as a function of the molecular weight of the solutes. The solid lines indicate the retention curves based on the structure parameters obtained with the i-SEC method (Table 1). The dashed lines indicate the retention curves based on the structure parameters obtained with mass transport measurements (Table 3). On the basis of the structure parameters obtained from i-SEC and mass transport measurements significant differences in the retention curves are predicted. The well-known cut-off value is often defined as the molecular weight for which the retention of the membrane is 90%. Table A1 shows the estimated values for the cut-off of the membranes. Both estimates for the cut-off of the RC-HP400A membrane are more than 100 kg.mole^{-1}. This implies that the membranes should show a significant extent of protein leakage. However, according to the specification sheets of Enka the high-flux membranes have a retention for the protein Bovine Serum Albumine (M=69 kg.mole^{-1}) of more than 95%. Furthermore, a substantial leakage of protein during the blood purification process would be highly undesirable. It may be that the RC-HP400A membranes are not isotropic but have a (thin) skin layer.

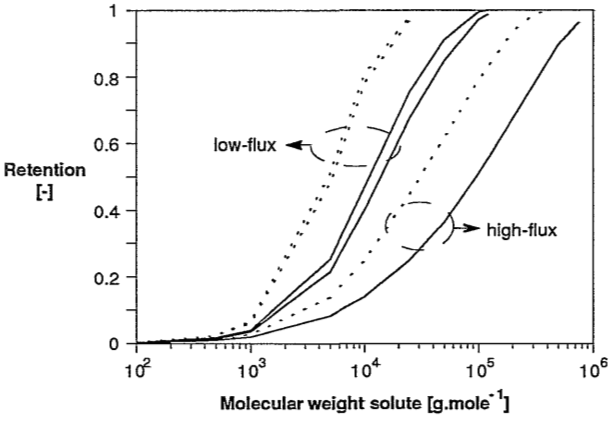

Figure A1 *Calculated retention curves as a function of the molecular weight of the solutes. Solid lines indicate curves based on the i-SEC data, the dashed lines are based on the mass transport data.*

It is assumed that the RC-HP400A fiber is composed as follows: a skin layer of 0.5 μm thick with a porosity of 0.7 and a pore radius of 2.6 nm and a support layer of 33.2 μm thick with a porosity of 0.824 and a pore radius of 5.6 nm. The porosity and pore radius of the skin layer are arbitrarily chosen equal to the values found for the low-flux membranes. A skin thickness of 0.5 μm is often reported for asymmetric ultrafiltration membranes.

With the parameters it can be calculated that in this case the cut-off drops to values which are identical with the values found for the low-flux membranes. The diffusive permeability of the skinned membrane, however, is only moderately affected. For solutes with a molecular weight of 0.2, 2 and 20 kg.mole^{-1} the reduction in diffusive permeability is 1, 4 and 67%, respectively. In particular the diffusive permeability of the smaller molecules is hardly affected.

Table A1 *Estimated cut-off values of the membranes, data calculated on the basis of the membrane structure parameters obtained from i-SEC and mass transport measurements.*

Membrane	I-SEC [kg.mole^{-1}]	Mass transport [kg.mole^{-1}]
cuprophan	64	15
hemophan	47	16
RC-HP400A	510	164

Parameters used:

$\rho = 1000$ kg.m^{-3} $\Delta p = 20$ kPa
$\eta = 6.95*10^{-4}$ Pa.s $N_a = 6.023*10^{23}$
T = 310 K

References:

[1] K.S. Spiegler, O. Kedem, Desalination, 1 (1966) 311
[2] A. Verniory, R. Du Bois, P. Decoodt, J.P. Gassee, P.P. Lambert, J. Gen. Physiol., 62 (1973) 489-507

6.7 Appendix B. Donnan exclusion of charged solutes

A cuprophan membrane with a fixed negative charge (R^-) is placed in a solution containing NaCl and positively charged creatinine (+co-ion). The ions of sodium, creatinine, chloride and the co-ion can diffuse from the solution to the membrane phase, although the sodium and creatinine ions can only diffuse in combination with their co-ion. The problem is simplified by assuming that only one salt is present in solution, i.e., X^+ and Cl^- ($[X^+] = [\text{creatinine}^+] + [Na^+]$). At equilibrium it follows that:

$$[X^+]_m.[Cl^-]_m = [X^+].[Cl^-] \qquad \text{(B1)}$$

where the subscript m refers to the membrane phase.

Because of electrical neutrality:

$$[X^+]_m=[Cl^-]_m + [R^-]_m \qquad \text{(B2)}$$

If $[X^+]=[Cl^-]$ it follows that:

$$\frac{[X^+]_m}{[X^+]} = \frac{1}{\sqrt{1 - \frac{[R^-]_m}{[X^+]_m}}} \qquad \text{(B3)}$$

The adsorption factor K_S is equal to the left-hand side of Eqn. B3.

The charge concentration $[R^-]_m$ is determined from charge density data of Table 5 in

Chapter 5 taking the volume fraction polymer of the swollen membrane into account. The concentration of the creatinine ion is taken as 1 mmole.dm^{-3}. The NaCl concentration is varied and added to the creatinine concentration. The creatinine concentration in the membrane and hence the adsorption factor K_S is then calculated from Eqn. B3 by iteration.

If both the permeant and the membrane are positively charged the electrical neutrality relation is given by:

$$[Cl^-]_m = [X^+]_m + [R^+]_m \qquad \text{(B4)}$$

And the adsorption factor becomes:

$$\frac{[X^+]_m}{[X^+]} = \frac{1}{\sqrt{1 + \frac{[R^+]_m}{[X^+]_m}}} \qquad \text{(B5)}$$

The results are further discussed in section 6.3 (Results and Discussion).

SUMMARY

Since the late 1960s cellulosic hollow-fiber membranes have been used in artificial kidneys, in which they act as a separation barrier for metabolic waste. The mass transport behavior of these membranes has been fairly well investigated since then. Relatively little, however, is known about the structure of the membranes. The objective of this thesis is to acquire fundamental knowledge about the structure and its relation to the performance of cellulosic hollow-fiber hemodialysis membranes. For this purpose various up-to-date membrane characterization techniques were used.

Throughout this thesis special attention is paid to three different types of hollow-fiber hemodialysis membranes: cuprophan®, hemophan® and RC-HP400A. The RC-HP400A fiber is a so-called high-flux type membrane. The cuprophan and RC-HP400A are made of a regenerated cellulose. The cellulose of hemophan fibers has been modified with a small amount of positively charged N,N-di-ethyl-aminoethyl (DEAE) ether groups.

Chapter 1 is a general introduction about hemodialysis and artificial kidneys. In this chapter recent trends in the development of new artificial kidneys, and the mass transfer in hollow-fiber artificial kidneys are discussed.

Chapter 2 gives a broad overview of the present knowledge about cellulosic hemodialysis membranes. The chapter is divided in three sections. The first section deals with the chemical and physical features of (water swollen) regenerated cellulose materials. In the second section the two main mass transport models proposed for the transport through cellulosic membranes are discussed. The third section deals with the choice for suitable characterization techniques. If a dry cellulosic membrane is brought in contact with water it swells and water filled channels or pores are formed through which mass transport can occur. Only in the water swollen state the membrane exhibits the properties that are required for the hemodialysis process. The characterization technique(s) to be used should therefore be capable to determine pores of a few nanometers in the wet state.

The characterization of cellulosic membranes by means of thermoporometry/calorimetry is discussed in chapter 3. Thermoporometry is a wet-state characterization technique to determine the pore size distribution and porosity of meso-porous membranes. It appears that in the case of water swollen cellulosic membranes the measurements are frustrated by anomalous recrystallization phenomena of melted ice. Owing to these phenomena, no reliable pore size distribution of the membranes can be obtained.

Measurements with a series of samples with different water content showed that the pore size distributions of the membranes are dependent on the water content. For all three membrane types it appears that above a water content of about 0.6 $g.g^{-1}$ a sudden change in the structure of the fibers occurs. Also the non-freezing water content of the fibers is dependent on the overall water content. For the low-flux fibers the non-freezing water content increases from 0.32 $g.g^{-1}$ to about 0.48 $g.g^{-1}$ at the equilibrium water content. For the RC-HP400A high-flux fiber the non-freezing water content increases from 0.33 to 0.73 $g.g^{-1}$.

Chapter 4 presents the characterization of cellulosic hemodialysis membranes by means of inverse size exclusion chromatography (i-SEC). With this technique the pore size distribution and porosity of a membrane can be determined and adsorption phenomena can be studied. The membranes show clear differences in pore size and porosity. The high-flux RC-HP400A membrane has a larger pore size as well as a higher porosity than the two low-flux membranes. It appears from the i-SEC measurements that the pore size distributions of the membranes are very narrow.
The test molecules creatinine and vitamin B12 both adsorb to the cellulosic membranes. The adsorption behavior of creatinine is strongly dependent on the NaCl concentration of the system indicating that an electrostatic interaction is present. The adsorption of vitamin B12 is not influenced by the NaCl concentration. The observations can be explained by assuming that cuprophan and RC-HP400A fibers are negatively charged whereas hemophan is positively charged due to the modification with DEAE. The net charge of the hemophan fibers is smaller.

In chapter 5 the mass transport through the membranes is discussed. The membranes show clear differences in permeability. The more swollen high-flux RC-HP400A fiber has a higher diffusive and hydraulic permeability. The permeation of creatinine through cuprophan, and to a lesser extent, through RC-HP400A is a strong function of the NaCl concentration in the system. It is shown that cuprophan has the highest (negative) charge density, the hemophan is slightly positively charged. The permeation data were used to obtain information about the pore morphology of the membranes. The parameters obtained are in good agreement with literature data for cuprophan. The RC-HP400A fibers have a larger pore size and a lower tortuosity. It appears from the permeability data for a range of polyethylene glycols that the calculated pore size increases with the size of the solute which may be an indication for the existence of a distribution of pore sizes.

Chapter 6 is a general discussion to compare the results of the thermoporometry, i-SEC and mass transport measurements. It is shown that although all the techniques give relevant information about the structure of the membranes there is some discrepancy between the results. With the i-SEC technique very sharp pore volume distributions are found. Thermoporometry

and mass transport measurements do not confirm this. Thermoporometry gives much smaller values for the porosity of the membranes. I-SEC yields somewhat larger pore sizes than the mass transport measurements. The difference can be explained by the difference in the characteristic size of the polyethylene glycols for both processes. From a combination of thermoporometry and i-SEC it appears that the non-freezing water of the membranes is at least partly accessible to solutes. The adsorption behavior of creatinine to the membranes can be explained qualitatively by a Donnan exclusion mechanism.

In an appendix to chapter 6, it is shown that the high-flux RC-HP400A fibers may have a (thin) skin layer with smaller pores. With such a skin layer it can be explained that even though the high-flux is more swollen and has larger pores no significant leakage of proteins from the blood is observed during the hemodialysis process.

RC-HP400A membraan bevat grotere poriën en heeft een lagere tortuositeit. Tevens zijn permeatiemetingen verricht met een reeks van polyethyleenglycolen van verschillende grootte. Het blijkt dat de, op grond van deze metingen berekende, poriegrootte toeneemt met de grootte van het gebruikte polyethyleenglycol molekuul. Dit zou een aanwijzing kunnen zijn voor het bestaan van een (brede) poriegrootteverdeling.

Hoofdstuk 6 is bedoeld om de resultaten van thermoporometrie, inverse uitsluitingschromatografie en stoftransportmetingen te vergelijken. Hoewel alle drie technieken waardevolle informatie over de struktuur van de membranen opleveren is er toch sprake van enige discrepantie tussen de resultaten van de verschillende metingen. Op grond van de i-SEC metingen is geconcludeerd dat de membranen zeer nauwe poriegrootteverdelingen hebben. Dit kon echter niet bevestigd worden met thermoporometrie of met stoftransportmetingen. Met thermoporometrie worden veel lagere waarden gevonden voor de porositeit van de membranen. De uitsluitingschromatografie techniek levert grotere waarden voor de poriegrootte dan de stoftransportmetingen. Het verschil kan verklaard worden door het verschil in karakterstieke grootte van de polyethyleenglycolen voor de verschillende processen. Uit een combinatie van de resultaten van i-SEC en thermoporometrie blijkt dat het niet-bevriezende of gebonden water op zijn minst gedeeltelijk toegankelijk is voor opgeloste stoffen. Het adsorptiegedrag van creatinine kan kwalitatief verklaard worden met een Donnan-exclusie mechanisme.

Uit een appendix bij hoofdstuk 6 wordt de indruk verkregen dat het RC-HP400A membraan mogelijk een dunne toplaag heeft met kleinere poriën. Op basis van zo'n toplaag kan verklaard worden dat, hoewel deze membranen meer gezwollen zijn en grotere poriën hebben ze toch niet of nauwelijks bloedeiwitten doorlaten tijdens het hemodialyseproces.

ZUSAMMENFASSUNG

Seit Ende der sechziger Jahre werden Membranen aus Zellulose-Hohlfasern für künstliche Nieren verwendet. Sie übernehmen dabei die Reinigung des Blutes von Abfallprodukten aus dem Stoffwechselprozeß bei Patienten mit nur ungenügend arbeitenden Nieren. Die Stofftransporteigenschaften dieser Membranen wurden inzwischen ausführlich untersucht. Im Gegensatz dazu ist aber über die Struktur der Membranen noch sehr wenig bekannt. Im Rahmen dieser Dissertation wurden grundlegende Untersuchungen zur Struktur und Morphologie von in Wasser gequollenen Zellulose-Membranen in Verbindung mit ihren Stofftransporteigenschaften durchgeführt. Für die Charakterisierung wurden verschiedene moderne Methoden genutzt.

Für die Untersuchungen wurden drei verschieden Typen von Hohlfasern verwendet: cuprophan®, hemophan® und RC-HP400A. Letztere Membran unterscheidet sich von den beiden erstgenannten durch ein hohes Durchflußvermögen. Die cuprophan- und RC-HP400A-Fasern bestehen aus regenerierter Zellulose. Die Zellulose von hemophan-Membranen ist mit einem geringen Anteil an positiv geladenen N,N-di-ethyl-aminoethyl (DEAE) ether-Gruppen modifiziert.

Kapitel 1 dieser Dissertation ist eine allgemeine Einleitung in Hämodyalyse und die Verwendung künstlicher Nieren. Es werden neuere Entwicklungen auf dem Gebiet der Verbesserung künstlicher Nieren und des Stofftransportes in künstlichen Nieren aus Hohlfasern beschrieben.

Kapitel 2 gibt einen grundlegenden Überblick über Zellulose-Hämodyalyse-Membranen. Das Kapitel ist in drei Teile untergliedert. Im ersten Teil werden die chemischen und physikalischen Eigenschaften gequollener und nicht gequollener Hämodyalyse-Membranen aus regenerierter Zellulose beschrieben. Teil 2 beschreibt die zwei wichtigsten Transportmodelle für den Stofftransport durch Zellulose-Membranen. Die Auswahl geeigneter Charakterisierungsmethoden wird in Teil 3 erläutert. Wird eine trockene Zellulose-Membran in Kontakt mit Wasser gebracht, so quillt sie. Dadurch entstehen mit Wasser gefüllte kleine Kanäle oderis Poren, die einen Stofftransport ermöglichen. Nur in diesem gequollenen Zustand besitzt die Membran die für die Hämodyalyse wesentlichen Eigenschaften. Die für die Charakterisierung der Membran genutzten Methoden müssen in der Lage sein, im nassen Zustand Poren in der Größe weniger Nanometer detektieren zu können.

Kapitel 3 beschreibt die Charakterisierung von Zellulose-Membranen

mit Hilfe von Thermoporometrie/Kalorimetrie. Thermoporometrie ist eine Methode, bei der im nassen Zustand die Porengrößenverteilung sowie die Porosität meso-poröser Materialien bestimmt werden können. Diese Methode scheint jedoch bei in Wasser gequollenen Zellulose-Membranen durch das Auftreten von Kristallisationserscheinungen des geschmolzenen Eises gestört zu werden. Aufgrund dieser Störeffekte können mit Thermoporometrie keine zuverlässigen Porengrößenverteilungen bestimmt werden. Messungen an Zellulose-Membranen mit unterschiedlichem Wassergehalt zeigten, daß die erhaltenen Porengrößenverteilungen vom Wassergehalt der Membranen abhängig sind. Bei einem Gehalt an Wasser von mehr als 0,6 g g^{-1} zeigten alle drei verwendeten Membrantypen (cuprophan®, hemophan®, RC-HP400A) eine plötzliche Veränderung der Membranstruktur. Die Menge an physikalisch gebundenem Wasser scheint ebenfalls vom totalen Wassergehalt der Membranen abzuhängen. Für die Hohlfasern mit geringem Durchflußvermögen erhöhte sich im vollständig gequollene Zustand der Anteil an physikalisch gebundenem Wasser von 0,32 g g^{-1} bis auf ca. 0,48 g g^{-1}. Für Hohlfasern mit hohem Durchflußvermögen stieg dieser Anteil von 0,33 g g^{-1} bis auf ca. 0,73 g g^{-1}.

In Kapitel 4 wird die Charakterisierung von Membranen mit invers-Ausschlußchromatographie (i-SEC) beschrieben. Mit dieser Methode können sowohl die Porengrößenverteilung als auch die Wechselwirkung verschiedener Stoffe mit dem Membranmaterial untersucht werden. Porengröße und Porosität der verwendeten Membranen zeigen deutliche Unterschiede. Dabei besitzt die Membran mit hohem Durchflußvermögen (RC-HP400A) sowohl größere Poren als auch eine höhere Porosität als die im Rahmen dieser Arbeit verwendeten Membranen mit geringerem Durchflußvermögen (cuprophan, hemophan). Aus den Ergebnissen der i-SEC Messungen kann ebenfalls geschlossen werden, daß alle untersuchten Membranen eine enge Porengrößenverteilung besitzen.
Die verwendeten Testmoleküle Kreatinin und Vitamin B12 adsorbieren wahrscheinlich an der Zellulose-Membran. Das Adsorptionsverhalten von Kreatinin wird durch die NaCl-Konzentration des Meßsystems stark beeinflußt, was auf einen elektrostatischen Wechselwirkungsmechanismus hinweist. Das Adsorptionsverhalten von Vitamin B12 ist unabhängig von der NaCl-Konzentration. Diese Erscheinungen können mit der Anwesenheit negativer Ladungen im Fall der cupophan- und RC-HP400A-Membranen erklärt werden. Die hemophan-Membranen besitzen aufgrund der Modifikation mit DEAE positive Ladungen, wodurch die resultierende Ladung erniedrigt wird.

In Kapitel 5 wird der Stofftransport durch die Membranen beschrieben. Die Permeabilitäten der untersuchten Membranen weisen große Unterschiede auf. Die stärker gequollenen RC-HP400A-Membranen besitzen sowohl eine

höhere hydraulische Permeabilität als auch eine höhere auf Diffusion beruhende Permeabilität. Die Permeation von Kreatinin durch cuprophan wird stark, die von Kreatinin durch RC-HP400A dagegen weniger von der NaCl-Konzentration beeinflußt. Messungen der Ladungsdichte ergaben, daß von den verwendeten Materialien cuprophan die höchste (negative) Ladungsdichte, hemophan dagegen eine schwach positive Ladung besitzt. Die aus den Stofftransportmessungen erhaltenen Ergenisse für Porengröße, Porosität und Tortuosität sind in guter Übereinstimmung mit den Literaturdaten für cuprophan. Membranen vom Typ RC-HP400A besitzen größere Poren und eine geringere Tortuosität. Weiterhin wurden Permeationsmessungen mit einer Reihe von Polyethylenglykolen verschiedener Größe durchgeführt. Die aufgrund dieser Messungen berechnete Porengröße nimmt scheinbar mit der Größe des verwendeten Polyethylenglykolmoleküls zu. Das könnte auf eine (breite) Porengrößenverteilung hinweisen.

In Kapitel 6 werden die Ergebnisse von Thermoporometrie, invers-Ausschlußchromatographie und Stofftransport miteinander verglichen. Alle drei verwendeten Charakterisierungsmethoden liefern wichtige Ergebnisse über die Membranstrukturen, wobei jedoch mit unterschiedlichen Methoden teilweise auch unterschiedliche Ergebnisse erhalten werden. Die i-SEC-Messungen weisen zum Beispiel auf eine enge Porengrößenverteilung hin, was aber durch Thermoporometrie- und Stofftransportmessungen nicht bestätigt werden kann. Mit der Thermoporometrie werden wesentlich geringere Porositäten erhalten. Die i-SEC-Methode führt zu größeren Werten für die Porengröße als Stofftransportmessungen. Diese Differenz kann durch einen Unterschied der charakteristischen Größe der Polyethylenglykolmoleküle in den verschiedenen Prozessen erklärt werden. Durch Kombination der Ergebnisse von Thermoporometrie und i-SEC kann geschlossen werden, daß das physikalisch gebundene Wasser zumindest teilweise für gelöste Stoffe zugänglich ist. Das Adsorptionsverhalten von Kreatinin kann qualitativ durch einen Donnan-Ausschluß Mechanismus erklärt werden.

Der Appendix zu Kapitel 6 gibt einen Hinweis darauf, daß RC-HP400A-Membranen möglicherweise Toplayer mit kleineren Poren besitzen. Das könnte eine Erklärung dafür sein, daß diese Membranen, obwohl sie stärker gequollen sind und größere Poren besitzen, nicht oder in nur geringem Maß Bluteiweißstoffe während der Hämodyalyse duchlassen.

LEKENSAMENVATTTING

Nieren vervullen een belangrijke funktie in het lichaam van de mens. Zo zorgen ze er onder andere voor dat afvalstoffen uit het bloed gefilterd worden en in de urine terechtkomen. Als de nieren niet of onvoldoende werken onstaat er een probleem; de afvalstoffen hopen zich op en het lichaam raakt vergiftigd. Om dit te voorkomen moet er ingegrepen worden. Dat gebeurt met een behandeling die hemo- of nierdialyse genoemd wordt. Voor zo'n behandeling moet de patiënt een aantal keren per week een paar uur naar het ziekenhuis (er zijn tegenwoordig ook andere behandelingen mogelijk). Tijdens de behandeling wordt het bloed van de patiënt schoon gemaakt met behulp van een kunstnier. Een belangrijk onderdeel van de kunstnier is het membraan of filter. Het membraan bestaat uit een dunne laag van een bepaald materiaal en heeft een heleboel heel kleine gaatjes of poriën. Die kleine gaatjes maken het mogelijk dat grote deeltjes, zoals bloedcellen en bloedeiwitten worden tegengehouden, terwijl de afvalstoffen, die vaak wat kleiner zijn, door het membraan heen kunnen. Op die manier kunnen de afvalstoffen afgescheiden worden. De gaatjes van het membraan zijn zo klein dat je ze met het blote oog niet kunt zien, zelfs met een goede microscoop lukt dat niet (zo maar). Toch is het belangrijk dat de gaatjes in het membraan precies de juiste grootte hebben. Als de gaatjes te klein zijn, kunnen de afvalstoffen er niet door en wordt het bloed niet schoon. Als de gaatjes te groot zijn, gaan ook de verkeerde stoffen, zoals eiwitten, door het membraan. Voor een fabrikant van kunstnieren is het belangrijk om snel te kunnen controleren of het gemaakte membraan de juiste eigenschappen heeft.

Een belangrijk doel van het onderzoek is geweest om methoden te vinden, waarmee je iets kunt zeggen over de grootte en het aantal gaatjes in een kunstniermembraan. In het bijzonder is er gekeken naar membranen die gemaakt zijn van cellulose; dit is een materiaal dat erg lijkt op huishoudfolie of cellofaan. Op grond van de gemeten eigenschappen is geprobeerd om een voorspelling te doen over hoe snel en hoe goed het membraan werkt.

LEVENSLOOP

Arnold Broek werd op 29 augustus 1965 geboren te Vlaardingen. Aan het Heldring College te Zetten behaalde hij in 1982 het HAVO diploma, en in 1984 het VWO diploma. In datzelfde jaar begon hij met een studie levensmiddelentechnologie, studieprofiel fermentatieleer, aan de Landbouwuniversiteit (Landbouwhogeschool) te Wageningen. De studie werd afgesloten met een hoofd- en een bijvak proceskunde en een stage bij het Norwegian Herring Oil and Meal Research Institute te Bergen, Noorwegen. Op 1 september 1989 werd het ingenieursdiploma behaald. Van 1 september 1989 tot 1 september 1993 was hij in dienst van de Universiteit Twente te Enschede. In de onderzoeksgroep membraantechnologie, onder leiding van prof. dr. C.A. Smolders en later prof. dr. ing. H. Strathmann, werd het in dit proefschrift beschreven onderzoek verricht. Sinds 18 oktober 1993 is hij in dienst van het Instituut voor Agrotechnologisch Onderzoek (ATO-DLO) te Wageningen.